


2012

Processing, Characterization And Performance Of Carbon Nanopaper Based Multifunctional Nanocomposites

Fei Liang
University of Central Florida

 Part of the [Materials Science and Engineering Commons](#)
Find similar works at: <https://stars.library.ucf.edu/etd>
University of Central Florida Libraries <http://library.ucf.edu>

This Doctoral Dissertation (Open Access) is brought to you for free and open access by STARS. It has been accepted for inclusion in Electronic Theses and Dissertations, 2004-2019 by an authorized administrator of STARS. For more information, please contact STARS@ucf.edu.

STARS Citation

Liang, Fei, "Processing, Characterization And Performance Of Carbon Nanopaper Based Multifunctional Nanocomposites" (2012). *Electronic Theses and Dissertations, 2004-2019*. 2400.
<https://stars.library.ucf.edu/etd/2400>

PROCESSING, CHARACTERIZATION AND PERFORMANCE OF CARBON NANOPAPER BASED MULTIFUNCTIONAL NANOCOMPOSITES

by

FEI LIANG

B.S. Donghua University, 2006

M.S. Donghua University, 2008

M.S. University of Central Florida, 2010

A dissertation submitted in partial fulfillment of the requirements
for the degree of Doctor of Philosophy
in the Department of Mechanical, Materials, and Aerospace Engineering
in the College of Engineering and Computer Sciences
at the University of Central Florida
Orlando, Florida

Fall Term
2012

Major Professor: Jihua Gou

©2012 Fei Liang

ABSTRACT

Carbon nanofibers (CNFs) used as nano-scale reinforcement have been extensively studied since they are capable of improving the physical and mechanical properties of conventional fiber reinforced polymer composites. However, the properties of CNFs are far away from being fully utilized in the composites due to processing challenges including the dispersion of CNFs and the viscosity increase of polymer matrix. To overcome these issues, a unique approach was developed by making carbon nanopaper sheet through the filtration of well-dispersed carbon nanofibers under controlled processing conditions, and integrating carbon nanopaper sheets into composite laminates using autoclave process and resin transfer molding (RTM).

This research aims to fundamentally study the processing-structure-property-performance relationship of carbon nanopaper-based nanocomposites multifunctional applications: a) Vibrational damping. Carbon nanofibers with extremely high aspect ratios and low density present an ideal candidate as vibrational damping material; specifically, the large specific area and aspect ratio of carbon nanofibers promote significant interfacial friction between carbon nanofiber and polymer matrix, causing higher energy dissipation in the matrix. Polymer composites with the reinforcement of carbon nanofibers in the form of a paper sheet have shown significant vibration damping improvement with a damping ratio increase of 300% in the nanocomposites. b) Wear resistance. In response to the

observed increase in toughness of the nanocomposites, tribological properties of the nanocomposite coated with carbon nanofiber/ceramic particles hybrid paper have been studied. Due to high strength and toughness, carbon nanofibers can act as microcrack reducer; additionally, the composites coated with such hybrid nanopaper of carbon nanofiber and ceramic particles shown an improvement of reducing coefficient of friction (COF) and wear rate. c) High electrical conductivity. A highly conductive coating material was developed and applied on the surface of the composites for the electromagnetic interference shielding and lightning strike protection. To increase the conductivity of the carbon nanofiber paper, carbon nanofibers were modified with nickel nanostrands. d) Electrical actuation of SMP composites. Compared with other methods of SMP actuation, the use of electricity to induce the shape-memory effect of SMP is desirable due to the controllability and effectiveness. The electrical conductivity of carbon fiber reinforced SMP composites can be significantly improved by incorporating CNFs and CNF paper into them. A vision-based system was designed to control the deflection angle of SMP composites to desired values. The funding support from National Science Foundation and FAA Center of Excellence for Commercial Space Transportation (FAA COE CST) is acknowledged.

To my Parents

ACKNOWLEDGMENTS

I would like to express my gratitude and appreciation to my advisor Dr. Jihua Gou, the director of the Composite Materials and Structures Laboratory (CMSL) at UCF. I'm really feeling grateful that he has provided me this great opportunity to join in the top level research group and work in composite materials area since fall 2008. His technical guidance, life counsel and continuous support are highly appreciated. He affects me not only with the serious research attitude by also with great personality. I would also like to express my sincere appreciation to Dr. Jiyu Fang, Dr. Ming Su, Dr. Nina Orlovskaya, and Dr. Yunjun Xu for serving on my committee and spending their valuable time evaluating my dissertation. I would like to express my special sincere gratitude to collaborators, Robert Sivilli from University of Central Florida, Dr. Haibao Lv from Harbin Institute of Technology, and Dr. Aixi Zhout from University of North Carolina at Charlotte for contributing their valuable time and providing numerous valuable suggestions and experimental help. My appreciation also goes to Mr. James McKee, our lab manager, for helping me carry out the experiment, order the materials, and proof reading.

Furthermore, my gratitude is also extended to Dr. Kevin Coffey and Cynthia Harle, of Advanced Materials Processing and Analysis Center (AMPAC) for their help in arranging all academic affairs. Special thanks must be extended to Stephanie Gavarrete, Jeanine Clements and Patricia Colyer, in the Department of Mechanical, Materials and Aerospace Engineering, for their help in arranging the traveling for me

to attend conferences.

Finally, sincere thanks go to my dear parents, for their patient, everlasting love, support, encouragement and understanding.

TABLE OF CONTENTS

LIST OF FIGURES	xii
LIST OF TABLES	xvii
CHAPTER ONE: INTRODUCTION	1
1.1. Motivation.....	1
1.2. Structure of the Dissertation	4
CHAPTER TWO: LITERATURE REVIEW	6
2.1. Processing of Carbon nanotubes/nanofibers/ graphene nanopaper	6
2.1.1. Vacuum/Pressure Filtration	6
2.1.2. Spin-Coating Method	7
2.1.3. Domino Pushing Method.....	8
2.1.4. Direct Synthesis.....	9
2.1.5. Electrophoretic Deposition.....	10
2.2. Processing of Nanocomposites	11
2.3. Multifunctional Polymer Nanocomposites	12
CHAPTER THREE: SYNTHESIS AND PROCESSING OF CARBON NANOPAPER AND NANOCOMPOSITES	15
3.1. Processing of Carbon Nanofiber Paper and its Hybrid Paper.....	15
3.2. Processing of Composites Coated with Nanopaper.....	17
CHAPTER FOUR: DAMPING CHARACTERIZATION AND ANALYSIS OF CARBON NANOFIBER BASED POLYMER COMPOSITE LAMINATES	22

4.1. Introduction.....	22
4.2. Materials and Damping test of carbon nanofiber paper-enabled nanocomposites.....	25
4.3. Results and Discussion	26
4.4. Summary.....	31
CHAPTER FIVE: TRIBOLOGICAL PROPERTIES OF THE NANOCOMPOSITES COATED WITH HYBRID NANOFIBER PAPER	
5.1. Introduction.....	32
5.2. Materials and Test Method	32
5.3. Results and Discussion	34
5.4. Summary.....	39
CHAPTER SIX: ELECTRICAL PROPERTIES OF NANOPAPER AND NANOCOMPOSITES AND THEIR APPLICATIONS	
6.1. Introduction.....	40
6.1.1. CNF-Based Nanocomposite for EMI shielding	40
6.1.2. CNF-Based Nanocomposite for lightning strike protection.....	42
6.2. Electrical property measurement of nanopaper and nanocomposites.....	43
6.3. EMI shielding application of CNF-based nanocomposites	45
6.3.1. Materials and Experiment methods	45
6.3.2. Electrical conductivity results of CNFs-based thin film	47
6.3.3. EMI SE Results	49

6.4. Lightning strike protection application of CNF-based nanocomposites	51
6.4.1. Materials and experiment methods.....	51
6.4.2. Electrical conductivity and Lightning strike tests	51
6.4.3. Damage characterization of composite panels after lightning strike.....	52
6.5. Summary.....	56
CHAPTER SEVEN: ELECTRO ACTUATION OF CARBON NANOFIBER-BASED	
SHAPE MEMORY POLYMER NANOCOMPOSITES	58
7.1. Introduction.....	58
7.2. Electro Actuation of SMP coated with carbon nanofiber paper	61
7.2.1. Materials	61
7.2.2. Fabrication of CNFs Paper and the CNFP-based SMP Composites	61
7.2.3. Results and Discussion	63
7.2.4. Control tests of SMP nanocomposites.....	71
7.3. Electro Actuation of continuous carbon fiber reinforced SMP nanocomposites.....	75
7.3.1. Row materials.....	75
7.3.2. Experimental Results and Discussion	75
7.4. Mechanical Property Degradation of Fiber Reinforced SMP Nanocomposites	78
7.5. Characterization results of shape recovery effect of carbon fiber reinforced	
SMP composites by vision based coordinate measurement system	83
7.6. Summary.....	84
CHAPTER EIGHT: COVELENT FUNCTIONALIZTION OF CARBON FIBERS	

WITH POLYHEDRAL OLIGOMERIC SILSEQUIOXANE AND THEIR	
APPLICATION IN SUPERHRDROPHOBICITY AND FLAME RETARDANCY	85
8.1. Introduction.....	85
8.2. Experimental.....	87
8.3. Measurements	89
8.4. Results and discussion	91
8.5. Summary.....	101
CHAPTER NINE: CONCLUSION AND FUTURE WORK.....	103
REFERENCE.....	106

LIST OF FIGURES

Figure 1. Schematic of spin-coating process	8
Figure 2 Schematic of Domino pushing method	9
Figure 3 Schematic of electrophoretic deposition process	11
Figure 4 Multi-step dispersion and microfiltration process of carbon nanofiber paper	16
Figure 5 Process of hybrid nanopaper	16
Figure 6 (a) Sample of fabricated carbon nanofiber paper, (b) SEM images of random CNF array.....	17
Figure 7 the schematic of VARTM processing	19
Figure 8 the schematic of stacking sequence of the vacuum bag system	20
Figure 9 Vacuum bag frame for autoclave	21
Figure 10 Connections between vacuum bag and autoclave	21
Figure 11 Regular composite beam and nanocomposite beam for damping test (left). Experimental setup for damping test (right)	26
Figure 12 Frequency response for the glass fiber reinforced composite beam with different thickness of carbon nanofiber paper as surface layer.....	30
Figure 13 Frequency response for the basalt fiber reinforced composite beam with different thickness of carbon nanofiber paper as surface layer.....	30
Figure 14 Frequency response for the carbon fiber reinforced composite beam with different thickness of carbon nanofiber paper as surface layer.....	31

Figure 15 The schematic of Tribometer (from Nanovea Inc.)	34
Figure 16 SEM images of pure CNF (left) and CNF with graphite flakes (right)	35
Figure 17 SEM images of CNF with SCFs (left) and CNF with graphite flakes, SCF (right)	36
Figure 18 SEM images of CNF with Al ₂ O ₃ and TiO ₂ (left), and CNF with all above nanoparticles (right)	36
Figure 19 SEM images of pure resin (left) and CNF with resin (right)	36
Figure 20 SEM images of CNF and graphite flakes with resin (left), and CNF, SCF with resin (right)	37
Figure 21 SEM image for G2 (left) and G4 (right) for tribology test	38
Figure 22 Summary of Average COF and Wear rate	39
Figure 23 Signatone Quad Pro system used for measuring sheet resistivity. Sample is placed under head and the head moves down and comes into contact with sample....	45
Figure 24 EMI SE measurement setup. Sample is placed in between two waveguides.	47
Figure 25 EMI shielding of carbon nanofiber samples, a) for the pure nanofiber papers, b) for the nanofiber papers with epoxy resin	51
Figure 26 Experimental rig for lightning strike tests	52
Figure 27 Surface damages of composite panels: (a) CP-CNFP-1; (b) CP-CNFP-2; (c) CP-CNFP-3.	54
Figure 28 Damage area and thickness of composite panels after lightning strike test: (a)	

CP-CNFP-1; (b) CP-CNFP-2; (c) CP-CNFP-3.....	55
Figure 29 SEM images of (a) CNFPs and (b) CNFPs infused with SMP resin.....	64
Figure 30 the electrical resistivity of different groups of sample..	65
Figure 31 Storage modulus, loss modulus and tangent delta curves for G1-G4 samples.	66
Figure 32 Camera Setup.....	67
Figure 33 Sample with placed colored dots (left) and painted dots (right)	69
Figure 34 reduced search area and associated dots.....	69
Figure 36 Idealized sample deformation over time	69
Figure 36 Series of photographs showing the macroscopic shape-memory effect of SMP composite for G1-G4..	70
Figure 37 Block diagram of control system.....	71
Figure 39 Circuit diagram of voltage Regulator	72
Figure 40 PI control response for varying values of k_p and k_i	73
Figure 41 Typical Proportional Gain Input	73
Figure 42 Typical Integral Gain Input.....	74
Figure 43 Typical Proportional Gain Input	74
Figure 44 Storage Modulus of SMP samples.....	77
Figure 45 $\tan\delta$ of SMP samples	77
Figure 46 Glass transition temperature of SMP sample	78
Figure 47 Three point bending samples	79

Figure 48 MTS machine for three point bending test	79
Figure 49 Flexural stress-strain curves of SMP samples	81
Figure 50 Ultimate strength of SMP samples	82
Figure 51 Flexural Modulus of SMP samples	82
Figure 52 Deflection Angle of sample with 0%, 35.1%, 55.2% fiber volume fraction	83
Figure 53 Illustration for the synthesis of CNF-g-POSS.....	88
Figure 54. Illustration for the preparation of nanopaper.	89
Figure 55 The schematic representation of the ASTM E1345-10 cone calorimeter test method.....	91
Figure 56 FTIR spectra of: (a) pristine CNTs; (b) CNT-g-POSS; (c) POSS.	92
Figure 57 Raman spectra of: (a) pristine CNF; (b) CNF-g-POSS.....	93
Figure 58 SEM images of: (a) surface of CNF paper, (b) POSS-g-CNF paper, (c) the 'wall' in (b) at high magnification.	94
Figure 59 Photo images of a 15 μ L water droplet on surfaces: (a) CNF film; (b) A droplet sticks on CNF-g-POSS film; (c) stays on CNF-g-POSS film; (d) the same measured CNF-g-POSS film after exposure to a high-humidity environment for three weeks.....	97
Figure 60 TGA results of pure POSS, CNF, and POSS-grafted-CNF	97
Figure 61 Pure resin panel after cone test.....	99
Figure 62 Resin with 1% CNF panel after cone test.....	99

Figure 63 Resin with POSS-grafted-CNF panel after cone test	100
Figure 64 the mass loss of the cone test.....	100
Figure 65 HHR of the cone tsest.....	101

LIST OF TABLES

Table 1 Damping ratio for glass fiber reinforced composites calculated by half-power bandwidth method.....	29
Table 2 Damping ratio for carbon fiber reinforced composites calculated by half-power bandwidth method	29
Table 3 Damping ratio for basalt fiber reinforced composites calculated by half-power bandwidth method.....	29
Table 4 Composition of Different Groups of Samples	34
Table 5 Properties of carbon nanofibers	46
Table 6 Electrical conductivity of carbon nanofiber papers	49
Table 7 Compositions and structure of CNFPs with large size of 18”×18”	51
Table 8 Resistivity of top surface of CNFPs and composite panels	52
Table 9 Flexural testing results of LS-CP-S-1, LS-CP-S-1 and LS-CP-S-1	56
Table 10 Thermal properties of particles, nanopaper with resin from TGA.....	98
Table 11 PHRR and Char of samples.....	98

CHAPTER ONE: INTRODUCTION

1.1. Motivation

Polymer-matrix composites (PMCs) consist of high strength and modulus fibers as the reinforcement and polymer resin as the matrix. In the structure of PMCs, the matrix binds the fiber together, keeps them rigid, and acts as a medium to transfer and distribute the externally applied load, while the fibers serve as the principal load-carrying members. The combination of fibers and resin shows a unique property which is not possessed by either of the fibers or matrix. Compared to metallic matrix composites (MMCs) and ceramic matrix composites (CMCs), the great advantages of the PMCs are their light weight, high specific strength, and high specific stiffness.

These unique mechanical advantages, combined with tolerability, ease fabrication and formability, make the PMCs materials as a great competitor to the traditional metallic materials and ceramic materials. The PMCs, also named as advanced composite materials, was mostly used for high tech area such as aircraft, military, space, and race car. Nowadays, these materials are used in the greatest diversity of composite applications and in the largest quantities including boat decking, transportation, wind turbine blades, sporting goods, infrastructure, furniture, and so on. For example, the newly developed Boeing 787 Dreamliner contains 50% fiber reinforced composite materials by weight [1]. The PMCs are growing rapidly with accelerating global demanding. According to reports, global polymer composites industry reached \$17.7 billion in 2010 with annual growth of 10%. End produce

market makes composites in 2010 were \$50.2 billion [2].

However, several shortcomings for PMCs limit their implementation. First, due to the nature of matrix and fibers, most of PMCs are not conductive. The insulation nature of the composite materials will lead to serious problems when they are used as structure materials of the aircraft and wind turbine blades. Due to the high possibility of lightning strike of the air craft and wind turbine blades, it can cost a great damage on these parts since the PMCs is nonconductive and there is no way to dissipate the huge energy from the lightning when they are stroked. Therefore, highly conductive polymer composites are with great demanding for this kind of application. Second, in resulting of PMCs structure, the polymer on the surface is easy to worn out due to the low strength and toughness of the polymer resin. The tribological property of PMCs is undesirable. Third, the mechanical properties of PMCs will deteriorate at environment with high humidity due to the moisture absorption of the matrix. Improving hydrophobicity of PMCs is other critical issue. Fourth, shape memory polymer is the most attractive smart material, due to its light weight and large strain rate. To actuate SMP by electricity is really challenging due to low conductivity of the SMP resin. To solve the as mentioned problem, nanoparticles, including carbon nanotubes (CNTs), Carbon nanofibers (CNFs), and few layer graphite were employed. Significant improvement of the mechanical and electrical properties has been achieved while several issues still remain, including the dispersion of CNFs and the viscosity increase of polymer matrix. To overcome these issues, a unique approach

was developed by making carbon nanopaper sheet through the filtration of well-dispersed carbon nanofibers under controlled processing conditions, and integrating carbon nanopaper sheets into composite laminates using autoclave process and resin transfer molding (RTM).

Therefore, the motivation of this study is to fundamentally study the processing-structure-property-performance relationship of carbon nanopaper-based nanocomposites multifunctional applications. Specifically, this work includes the following:

1) Vibrational damping. Carbon nanofibers with extremely high aspect ratios and low density present an ideal candidate as vibrational damping material; specifically, the large specific area and aspect ratio of carbon nanofibers promote significant interfacial friction between carbon nanofiber and polymer matrix, causing higher energy dissipation in the matrix. Polymer composites with the reinforcement of carbon nanofibers in the form of a paper sheet have shown significant vibration damping improvement with a damping ratio increase of 300% in the nanocomposites.

2) Wear resistance. In response to the observed increase in toughness of the nanocomposites, tribological properties of the nanocomposite coated with carbon nanofiber/ceramic particles hybrid paper have been studied. Due to high strength and toughness, carbon nanofibers can act as microcrack reducer; additionally, the composites coated with such hybrid nanopaper of carbon nanofiber and ceramic particles shown an improvement of reducing coefficient of friction (COF) and wear

rate.

3) High electrical conductivity. A highly conductive coating material was developed and applied on the surface of the composites for the electromagnetic interference shielding and lightning strike protection. To increase the conductivity of the carbon nanofiber paper, carbon nanofibers were modified with nickel nanostrands.

4) Electrical actuation of SMP composites. Compared with other methods of SMP actuation, the use of electricity to induce the shape-memory effect of SMP is desirable due to the controllability and effectiveness. The electrical conductivity of carbon fiber reinforced SMP composites can be significantly improved by incorporating CNFs and CNF paper into them. A vision-based system was designed to control the deflection angle of SMP composites to desired values.

5) Superhydrophobicity and fire retardancy. Develop coating material on the surface of the composites by covalent functionalization of carbon nanofibers with polyhedral oligomeric silsesquioxane (POSS) for superhydrophobicity and fire retardancy.

1.2. Structure of the Dissertation

The structure of the dissertation from Chapter 2 to Chapter 8 is organized by the following sequence. Chapter 2 reviews the processing of nanocomposites, and processing approaches of nanopaper, properties of multifunctional polymer composites. Chapter 3 discusses the composites manufacture and processing, including nanopaper fabrication and fiber reinforced nanocomposites processing.

Chapter 4 focuses on damping property of carbon nanofiber paper composites. Chapter 5 discusses the tribological properties of the nanocomposites coated with hybrid nanopaper. Chapter 6 analyzes high conductive carbon nanofiber paper nanocomposites for EMI and lightning strike protection application. Chapter 7 focuses on electro-actuation of SMP CNFP nanocomposites by resistivity heat. Chapter 8 discusses the covalent functionalization of carbon nanofibers with POSS and their applications in superhydrophobicity and fire retardancy. The dissertation ends in Chapter 9, where conclusion and future work are proposed.

CHAPTER TWO: LITERATURE REVIEW

2.1. Processing of Carbon nanotubes/nanofibers/ graphene nanopaper

There are various methods to manufacture carbon nanotube paper. The manufacturing process can be divided into two categories: one-step method and two-step method. For the two-step method, carbon nanotubes are synthesized first and the paper is made from the nanotubes. In one-step method, carbon nanotube paper is grown directly. The two-step method is the main process to make carbon nanotube paper, including vacuum/pressure filtration, spin-coating, and domino pushing method.

2.1.1. Vacuum/Pressure Filtration

Since the as received nanoparticles are in the form of bundle or cluster, ultrasonication is employed to de-bundle them before the vacuum/pressure filtration processing. The nanoparticles are mixed with the water or acetone, then are put into the sonicator. The process utilizes ultrasound energy to agitate nanoparticles. It is usually carried out by an ultrasonic bath or a horn/probe. During the process, the ultrasound propagates by a series of compression. When it passes through the solvent medium, attenuated waves are induced, promoting the “peeling off” of CNFs that located at the outer parts of the CNF bundles/agglomerates. As a result, the individual nanoparticles are separated and high quality dispersed suspension is achieved [3].

Filtration method is a process in which the suspension of carbon nanotubes is filtrated through a filter paper to make a free-standing non-woven mat [4]. The entire process can be divided into four steps: (1) preparation and purification of carbon nanotubes; (2) uniform dispersion of carbon nanotubes into a solvent to form a stable suspension; (3) filtration of the suspension of carbon nanotubes under vacuum or pressure; and (4) drying the nanotube paper in a vacuum oven. The advantage of this method is low cost and easy manufacturing. However, high degree of curviness and easy aggregation of the nanotubes may result in the brittleness of the nanotube paper.

2.1.2. Spin-Coating Method

A uniform carbon nanotube paper is produced by spin-coating from a highly concentrated nanotube dispersion, which is stabilized by chemical oxidation [4]. In this process, the solution of purified carbon nanotubes is filled into a high speed spinning glass panel. The thickness of the nanotube paper can be controlled by changing the concentration of the nanotubes and the speed of spinning. High quality of the nanotube paper can be obtained with uniform surface and much thinner thickness, which lead to potential applications in the field of solar battery. Aligned MWCNTs are produced and aligned CNT-based membrane electrode is used as the anode material in a rechargeable lithium-ion battery. Figure 1 shows the procedure of the spin-coating method.

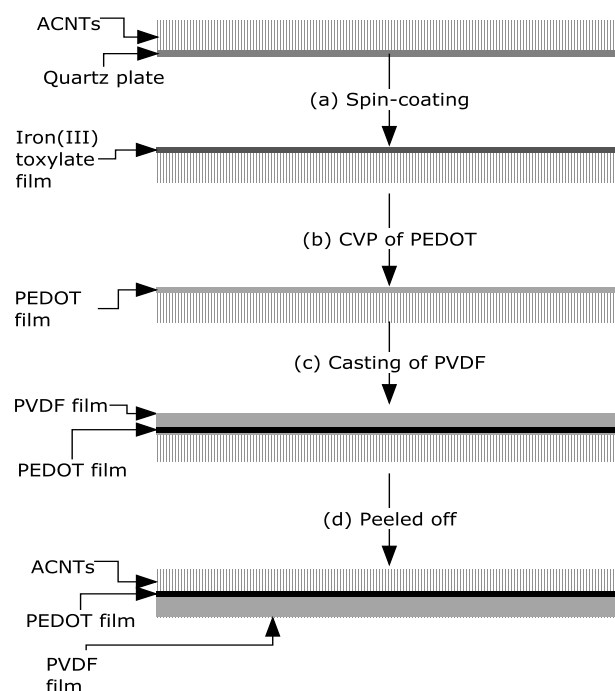


Figure 1. Schematic of spin-coating process [5]

2.1.3. Domino Pushing Method

A simple but effective macroscopic manipulation of carbon nanotube arrays called “domino pushing” has been developed to make aligned thick carbon nanotube papers [6]. The schematic of domino pushing method is shown in Figure 2. Firstly, the nanotube array is covered with a piece of micro-porous membrane. All the nanotubes in the array are forced down to one direction by pushing a cylinder, which is placed on the nanotube array with a constant pressure. All the nanotubes in the array are attracted together due to strong Van der Waals forces and form an aligned carbon nanotube paper. The aligned carbon nanotube paper is then peeled off from the silicon substrate with the membrane. Ethanol is spread on the micro-porous membrane and permeates through the membrane, and then the aligned nanotube paper can be peeled

off from the membrane easily. The curviness and aggregation of the nanotubes can be avoided with this method. However, the impurity stays with the nanotubes. The domino pushing method is more complicated than the filtration and spin-coating process.

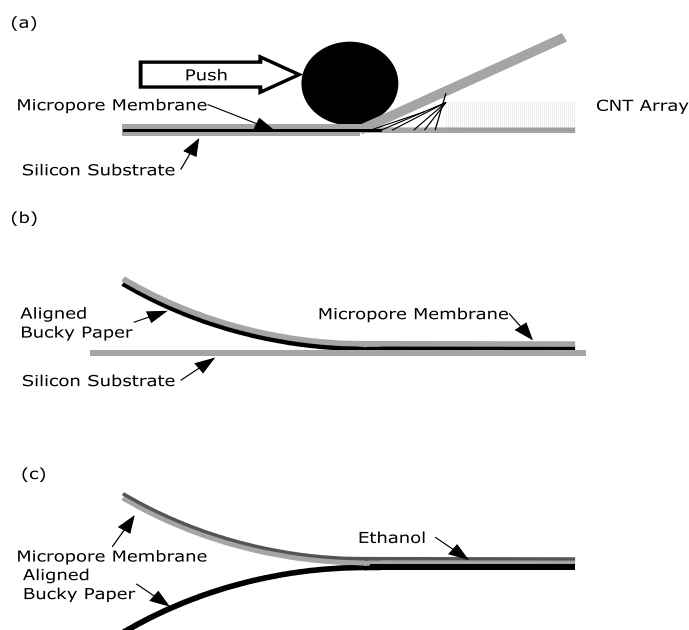


Figure 2 Schematic of Domino pushing method [6]

2.1.4. Direct Synthesis

In this method, carbon nanotube paper is in-situ synthesized by using trichlorobenzene (TCB) as a precursor. There are barely reports on the one-step method in which carbon nanotube paper is grown by CVD method. Ferromagnetic carbon nanotube paper filled with Fe nanowires (Fe-CNT) was in-situ synthesized without using any surfactant or acid treatment [7]. The one-step method is much simpler than the two-step method. The organic solvent can be avoided in one-step process. Meanwhile, good mechanical properties can be obtained. However, high

impurity content limits the applications of carbon nanotube paper made by the one-step method.

2.1.5. Electrophoretic Deposition

An electrophoretic deposition (EPD) process has been developed to fabricate the graphene paper [8]. The film is composed of overlapped and stacked platelets of reduced graphene oxide. Figure 3 shows the experiment setup and cross-sectional SEM image of the EPD-GO film. GO was dispersed in water and sonicated at room temperature. After the preparation of colloidal suspensions of individual GO platelets in purified water, EPD-GO was deposited on stainless steel, and on various other electrically conductive substrates. Typical concentrations of GO and applied direct current (DC) voltage were 1.5 mg/mL and 10 V, respectively. The deposition time was in the range of 1-10 min. The GO platelets migrated toward the positive electrode when a DC voltage was applied. The deposition rate depended on several factors including the concentration of the GO suspension, the applied DC voltage, and the conductivity of the substrate. A smooth film was deposited on the stainless steel positive electrode in a short time period with 10 V of applied potential. After the deposition, the samples were air dried at room temperature. By varying the current and time, films with the thickness in the range between several hundreds of nanometers and tens of micrometers could be deposited.

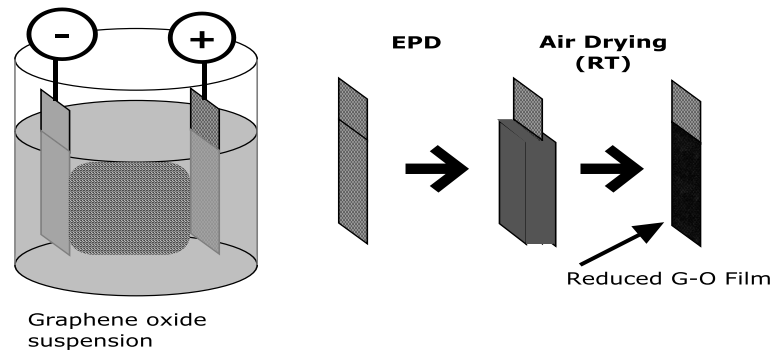


Figure 3 Schematic of electrophoretic deposition process [8]

2.2. Processing of Nanocomposites

Nanoparticles have been used as additives into polymers to achieve high performance nanocomposites. There are several different synthesis methods for polymer nanocomposites including high shear mixing, solution mixing, melt mixing, in-situ polymerization, emulsion polymerization, and so on. All these processing approaches have their own advantages as well as disadvantages. In general, the goal is to achieve the nanoscale dispersion of the nanoparticles and significantly improve the properties of the nanocomposites.

The high shear mixing method is the most intuitive way and most widely used method to incorporate the nanoparticles into polymer. The advantage for this method is low cost and free of solvent, while the disadvantage is even dispersion of the nanoscale is hard to achieve. The advantage of solution mixing is the viscosity of resin is controlled in a very low degree so that high extents of dispersion of nanoparticles in polymer can be achieved, while the limitation is this method needs lots of solvents for the processing which is not cost effective and environmentally

friendly. Melt mixing is other popular approach to syntheses nanocomposites. For this method, the nanofillers are directly mixed with the polymer at high temperature which makes it solvent free. However, serious degradation of the polymer at high temperature will occur, which lead to the decrease of the mechanical properties of the nanocomposites. In-situ polymerization method requires the nanofillers can be dispersed evenly in solvent and the monomer of the polymer can also be dissolved into the same solvent. The low viscosity of this method leads to a better dispersion of the nanofillers and the subsequent polymerization of the monomer allows the polymer uniformly interacting with nanofillers.

2.3. Multifunctional Polymer Nanocomposites

Due to the light weight, good chemical resistance and lower manufacturing costs, polymer matrix composites have been widely used to automobile, aerospace, recreational goods, infrastructure, electronic devices, etc. In last 20 years, nanomaterials and nanotechnology have drawn tremendous attention due to their excellent mechanical, electrical, and thermal properties and their great potential application in sensing, solar cell, super capacitor, tribological, catalytic, biomedical, fuel cell, battery and so on. Great combination of excellent properties of polymer and nanomaterials leads to a unique concept of multifunctional polymer nanocomposites. Multi-functions usually have structural advantage with other functions including energy storage, actuation, thermal management, health monitoring, electromagnetic interference shielding, and biological. A significant advantage of multifunctional

materials used to structural application is large weight saving due to the reduction in number of multiple monofunctional components. The multifunctional polymer nanocomposites have a rapid development and a number of achievements in the fields of both academics and industries have been reported. Zhang et al [9] developed a vertically aligned self-supporting multifunctional carbon nanotubes sheet, which can be used for the microwave bonding of plastics and for making transparent, highly elastomeric electrodes; planar sources of polarized broad-band radiation; conducting appliqué and flexible organic light-emitting diodes. Veedu et al [10] grew multi-walled carbon nanotubes on the surface of micro-fibre fabric cloth layouts to create 3D effect between plies under loading, which exhibited remarkable improvements in the interlaminar fracture toughness, hardness, delamination resistance, in-plane mechanical properties, damping, thermoelastic behaviour, and thermal and electrical conductivities making these structures truly multifunctional.

One of the shortcomings of the polymer based materials is nonconductive, which limited their application. Incorporating adequate electrical conductive nanoparticles into polymer composites will make a great benefit to the increasing demand of lightning strike protection of polymer composites constructed aircraft and electromagnetic interference shielding of electron devices. Moreover, low thermal conductivity of polymer composites also could be a problem to the application of electronic packaging which requires high thermal conductivity to dissipate heat.

In this research, we used the carbon nanofiber paper as a platform material,

incorporated with other nanoparticles and integrated with the polymer composites to tailor the electrical, thermal, and mechanical properties of the polymer nanocomposites. The multifunctional polymer nanocomposites have demonstrated the capability for the application of damping, tribological, lightning strike protection, EMI shielding, and actuation.

CHAPTER THREE: SYNTHESIS AND PROCESSING OF CARBON NANOPAPER AND NANOCOMPOSITES

3.1. Processing of Carbon Nanofiber Paper and its Hybrid Paper

The multi-step process of carbon nanofiber paper is shown in Figure 4. A high intensity sonicator (600-watt Sonicator 3000 from Misonix Inc.) was used to evenly disperse the carbon nanofiber and the facile filtration method was employed to fabricate the carbon nanofiber paper. In detail, the nanofibers were divided into several parts evenly, and then were transferred into three 1000ml beakers and 400 ml deionized water was added. The solution was sonicated using a sonicator for with 30 min. After that, the solution was cooled down to room temperature and 10 drops of surfactant (Triton-X100) were added into the solution. Then the solution was sonicated twice again with 30 min interval and was cooled down to room temperature. Finally, the as-prepared three suspensions were sonicated two minutes and immediately transferred into filtration system. However, not all the nanoparticles are suitable to be dispersed by the sonicator. For example, the nickel nanostrands with dedicate nanostructure can be severely damaged by the high intensity sonication. Therefore, the process of hybrid paper is different (Figure 5). The boiling water method was employed to disperse the nickel nanostrands in the deionized water and then mixed with the carbon nanofiber suspension by a high shear mixer.

The carbon nanofiber paper was made by filtering the as-prepared suspension through 0.4 μ m hydrophilic polycarbonate membrane under a high-pressure filtration

system (100 Psi). Once the paper was made, the filter with the carbon nanopaper was carefully removed and placed onto a piece of paper where the filter was detached. The papers were about 12.5 cm in diameter, as shown in Figure 6. The remaining paper was put into oven at temperature of 120°C for two hours.

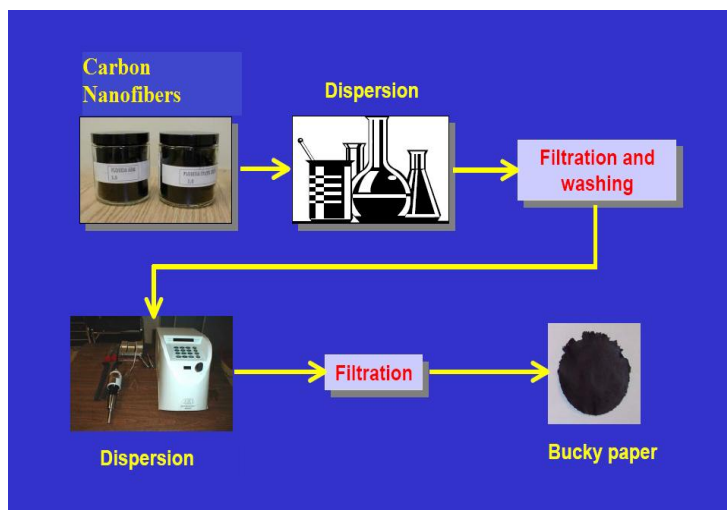


Figure 4 Multi-step dispersion and microfiltration process of carbon nanofiber paper

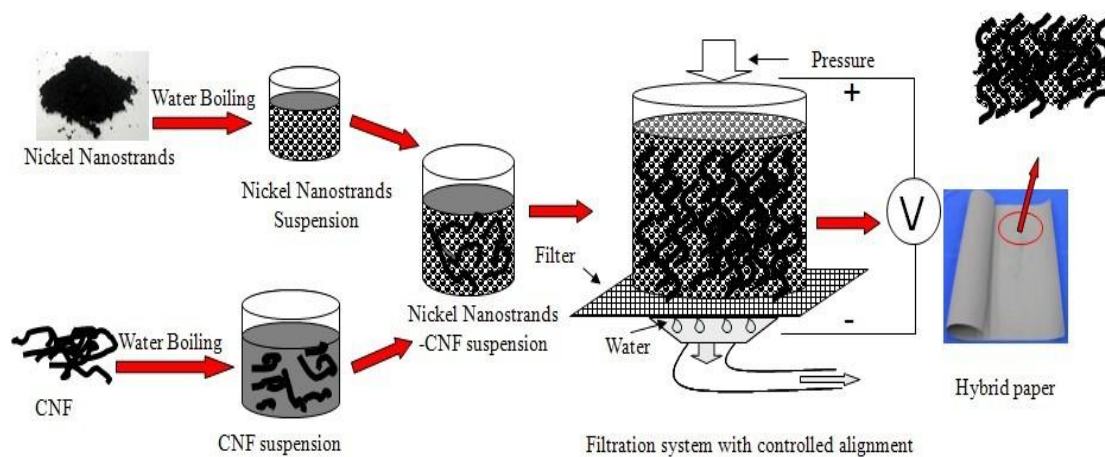


Figure 5 Process of hybrid nanopaper

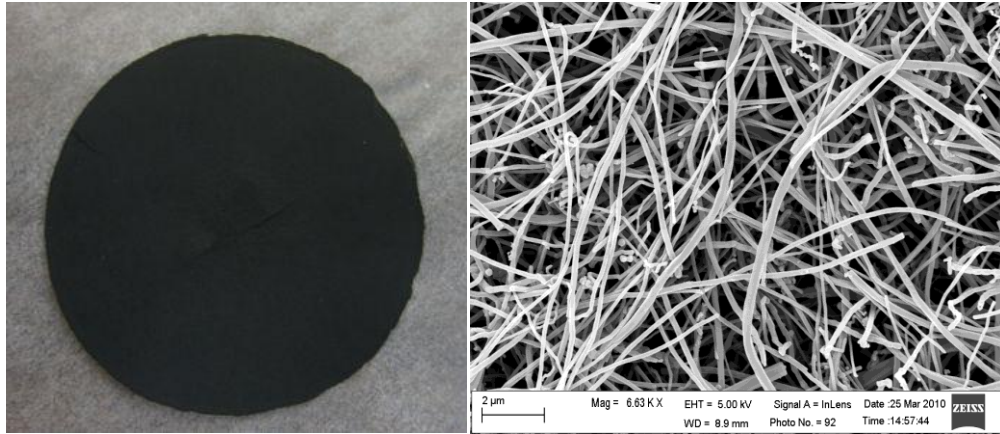


Figure 6 (a) Sample of fabricated carbon nanofiber paper, (b) SEM images of random CNF array

3.2. Processing of Composites Coated with Nanopaper

There are a variety of methods to manufacture the fiber reinforced polymer composites. The first technique used to fabricate the composites is the manual lay-up. In this method, one layer of the dry fabric is laid in the mold and then the liquid resin is poured, brushed, or sprayed on the fabric. The roller is employed to evenly distribute the resin and remove the air bubbles. Then another layer of the fabric is laid on the top and the previous sequence is repeated until the desired thickness of composites is obtained. This method is simple and cost effective. However, the quality of the product is highly depended on the experience and lots of air bubbles could be created during the resin spreading process. Also, the lay-up method cannot achieve high fiber volume fraction composites. Another widely used method is the vacuum assist resin transfer molding (VARTM) process. Figure 7 shows the schematic of VARTM process. The nanopaper is laid on the mold and the fabric is put on the top of the nanopaper. Then peel ply and flow media are applied on it. A plastic vacuum

bag is used to seal the part. Resin is sucked into the vacuum bag by the vacuum pressure applied in the outlet. The advantages of this method lie in the control of the voids, thickness of the laminates, and the fiber volume fraction. Moreover, this method significantly reduces the tooling cost. The most common issue of VARTM process is the age of the bag. The bag leak often occurs between the interface of the sealant and the vacuum bag, which causes the bag failure and voids in the laminates. The main liquid molding method is the resin transfer molding (RTM), which widely used in the automotive industry. The products made by a RTM process have good finish on the surface and the voids can be significantly reduced. In our experiments, the CNFPs were incorporated onto the surface of traditional carbon fiber mats through resin transfer molding (RTM) process. In the RTM process, the CNFP was first placed on the bottom of the mold, the fabric mats were laid down on the top. After the resin filled the mold, it cured at different curing cycle which depends on the resin system. The big advantage of the RTM process is good resin penetration through the low permeability nanopaper, such as layered-structure graphene nanopaper. A 300-psi pressure system was developed to achieve the good resin impregnation of the nanopaper.

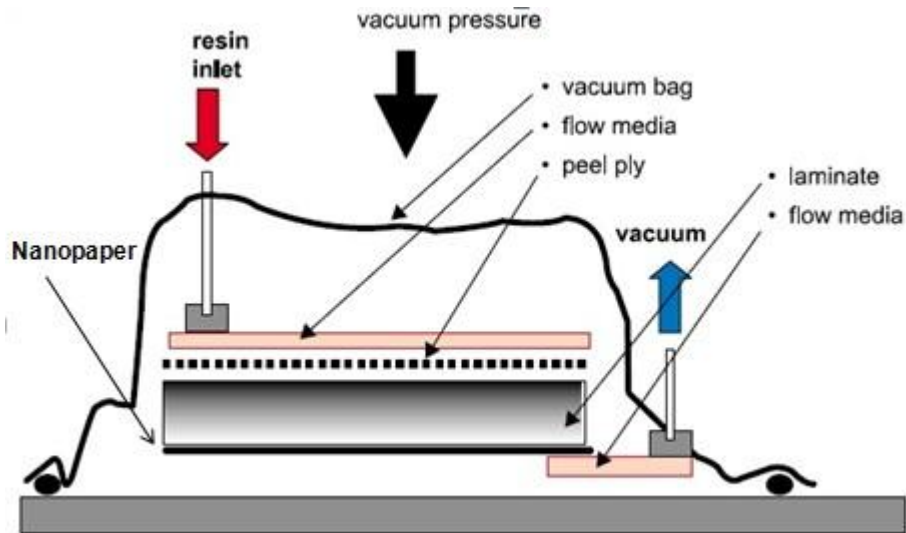


Figure 7 the schematic of VARTM processing

Autoclave is the most advanced composites manufacturing process. This process provides higher pressure and void elimination. Several parts can be cured in the autoclave at the same time. Autoclave is extensively used for high-performance parts such as aerospace parts. Another advantage of autoclave is that both vacuum and pressure can be applied, which greatly reduced the void content even for the chemical reaction with lots of air bubbles. In this study, autoclave processing has been employed to fabricate fiber reinforced SMP nanocomposites. As the most widely used composites processing facility, autoclave processing has incomparable advantages. The processing temperature can vary from 20°C to 425 °C, and the pressure can achieve as high as 200 psi (13.6 atm). The vacuum degree can reach about -30in Hg. Liquid SMP resin (part A and part B) was dried at less than -27inHg for 3 hours. The die was dried for more 3 hours at 70°C. The material stacking sequence (from bottom to top) for the vacuum bag tooling in autoclave follows:

release plastic film, breath fabric, aluminum frame, silicon-based rubber breath fabric, and cork. The release plastic allows the cured composites easily come off from the tooling. The breach fabric provides the space for the air/gas generated from the curing reaction which great decrease the air bubble volume fraction in the composites. The silicon-based rubber will keep the composites panel flat. The cork absorbs the extra resin. When the resin and die (aluminum frame) were completely dried, the carbon nanopaper was put into the die and the carbon fabrics were laid on the top of nanopaper. Part A and part B were mixed for 2 minutes at 60 rpm and then were poured into the die. The vacuum bag tooling was closed and the -27 inHg vacuum was applied immediately and stayed on through the whole process. During the curing cycle, 15 psi pressure was applied for 5 minutes then increase up to 50 psi. The temperature increased to 75°C after 5 minutes. The curing process ended after 3 hours.

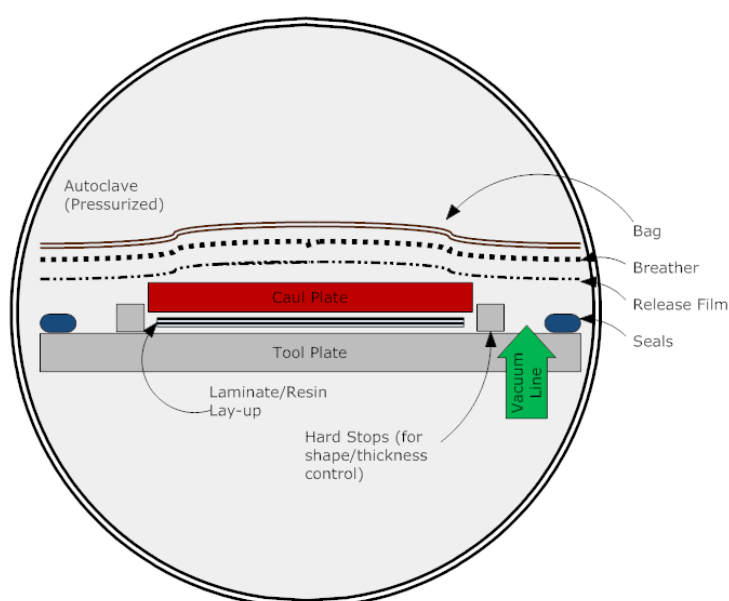


Figure 8 the schematic of stacking sequence of the vacuum bag system

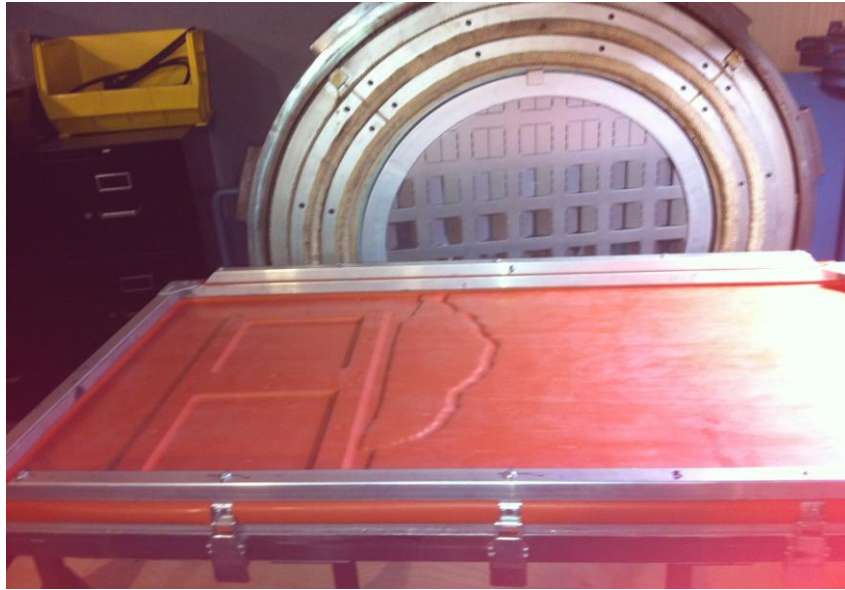


Figure 9 Vacuum bag frame for autoclave

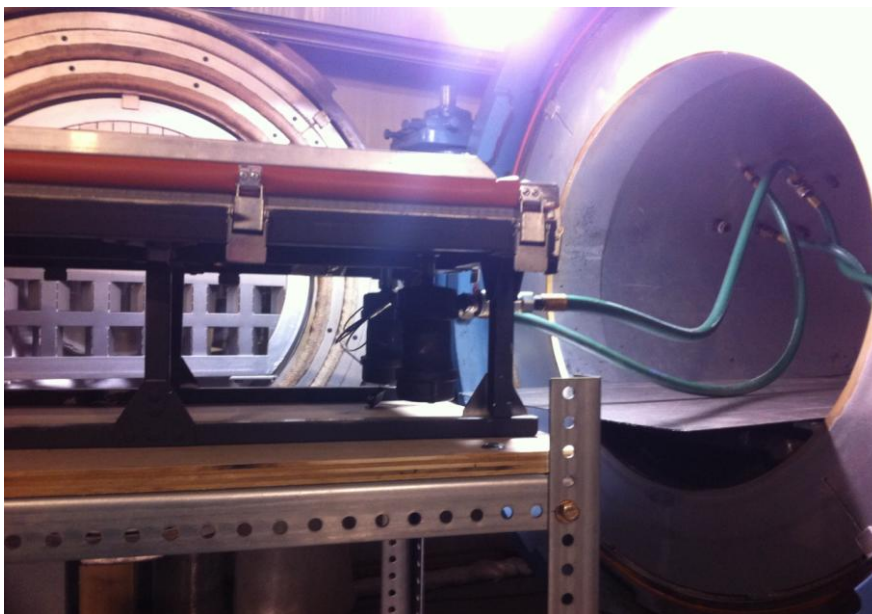


Figure 10 Connections between vacuum bag and autoclave

CHAPTER FOUR: DAMPING CHARACTERIZATION AND ANALYSIS OF CARBON NANOFIBER BASED POLYMER COMPOSITE LAMINATES

Polymer matrix composites reinforced by carbon nanofibers (CNFs) are rapidly gaining popularity in vibration damping applications. The large specific area ($1000 \text{ m}^2/\text{g}$) and aspect ratio (>1000) of CNFs, which promote significant interfacial friction between carbon nanofibers and the polymer matrix, cause much higher energy dissipation in the polymer matrix. Nanocomposite combined with carbon nanofibers in the form of paper sheet have proved significant improvement in vibration damping compared to pure matrix materials.

4.1. Introduction

The vibration in the dynamic systems, such as turbine blades in aircraft, is lean to severe due to resonance, limit cycle, or aeromechanical instability conditions. Increasing the damping effect can lead to reduction of system loading, alleviation of fatigue of structural components, and decrease of cabin noise. Therefore, it is obviously significant to explore structural components with high levels of inherent structural damping for a wide variety of applications in wind energy, aircraft, and automobile systems. Passive and active damping is two main methods of enhancement the damping effect for composites. In passive system, vibrations are diverted into special materials or structural components that dissipate the vibration energy as heat due to the friction of different components. Viscoelastic materials have

been embedded into composite structures to improve the damping ratio. In the active systems, a certain control strategy is implemented on the composite structures instrumented with actuators and sensors to actively control the vibration signal. The structures are moved in opposition to the vibration to effectively cancel the vibration out.

Viscoelastic [11] and elastomeric [12] materials, considered as conventional materials for vibration damping, have proved their usefulness in energy dissipation. However, poor thermal stability [13], and low stiffness and strength limit their application for the enhancement of vibration damping property of composite structures. For example, the performances of commercial damping films will greatly loss when the operating temperature is higher 60°C [14]. Moreover, the stiffness of viscoelastic materials is much lower than the host composite structure. The integration of viscoelastic materials within composite structures poses significant technical challenges [14]. For example, when the damping materials are co-cured with the host composites, the viscoelastic material experiences the same temperature cycle of the curing and the maximum temperature is below than that of the composite curing cycles. In order to overcome these limitations, novel materials for structural damping and stiffliess augmentation in composite systems should be explored.

Since carbon nanotubes (CNTs) were first discovered by Iijima [15], researchers found CNTs have astonishing mechanical properties and that they provide a way of exploiting the enormous strength associated with sheets of graphite in fiber

geometry. Both theoretical and experimental studies [16-24] have revealed that carbon nanotubes and carbon nanofiber (CNTs/Fs) with their nanoscale dimension, high aspect ratio, and off-axis elasticity, provide excellent properties for application to engineering systems. They are significantly lighter than traditional engineering materials due to their hollow shell structure. Therefore, in composites with CNTs/Fs fillers, it is expected that high damping can be achieved by taking advantage of the weak bonding and interfacial friction between individual CNTs and resin. The debonding mechanism and its effect on the enhancement for damping characteristics of CNT-filled composites have been to be investigated. Recently, the molecular dynamics (MD) methods have been used by Buldum and Lu [25] to study the interfacial sliding and rolling of carbon nanotubes. In the “stick-slip” mechanism, a nanotube first sticks and then slips suddenly when the force exerted on it is sufficiently large. Moreover, hysteresis in the plot of force versus distance shows that the energy is dissipated during the “stick-slip” motion. Development of experimental techniques such as the atomic force microscope (AFM), enable the study of friction at the nanometer scale. Holscher’s research [26] verified the “stick-slip” mechanism by using an AFM tip applied to pyrolytic graphite. Koratkar et al [22] studied vibration of epoxy thin films containing dense packing of multi-walled carbon nanotubes (MWNTs) by direct shear testing. It was reported that the thin film causes than up to 1400% increase in loss factor compared to the baseline epoxy. They found two possible mechanisms that could be responsible for the increase in the mechanical

damping: (a) the energy dissipation caused by the interfacial sliding at the nanotube-polymer interface and (b) the energy dissipation caused by the interfacial stick-slip sliding at the nanotube-nanotube interface. Nader et al [27] studied the damping properties of carbon nanotube-based epoxy composites. They found up to 700% increase in damping ratio by adding 5.0 wt% MWNTs into epoxy compared to neat epoxy. A maximum damping ratio was observed for both MWNT and single walled CNTs (SWNT) based nanocomposites. The MWNTs were found to be better reinforcements for damping enhancement. Finegan et al [28] developed an analytical model by using the elastic-viscoelastic correspondence principle to predict the damping properties of carbon nanofiber/polypropylene composites. They found that the composites with very low fiber aspect ratios have higher damping properties than those with high fiber aspect ratios. These investigations highlight the importance of studying the interfacial friction between the nanotubes and the resin in CNT-based composites in vibration damping. However, all of these researches are limited to the local molecular interaction between CNTs and resin. In order to have direct impact to the field of vibration damping, a structure or system level approach is needed to examine the damping mechanism and characteristics of CNT-based composites.

4.2. Materials and Damping test of carbon nanofiber paper-enabled nanocomposites

In this study, three kinds of fiber reinforcement have been used, which includes glass fabric, carbon fabric, and basalt fabric. To investigate the effect of

carbon nanofiber paper to damping properties of the nanocomposite, different thickness carbon nanofiber paper are applied on the surface of composite, which including 0.5mm, 1.0mm,1.5mm.

The regular composite beam without carbon nanofiber paper and the nanocomposite beam with carbon nanofiber paper were used as the specimens for damping test. For each beam, a PZT (lead zirconate titanate, a type of piezoceramic material) patch (20mm ×20mm) was attached on one side as an actuator to excite the beam and a smaller PZT patch (10mm × 8mm) was attached on the other side of the beam as a sensor to detect the beam's vibration, as shown in Figure 11.

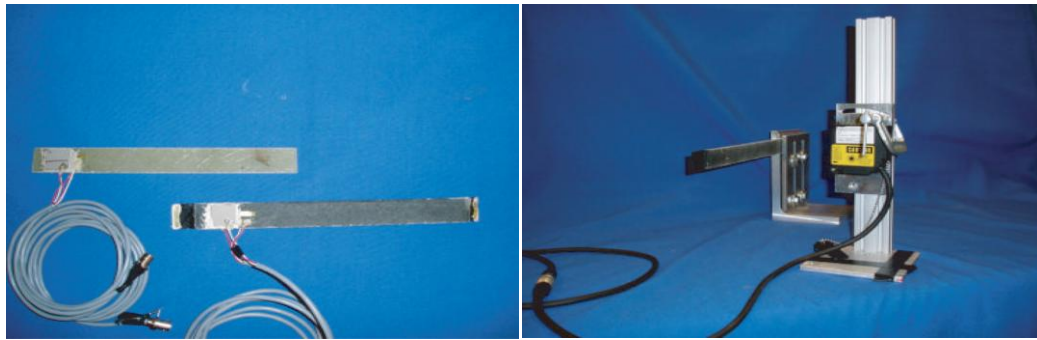


Figure 11 Regular composite beam and nanocomposite beam for damping test (left).
Experimental setup for damping test (right)

4.3. Results and Discussion

The damping test was conducted on the composite laminates with carbon nanopaper sheet as surface layer. During the damping test, sweep sinusoidal signals were used as the excitation source for the PZT actuator to obtain the frequency response of the system. The sweep sine was from 100Hz to 10,000Hz to excite the subsequent modes. The sweeping period of both sweep sins was set to 20 seconds.

The sampling frequency was set to 40 kHz. For the nanocomposite beam with carbon nanopaper sheet in different thickness as the surface layer, the time responses of both the sweep sine excitation are shown in Figure 12~14, respectively. The peak value in the sweep sine response represents resonance at a certain natural frequency. From the sweep sine responses, it can be clearly seen that the peak of first mode, second mode and third mode are significantly reduced for the nanocomposite beam, which indicates that the nanocomposite plate has improved damping property.

To estimate the damping ratio for each mode, the half-power bandwidth method was used. Corresponding to each natural frequency, there is a peak in the magnitude frequency plot of the system. 3 dB down from the peak, there are two points corresponding to half-power point. A larger frequency range between these two points means a larger damping ratio value. The damping ratio is calculated by using the following equation:

$$2\zeta = \frac{\omega_2 - \omega_1}{\omega_n} \quad (1)$$

where ω_1 , ω_2 are the frequencies corresponding to the half-power point, ω_n is the natural frequency corresponding to the peak value, and ζ is the damping ratio. All the data in the tables below is converted from the figures. Table 1 shows the damping ratio for glass fiber reinforced composites coated with different thickness of carbon nanofiber paper. The thickness of the nanopaper is 0 mm, 0.5 mm, 1 mm, and 1.5 mm, respective. For each sample, five peak values of damping ratio were shown due to resonance at the multiple nature frequencies. The higher value of the damping ratio

represents the better damping effect. Comparing the damping ratio of the sample at different frequencies, the damping ratio increased as the vibration frequency increased. At higher frequency, more friction between the carbon nanofiber and the resin were created. However, comparing the damping ratio of different sample at the same frequency, the sample coated with 1mm carbon nanofiber paper shown the best damping effect. Theoretically, the damping effect will increase as the thickness of the carbon nanofiber paper increase due to more area of contact surface. However, for the sample coated with 1.5 mm carbon nanofiber paper, damping ratio decreased due to the poor resin penetration and voids of the composites panel. Table 1-3 and the figure 12-14 show the first three modal frequencies and associated damping ratio of three different fiber reinforced composite beams. Similar results were shown for carbon and basalt fiber reinforced composites. Overall, from the damping ratio comparison, it is clear that the damping ratio of the nanocomposite beam has increased up to 300% at the 2nd mode and 3rd mode frequencies. However, there is little change in mode frequencies, which means that there is slight change in the stiffness of the composites. This demonstrates an advantage of nanocomposite over regular composite with viscoelastic layers. The regular composites with viscoelastic layers will sacrifice in reduced stiffness, though damping is improved.

Table 1 Damping ratio for glass fiber reinforced composites calculated by half-power bandwidth method

	Natural frequency (Hz)	Pure glass fiber	Pure glass fiber with 0.5mm CNF	Pure glass fiber with 1 mm CNF	Pure glass fiber with 1.5 mm CNF
1st mode	1.0254e+003	0.0096	0.0044	0.0074	0.0062
2nd mode	1.9751e+003	0.0062	0.0049	0.0096	0.0088
3rd mode	3.2129e+003	0.0059	0.0066	0.0137	0.0099
4th mode	4.6387e+003	0.0037	0.0063	0.0113	0.0092
5th mode	6.3672e+003	0.0074	0.0104	0.0073	0.0107

Table 2 Damping ratio for carbon fiber reinforced composites calculated by half-power bandwidth method

	Natural frequency (Hz)	Pure carbon fabric	Pure carbon with 0.5mm CNF	Pure carbon with 1 mm CNF	Pure carbon with 1.5 mm CNF
1st mode	1.5112e+003	0.0057	0.0034	0.0055	0.0089
2nd mode	2.8101e+003	0.0065	0.0025	0.0064	0.0061
3rd mode	4.5239e+003	0.0076	0.0052	0.0074	0.008
4th mode			0.0064	0.0071	0.007

Table 3 Damping ratio for basalt fiber reinforced composites calculated by half-power bandwidth method

	Natural frequency (Hz)	Pure basalt fiber	Pure basalt fiber with 0.5mm CNF	Pure basalt fiber with 1 mm CNF	Pure basalt fiber with 1.5 mm CNF
1st mode	1.0522e+003	0.0097	0.0078	0.0097	
2nd mode	2.0483e+003	0.0138	0.0078	0.0081	0.0066
3rd mode	3.2837e+003	0.0078	0.0073	0.0081	0.0082
4th mode	4.8022e+003	0.0087	0.0038	0.0081	0.0044

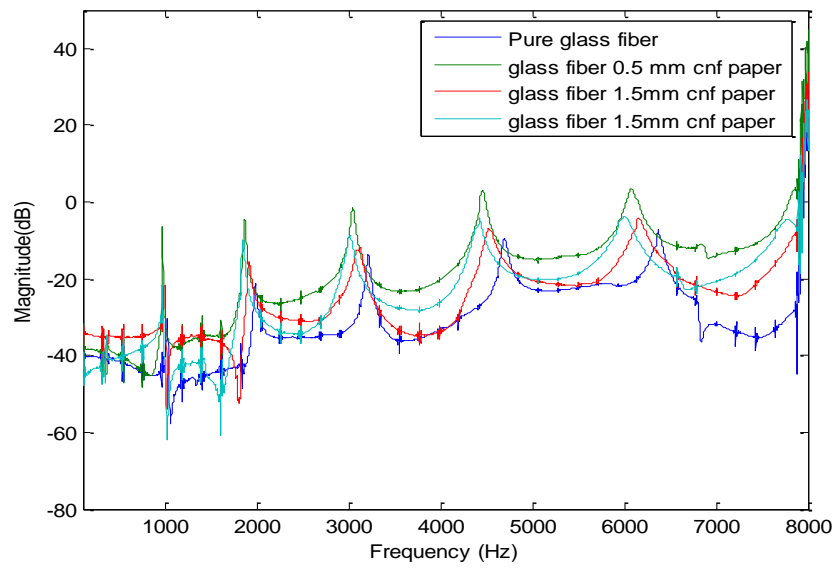


Figure 12 Frequency response for the glass fiber reinforced composite beam with different thickness of carbon nanofiber paper as surface layer

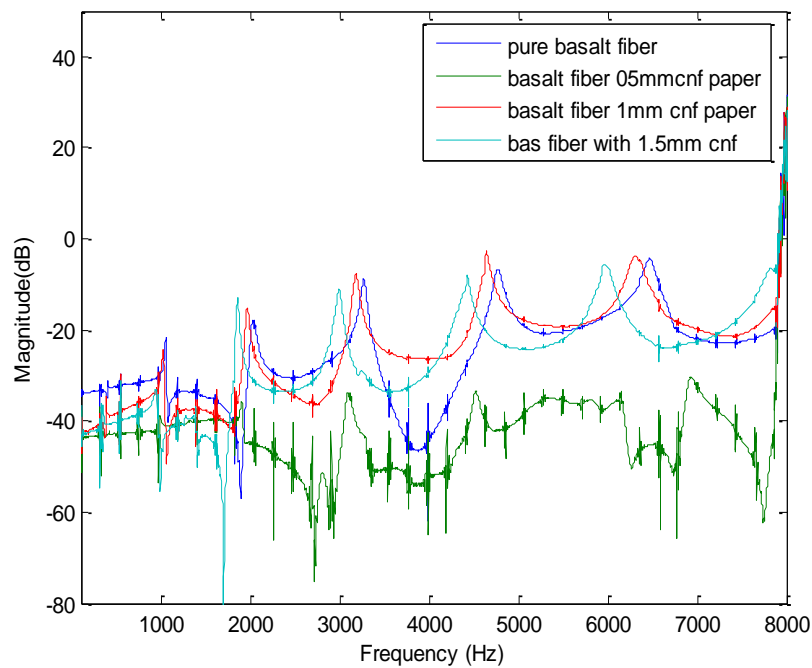


Figure 13 Frequency response for the basalt fiber reinforced composite beam with different thickness of carbon nanofiber paper as surface layer

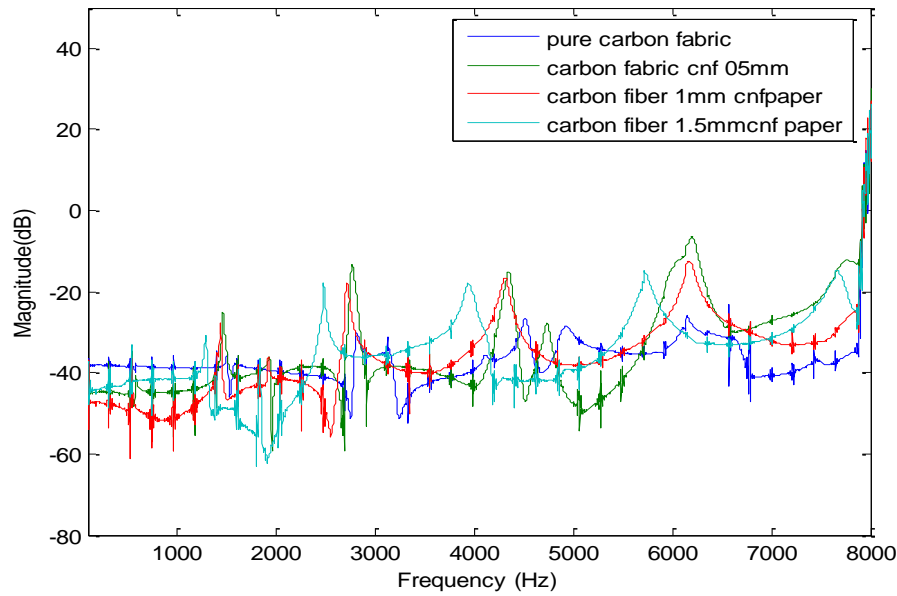


Figure 14 Frequency response for the carbon fiber reinforced composite beam with different thickness of carbon nanofiber paper as surface layer

4.4. Summary

The damping properties of the composites coated with carbon nanofiber paper were investigated. The damping tests show up to 300% increase of the damping ratios at high frequencies and subtle change in stiffness of composite laminates due to the incorporation of carbon nanofiber paper. The friction between the surface of the carbon nanofiber and the resin is expected to be responsible for the energy dissipation in the nanocomposites. Due to the large surface area of carbon nanofiber, significant enhancement of vibrational damping was achieved.

CHAPTER FIVE: TRIBOLOGICAL PROPERTIES OF THE NANOCOMPOSITES COATED WITH HYBRID NANOFIBER PAPER

5.1. Introduction

The smooth surface of blades can be greatly damaged by the erosion of the wind carrying large amounts of sand and water droplets and which significantly deteriorates aerodynamic performance and reduces machine power output. The potential for erosion depends on the force at which the particulate matter impacts the airfoil which related to geometric shapes and the relative velocities of both the airfoil and the impacting particle. Wind speed and rotational speed of the blade determine impact velocity. According to the research of van Rooij and Timmer [29], the effect of roughness on a blade's aerodynamic performance depends on the geometric design of the blade, such that a blade may be adapted to induce minimal energy loss. However, surface roughness changes during operation due to erosion, and will typically always lead to unpredicted energy losses. So, it's significant to develop a coating material to improve the impact wear properties of Blades. In this research, hybrid nanopapers were develop and incorporated on the surface of composite panels.

5.2. Materials and Test Method

Six groups of sample have been prepared, which are shown in Table 4. Different types of Nanoparticles are added into carbon nanopaper to from the hybrid nanopaper. To evaluate many samples in a short amount of time, pin-on-plate testing

was performed on a tribometer manufactured by Microphotonics (Irvine, CA). The schematic picture below (Figure 15) shows pin-on-plate testing for tribology. Basically, in pin-on-plate mode, the pin (or ball) is loaded with dead weights and pressed against the plate (coated laminate) that is then spun at a given speed. A flat or a sphere shaped indenter is loaded on to the test sample with a precisely known force. The indenter (a pin or a ball) is mounted on a stiff lever, designed as a frictionless force transducer. As the disk is rotated, resulting frictional forces acting between the pin and the disk are measured by very small deflections of the arm using a strain gage sensor. Other testing conditions used were 200 rpm, load of 10N, radius 5 mm, and test time of up to 20 minutes for promising candidates. The ball diameter is 6mm, and the revolution is 4000. Testing was completed with these conditions at room temperature. During the test, the instrument gives real-time outputs of frictional force, coefficient of friction (COF), temperature of the pin/ball, wear depth, and wear factor for the sample.

Table 4 Composition of Different Groups of Samples

Sample(g)	Carbon Nanofiber(CNF)	Graphite(Gr)	Short Carbon Fiber(SCF)	AL ₂ O ₃	TiO ₂
G1	2.4	0	0	0	0
G2	1.8	0.6	0	0	0
G3	1.8	0	0.6	0	0
G4	1.8	0.3	0.3	0	0
G5	1.8	0	0	0.3	0.3
G6	1.8	0.15	0.15	0.15	0.15

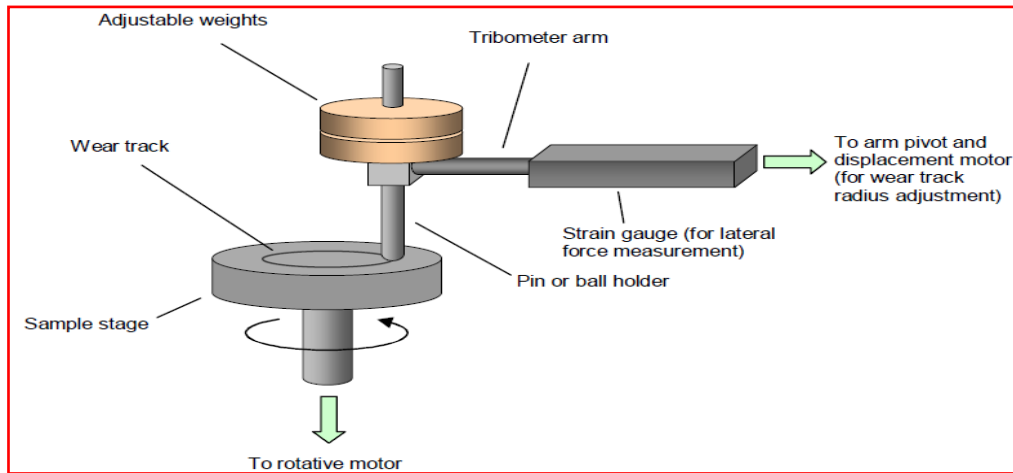


Figure 15 The schematic of Tribometer (from Nanovea Inc.)

5.3. Results and Discussion

SEM images of the carbon nanopaper with different kinds of nanoparticles are showed in Figure 16~20. In figure 16 (left), CNFs were well dispersed without any clusters which indicate that the coating layers are homogenous. Because of high strength and toughness, carbon nanofiber can act as micro-crack reducer. Once the

crack is created, the tough carbon nanofiber can stop the crack propagation through the whole composites. In figure 16 (right), the layered structure graphite flakes were evenly distributed into CNFs. Because of layered structure, graphite flakes has self-lubricant ability which can act as friction reducer to decrease the damage on the polymer surface. In figure 17 (left), micron sized short carbon fiber were incorporated with CNFs. Short carbon fiber has good compressive strength and creep resistance, which can absorb the energy and reduce the damage. Besides, it acts as a frame of the whole matrix system which greatly improves the stress transfer of the composites. In figure 18, Nano- Al_2O_3 and Nano- TiO_2 were dispersed on the surface of CNFs. The surface hardness can be significantly increased by adding those ceramic nanoparticles. They also act as a spacer to protect matrix by so called “rolling effect”, then reduce friction coefficient. To investigate the synergistic effect of those particles, all particles mentioned above were mixed together with certain composition (table 4). Figure 19, 20 are the SEM images of coating materials after resin infusion, which shown Good adhesion between resin and nanoparticles.

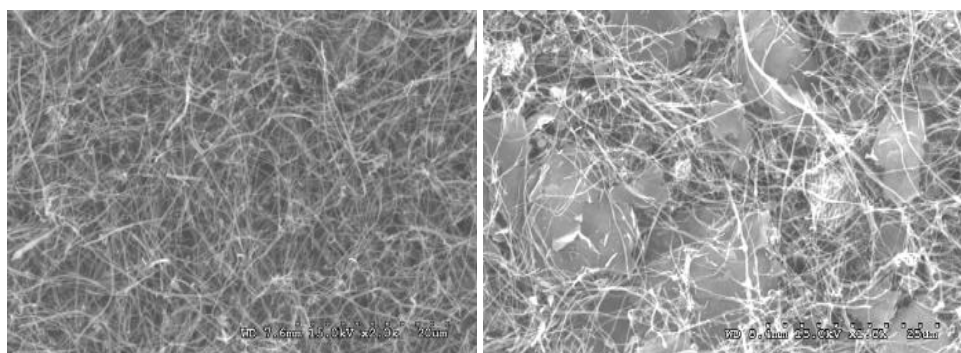


Figure 16 SEM images of pure CNF (left) and CNF with graphite flakes (right)

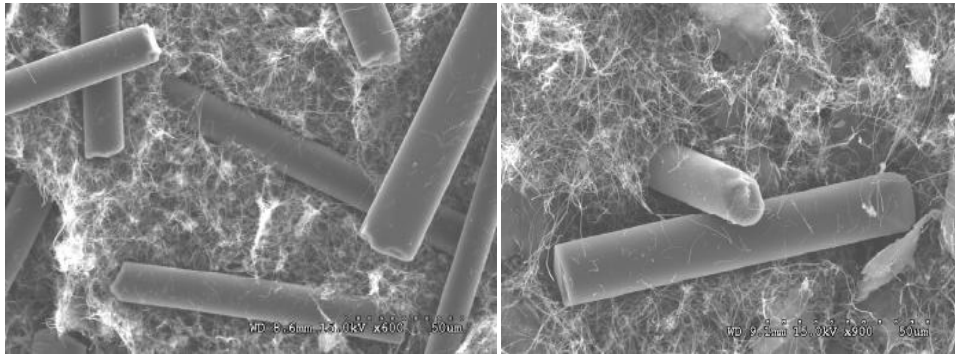


Figure 17 SEM images of CNF with SCFs (left) and CNF with graphite flakes, SCF (right)

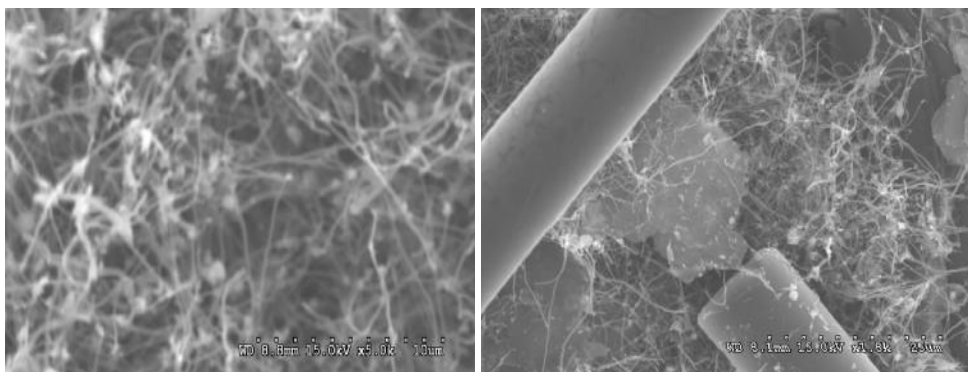


Figure 18 SEM images of CNF with Al_2O_3 and TiO_2 (left), and CNF with all above nanoparticles (right)

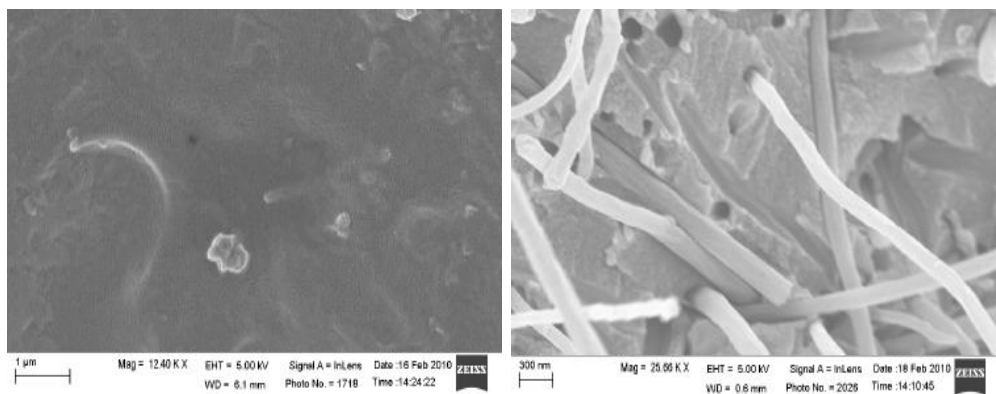


Figure 19 SEM images of pure resin (left) and CNF with resin (right)

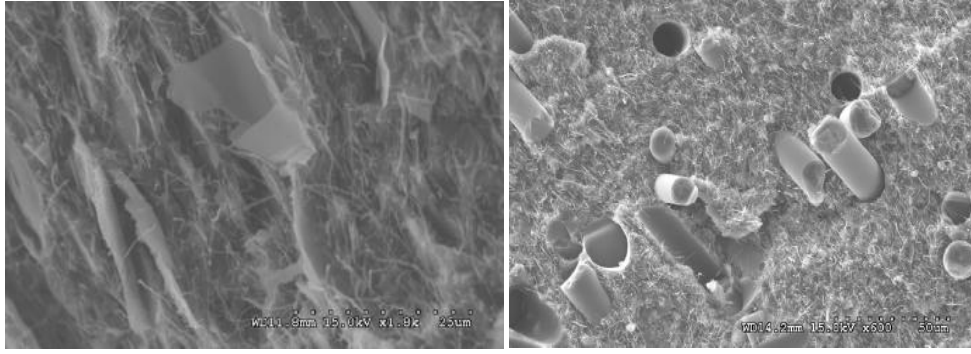


Figure 20 SEM images of CNF and graphite flakes with resin (left), and CNF, SCF with resin (right)

The coefficient of friction and ware rate results from the tribometer testing for six groups of sample are shown in Figure 22. The ware rate W_s of the specimens was calculated according to the following equation:

$$W_s = \frac{\Delta m}{\rho \times F_n \times L} \quad (\text{mm}^3/\text{Nm}) \quad (2)$$

where Δm is the specimen's mass loss, ρ is the density of the specimen, F_n is the normal load applied on the specimen during sliding, L is the total sliding distance.

The control is the carbon nanofiber paper used as a coating without any additives. As

you can see, G6 exhibit the lowest coefficient of friction (COF), which is due to the

synergistic effect of different particles. Great combination of mechanical properties of

those nanoparticles resulted in better tribological performance of nanocomposite.

COF is one of the important performance parameter for friction and wear applications;

and it has shown to be a very good indicator of the wear of a material in part-on-part

wear applications. It is not always the case, however usually a lower COF material in

this test is expected to better tribological performance. This is related to the way of

the instrument calculates the COF value. The torque of the arm is used in this

calculation. Even COF is a material property; it varies greatly based on how the measurement is performed. G2 exhibit the lowest wear rate, which is due to the self-lubricant of graphite particles. As we see, when the graphite and short carbon fiber were added into the CNF paper separately, samples show both low COF and low wear rate. But, G4 shows the highest wear rate, this is probably due to the poor quality of the sample. Figure 21 shows the SEM surface morphology of G2 and G4. The SEM image of sample G2 shown very little scratch, and the surface was pretty smooth which indicated the great wear resistance of the composites. This is contribution of the synergistic effect of tough carbon nanofiber and the self-lubricant graphite. However, the SEM image of sample G4, with highest wear rate, shown the great damage on the surface. The micron-sized short carbon fiber was ploughed out and the resin was scrunch of from the surface. Lots of voids can be seen, which indicated the poor adhesion between the resin and the nanoparticles.

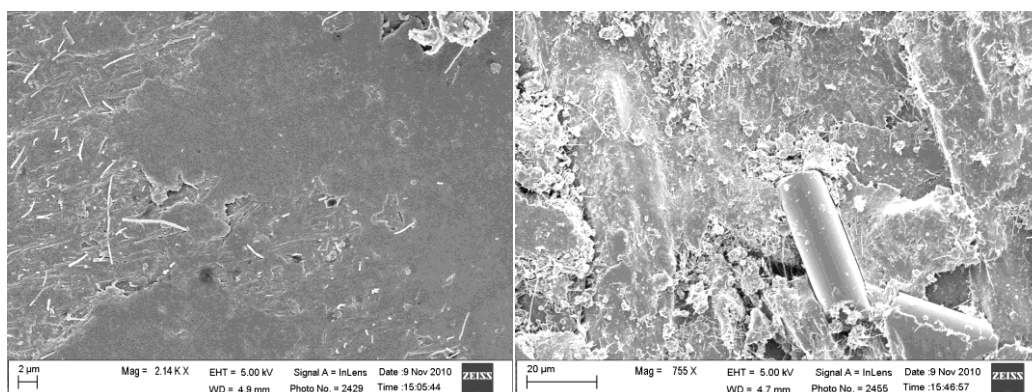


Figure 21 SEM image for G2 (left) and G4 (right) for tribology test

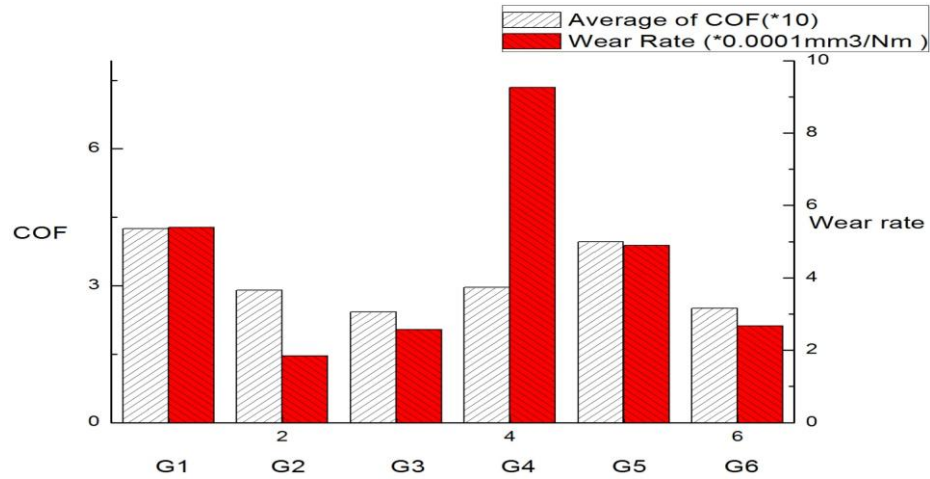


Figure 22 Summary of Average COF and Wear rate

5.4. Summary

In this study, multifunctional carbon nanofiber (CNF) paper was developed and optimized as a platform material. Carbon nanofiber paper was integrated into polymer composites through the VARTM process, which is compatible with the manufacturing process of wind turbine blades. This CNF paper-based nanocomposite has good impact-friction resistance with the wear rate as low as $1.78 \times 10^{-4} \text{ mm}^3/\text{Nm}$. Carbon nanofiber paper can be used for sand erosion mitigation of wind turbines by incorporating other nanoparticles, which could provide effective protection for wind turbines installed in desert.

CHAPTER SIX: ELECTRICAL PROPERTIES OF NANOPAPER AND NANOCOMPOSITES AND THEIR APPLICATIONS

Carbon nanofibers with extremely high aspect ratios possess high electrical conductivity. Combined with low density, carbon nanofibers have a wide range of applications, such as electromagnetic interference (EMI) shielding, lightning strike protection, as well as electro-actuating the shape memory polymer composites. In this study, porous, flexible, nonwoven papers of nanofibers are first prepared by the papermaking process. Carbon nano-films are fabricated by incorporating the epoxy into carbon nanopapers. To increase the conductivity of the carbon nanofiber papers, carbon nanofiber was modified with nickel nanostrands and the papers were fabricated by the papermaking process. The papers then act as a surface layer on the composite panels or carbon nano-films. The conductivity and shielding effectiveness (SE) of carbon nanopapers/nanofilms and the lightning strike tolerance, shape memory effect (SME) on these composite panels are measured in this study, respectively. The test results showed a good correlation between the EMI shielding/lightning strike tolerance/SME and the surface electrical conductivity.

6.1. Introduction

6.1.1. CNF-Based Nanocomposite for EMI shielding

Electromagnetic interference (EMI) has become a critical issue in the last several years with the development and advancement of electrical devices. The interference can cause detrimental damage to the performance of televisions and

mobile phones, computers, underground transformers, and various medical, military, and aircraft systems [30-44].

The shielding of the electromagnetic radiation is an extremely important approach in order to allow electronic devices to function properly. There are three main mechanisms of shielding: reflections, absorptions, and multiple reflections. For reflections to act as the shielding mechanism, mobile carriers such as electrons or holes must be present to interact with the electromagnetic field. Because of the presence of the mobile carriers, the shield tends to be electrically conductive. In order for absorption to block radiation, the shield needs to have electric and/or magnetic dipoles that can interact with the electromagnetic field. Absorption loss increases against frequency, while reflection loss shows the opposite trend. Multiple reflections require large surface areas or interface areas within the shield and are usually present in porous and foam materials, where there are many interfaces present [30, 33, 35-40].

The shielding effectiveness (SE) of the material depends on the skin effect. At high frequencies, electromagnetic radiation will only interact with the shallow surface of the material. When the depth of the field drops to $1/e$ of the incident wave, the skin depth (δ) is given by

$$\delta = \frac{1}{\sqrt{\pi f \mu \sigma}} \quad (3)$$

where f (Hz) is the frequency, μ is the magnetic permeability, and σ is the electrical conductivity in $\Omega^{-1}\text{m}^{-1}$. Therefore, the skin depth decreases with increasing frequency, permeability, and conductivity [30, 33, 40].

The extremely high aspect ratios (length/diameter) of carbon nanofibers allow for multiple reflections and absorptions to dominate the SE. They have similar shielding properties as metals but with significantly lower loading capabilities. This can be translated into a lower weight, a lower cost, and more design flexibility [30, 39, 43-48]. The aim of this study is to investigate and report the SE performance of various carbon nanofiber papers and the methods to increase the SE of the carbon nanofiber papers.

6.1.2. CNF-Based Nanocomposite for lightning strike protection

Aircrafts often trigger lightning strikes when flying through a heavily charged region of a cloud. Usually, lightning strikes occur in obtrusive regions such as the nose or wing tips. The airplane then flies through the lightning flash, which reattaches itself to the fuselage at other locations while the airplane is in the electric "circuit" between the regions of opposite polarity. The current travels through the conductive exterior skin of the aircraft and exits at the other end of the airplane such as the tail. Therefore, the principle of lightning strike protection is to provide a safe conductive path on the exterior skin. With highly conductive skins, most of the lightning current remains on the exterior skin, without serious damage to the air craft. Most of aircraft skins are primarily made of aluminum, a very good electrical conductor [49]. Modern aircrafts are made of advanced composite materials, which are significantly less conductive than aluminum. Being struck by lightning, the composites are damaged quickly due to the temperature rise from the resistive heating and serious degradation

at the lightning attachment points. Hence, it is necessary to develop advanced composites with high electrical conductivity.

Due to the high electrical conductivity, Carbon nanotubes (CNTs) and carbon nanofibers (CNFs) are highly sought-after candidate materials to replace traditional metallic materials for lightning strike protection of aircrafts. Although various methods have been used to disperse CNTs or CNFs into polymers, the resulting nanocomposites could not achieve high electrical conductivity to meet the requirements of lightning strike protection. Another issue is that the high loading level required to achieve high conductivity introduces processing challenges such as heavy re-agglomeration and high viscosity [50]. In addition, the increase of conductivity is limited beyond their percolation threshold due to the lack of effective connection among nano-fillers. Carbon nanofiber papers (CNFP) have been developed to achieve high loading level of nanoparticles on the skin surface of composites through vacuum-assisted resin transfer molding process [51, 52]. In order to meet the requirements of lightning strike protection of composites, the electrical pathway of CNFP was modified with nickel nanostrands in the nanofiber network structures, in which nickel nanostrands could efficiently bridge individual CNFs.

6.2. Electrical property measurement of nanopaper and nanocomposites

The electrical resistivity of the CNFP and composite panels were measured with the SIGNATONE QUADPRO system, incorporated with a four-point cylindrical probe. The four-point probe apparatus has four probes in a straight line with an equal

inter-probe spacing of 1.56 mm.

The electrical resistivity of the neat SMP and their hybrid filler filled composites were first measured by a standard four-probe method (SIGNATONE QUADPRO system) using a precision multi-meter incorporated with a four-point cylindrical probe. The apparatus has four probes in a straight line with an equal inter-probe spacing of 1.56 mm. The radius of the probe needle is 100 μm . A constant current passes through two outer probes and an output voltage is measured across the inner probes with the voltmeter. The electrical resistance was calculated as:

$$R_s = 4.5 \frac{V}{I} \quad (4)$$

where R_s is the electrical resistance, V is the voltage applied on the outer two probes, and I is the electrical current passed through inner two probes.

Furthermore, the electrical resistivity (ρ) and conductivity (σ) were calculated as:

$$\rho = R_s \frac{A}{l} \text{ and } \sigma = \frac{1}{\rho} \quad (5)$$

where A and l are the cross-sectional area and distance between two electrodes, respectively.

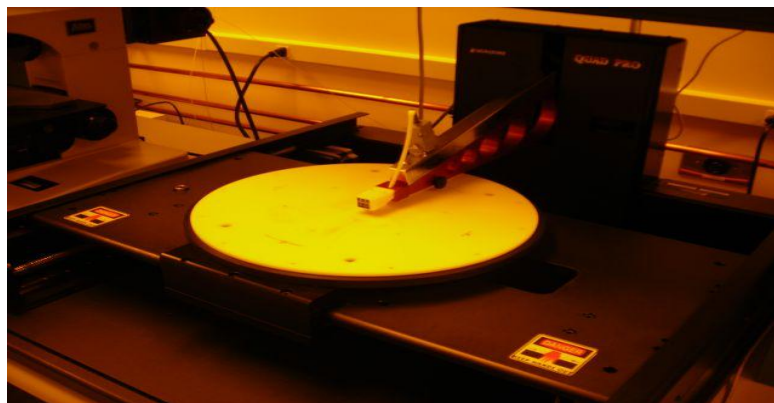


Figure 23 Signatone Quad Pro system used for measuring sheet resistivity. Sample is placed under head and the head moves down and comes into contact with sample.

6.3. EMI shielding application of CNF-based nanocomposites

6.3.1. Materials and Experiment methods

Pyrograf-IIITM carbon nanofibers (PR-PS-25) were supplied from Applied Sciences Inc., Cedarville, Ohio. The nanofibers have diameter of 100-150 nm and length of 30-100 μm . BYK surfactant provided by NanoLab (Newton, MA) is used to acquire a stable dispersion of the carbon nanofibers in the deionized water. The epoxy, supplied from Eastman Chemical Company was used as the matrix. The epoxy resin was mixed with the hardener at a weight ratio of 100:26.5. The curing temperature is 177 $^{\circ}\text{C}$ and curing time is 2 hrs. The specific properties of the fibers are shown in Table 5.

Table 5 Properties of carbon nanofibers

Sample Name	Nanofiber Type	Nanofiber Grade	Diameter (nm)	Nanofiber Content (g)
S1	PR-19	PS	100-200	1.2
S2	PR-24	PS	100-200	1.2
S3	PR-24	OX	100-200	1.2
S4	PR-25	PS	100-200	1.2
S5	PR-25	HHT	100-200	1.2
S6	PR-25&10 % nickel nanostrand	HHT	100-200	1.2
S7	PR-25&20 % nickel nanostrand	HHT	100-200	1.2

Note: PS: Cleaned fiber. HHT: high-temperature heat treated. OX: Oxide.

The fabrication of hybrid paper of CNFs and nickel nanostrands is similar to the procedures of making pure CNFs paper. However, there still some difference. The chemical bonds between nickel atoms will be destroyed when the nickel nanostrands were sonicated, because the bond energy between nickel nanostrands is smaller than the energy provided by sonicator. So water boiling method was used for the dispersion of nickel nanostrands. The nickel nanostrands were put into the deionized water by weight fraction of 10% and 20%, it was boiled for 1 hour. Mixed these two solutions together, boiled for another 1hour. When it cooled down, and then filtered the solution. After that the nanopaper was put into oven at temperature of 120°C for two hours. Then the hybrid papers were infused with epoxy resin by RTM method and cured in 2 hours at temperature of 177°C.

EMI Shielding Effectiveness (SE) was measured using an Agilent N5230A

PNA-L Network Analyzer and waveguides as shown in Figure 24. This test setup was calibrated to the reference planes at the coax-waveguide adaptors using Agilent 85052D 3.5mm SOLT calibration standards. This measurement was performed between 5.38 and 8.18 GHz with an IF bandwidth of 3 kHz. The SE is measured in terms of decibels (dB) and is expressed as

$$SE = 10 \log \frac{P_1}{P_2} \quad (6)$$

where P_1 and P_2 are the power of incident and transmitted waves, respectively.



Figure 24 EMI SE measurement setup. Sample is placed in between two waveguides.

6.3.2. Electrical conductivity results of CNFs-based thin film

The electrical conductivities of the samples are shown in Table 6. Since carbon nanofibers have excellent electrical properties, it was anticipated that the carbon paper samples would provide desired conductivity, which can be seen in Table 2. Pr25hht shows better conductivity values than that of PR-19 and PR-24. High heat treated caused a dramatic increase in the conductivity because the degree of crystalline order was allowed to increase. A significant increase of the conductivity was observed by using nickel nanostrand to modify carbon nanofiber. The carbon

nanofiber is well- dispersed, and the conductivity of S5 is better than that of S1~S4.

When the epoxy resin was incorporated into the paper, the conductivity of the sample increases compared with the corresponding paper. This is due to the highly entangled carbon nanofibers become more compact caused by the shrinkage of the epoxy resin, such as S2 and S5. However, in some cases, it was found that the conductivity decreased after incorporated into the resin, probably this is due to too much resin was used, we observed there is a layer which only contained the resin on the top surface of the nanopaper. Due to the lower dielectric constant of resin compared with carbon nanofiber, therefore, the conductivity decreases in those cases.

Table 6 Electrical conductivity of carbon nanofiber papers

Sample Name	Thickness(mm)	Conductivity(S/m)
S1	0.458	28.1
S1 with epoxy(ep)	0.997	10.0
S2	0.725	1.40
S2 with epoxy	0.400	20.1
S3	0.489	3.10
S3 with epoxy	0.467	2.15
S4	1.088	1.10
S4 with epoxy	0.665	7.20
S5	0.683	69.9
S5 with epoxy	0.686	78.8
S6	0.400	127
S6 with epoxy	0.740	32.8
S7	0.420	136
S7 with epoxy	1.000	60.2

6.3.3. EMI SE Results

The effectiveness of shielding is extremely important in protecting electrical equipment in the airplane and also allowing electronics devices to operate continuously under the lightning strike conditions. An SE value ranging from 20 to 30 dB is desirable for many commercial applications. For instance, 20 dB SE represents only 1% energy transfer through the shielding material. The higher the SE value, the less energy passes through the material and creates more effective shielding [49-51].

The EMI SE was tested between 5.38 and 8.18 GHz. Each sample was tested five times and 12801 data points were collected for each test. Very consistent measurement results were observed in all the tests. The measured SE ranges approximately from 25 to 52 dB as shown in Figure 25. It is observed that the SE of the carbon nanofiber papers exceeds the requirement of commercial applications. As seen in figure 25 a), S2 exhibits the lowest SE among all the samples due to the poor dispersion of nanofibers, which decreases the specific surface area. S5, S6, and S7 have the best SE performance. This is because the heat treatment of the nanofibers increases the degree of crystalline order. As a result, the electrical conductivity is increased. However, when S6 is mixed with resin, SE drops dramatically as shown in figure 21b. This decrease of the conductivity is very likely caused by the large amount of resin covered on its surface. It is noted that the S7 with resin exhibits the highest value of shielding effectiveness, in which the carbon nanofibers were modified with nickel nanostrands. This phenomenon shows that the nickel nanostrands have a positive effect on the EMI shielding. It can provide a practical method to obtain better EMI effect through adding nickel nanostrands. Further detail work will be conducted in this direction. By comparing the measurement results from the electrical conductivity and shielding effectiveness tests, a clear correlation between the two can be observed.

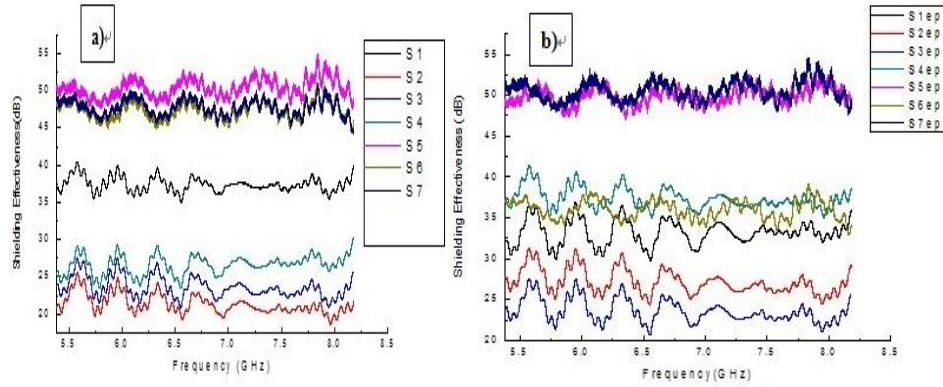


Figure 25 EMI shielding of carbon nanofiber samples, a) for the pure nanofiber papers, b) for the nanofiber papers with epoxy resin

6.4. Lightning strike protection application of CNF-based nanocomposites

6.4.1. Materials and experiment methods

Same procedures as above are used to make the 18"×18" papers with different weight ratio of nickel nanostrands. Three different papers labeled as CNFP-1, CNFP-2 and CNFP-3 were fabricated from the papermaking process, as shown in Table 7. Then the hybrid papers were infused with epoxy resin by RTM method and cured in 2 hours at temperature of 170°C.

Table 7 Compositions and structure of CNFPs with large size of 18"×18"

CNFP identification	PR-PS-25 carbon nanofibers (g)	Nickel nanostrands (g)	CNFP structure
CNFP-1	9.75	9.75	Monolayer paper with binder
CNFP-2	6.94	19.55	Bi-layer paper with latex binder
CNFP-3	6.94	19.55	Monolayer without binder

6.4.2. Electrical conductivity and Lightning strike tests

The electrical test procedures are the same as 3.1.1. For the lightning strike

tests, three 18"×18" panels were subjected to a Zone 2A (swept stroke) direct effects attachment using a peak current amplitude of 100 kA. For the Zone 2A test, all the areas of the aircraft surfaces, where a subsequent return stroke is likely to be swept with a low expectation of flash hang on. During lightning strike tests, the composite panels were positioned with carbon nanofiber paper surface facing the lightning simulation hardware. The entire panel was heavily grounded along its perimeter to direct the current path. The experimental test rig was set up as shown in Figure26.



Figure 26 Experimental rig for lightning strike tests

Table 8 Resistivity of top surface of CNFPs and composite panels

CNFP Identification	Conductivity (S/m)	Resistance (Ω /sq)	Panel Identification	Conductivity (S/m)	Resistance (Ω /sq)
CNFP-1	3.33E+01	116.40	CP-CNFP-1	2.22E+02	17.34
CNFP-2	9.09E+03	0.42	CP-CNFP-2	3.10E+04	0.12
CNFP-3	8.33E+03	0.42	CP-CNFP-3	3.41E+04	0.10

6.4.3. Damage characterization of composite panels after lightning strike

Three large size composite panels with 18" ×18" (CP-CNFP-1, CP-CNFP-2, and CP-CNFP-3) were tested with lightning strike. Figure 27 shows the surface damage of these composite panels after lightning strike. Clearly, CP-CNFP-1 had the

largest damaged area, where ~5.9% area of the paper was damaged. The carbon fiber mats underneath the nanofiber paper was obviously damaged. However, only ~3.3% and ~1% area of the paper were damaged in the CP-CNFP-2 and the CP-CNFP-3, respectively.

An ultrasonic testing was conducted on the composite panels in order to further confirm the damages caused by lightning strike. In the ultrasonic testing, the thickness readings were taken from the back of the panels to determine the thickness of the undamaged laminate. The thickness distribution of the undamaged laminate is shown in Figure 28. The 3D graphs clearly show that the CP-CNFP-1 had the most seriously damaged area and depth. It had a damaged area of 17 grids and each grid is 2.54 cm \times 2.54 cm. However, the CP-CNFP-2 and the CP-CNFP-3 had a damaged area of 10 and 7 grids, respectively. However, the CP-CNFP-2 had its damaged depth in the range of 0.15–0.18 cm. The CP-CNFP-3 had their damaged depth in the range of 0.08–0.10 cm. Based on the original thickness of the panels of 0.25 cm, the CP-CNFP-1 had its depth of 60–70 % damaged on the area of 110 cm². The CP-CNFP-3 was damaged in 30–40% of its thickness on the area of 45 cm².

During the lightning strike, the flow of lightning current may degrade the mechanical properties of composite structures. Starting in the middle of the damaged section, 2.54 cm strips were cut for the flexural testing along the same grid pattern used to map the panels in the ultrasonic testing. The flexural testing was conducted with the damaged side of the panel in tension. The specimen first tested was from the

middle of the damaged area. Using the ultrasonic testing map as guidance, several other specimens per panel were selected from the damaged section out to undamaged panel. Only the specimen located on Column 8 had a slightly smaller flexural strength and modulus than the average values for the CP-CNFP-3, as shown in Table 9. Clearly, the lightning strike had no serious degradation to the mechanical properties and structural integrity of the CP-CNFP-3. Similar results were obtained for the CP-CNFP-2. However, the flexural strength and modulus had seriously decreased for the CP-CNFP-1. The flexural strength was decreased to 38.4% for the specimen located on Column 8. It is clear that the CNFP-3 could efficiently protect the composite panel during lightning strike due to its highly conductive surface. The lightning currents could spread out sufficiently so as not to produce a high temperature rise on the CP-CNFP-3. The CNFP-1 failed the lightning strike test due to its low conductivity. The binder was found to slightly lower the lightning tolerance and flexural strength although the CP-CNFP-2 had similar electrical resistivity.

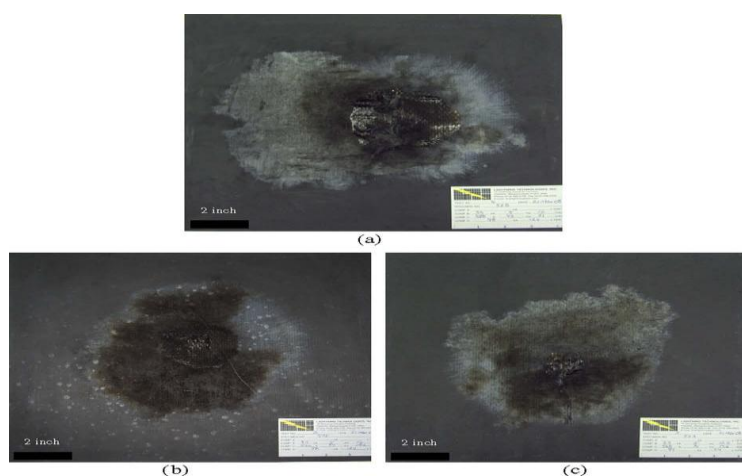


Figure 27 Surface damages of composite panels: (a) CP-CNFP-1; (b) CP-CNFP-2; (c) CP-CNFP-3.

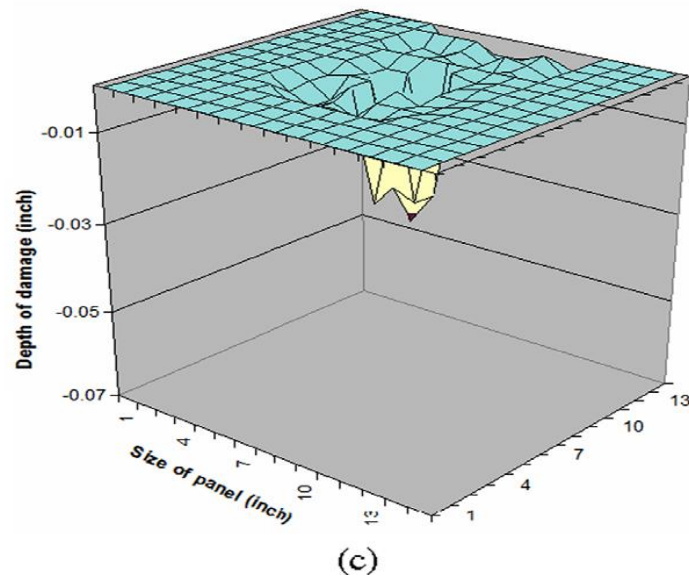
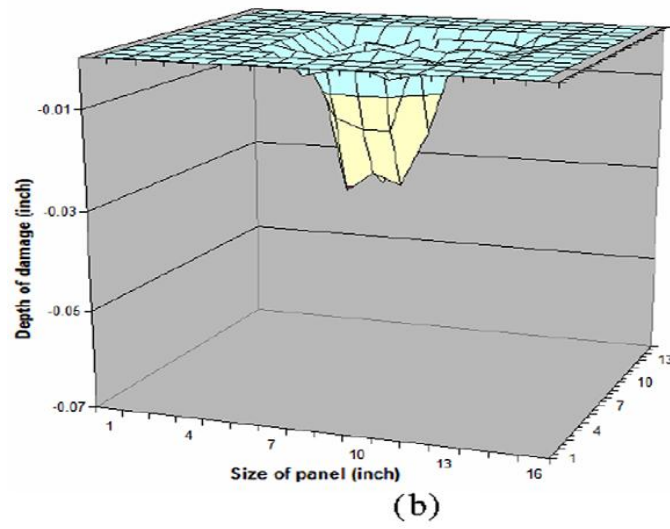
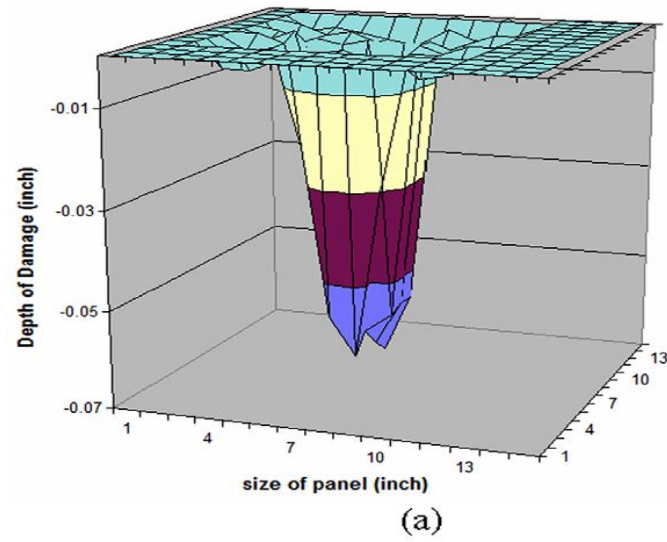


Figure 28 Damage area and thickness of composite panels after lightning strike test: (a) CP-CNFP-1; (b) CP-CNFP-2; (c) CP-CNFP-3.

Table 9 Flexural testing results of LS-CP-S-1, LS-CP-S-1 and LS-CP-S-1

LS-CP-S-1					
SAMPLE I.D.	WIDTH (in)	DEPTH (in)	FLEXURAL STRENGTH (psi)	FLEXURAL MODULUS (psi)	LOCATION OF SAMPLE TESTED
F1	0.9640	0.0935	43,360	4.496E+06	Column 8
F2	0.9010	0.0910	46,640	5.191E+06	Column 9
F4	0.9025	0.0935	44,920	4.693E+06	Column 11
F6	0.9235	0.0925	46,245	4.911E+06	Column 13
LS-CP-S-2					
F1	0.9710	0.0980	15,585	3.605E+06	Column 8
F2	0.8800	0.0995	34,365	3.610E+06	Column 9
F4	0.9355	0.0985	40,714	4.044E+06	Column 11
F6	0.9130	0.0980	40,576	4.127E+06	Column 13
F8	0.8905	0.0980	40,743	4.256E+06	Column 15
LS-CP-S-3					
F1	0.8490	0.0960	43,128	4.617E+06	Column 8
F2	0.9165	0.0975	41,836	4.408E+06	Column 9
F4	0.9000	0.0960	45,327	4.746E+06	Column 11
F6	0.8665	0.0955	46,704	5.037E+06	Column 13
F8	0.9645	0.0950	46,457	4.943E+06	Column 15

6.5. Summary

In this study, porous, flexible, nonwoven papers of nanofibers are first prepared by the papermaking process. Five different types of nanofiber are used to make the papers. Carbon nanofilms are fabricated by adding the epoxy into carbon nanopapers. In order To increase the conductivity of the carbon nanofiber papers, the nickel nanostrands were used to modify the carbon nanofiber. Similar procedures are used to make the 18'' × 18'' papers with different weight ratio of nickel nanostrands. The papers act as a surface layer on the composite panels. The conductivity and shielding effectiveness (SE) of carbon nanopapers/nanofilm and the lightning strike

tolerance on these composite panels are measured in this research. The best result was observed in the case of PR-25 (HHT) nanofiber with load of 20 wt% nickel nanostrands, which exhibits a conductivity of 136 S/m and has the highest SE value in the 5.38 GHz to 8.18 GHz range. Furthermore, a method of applying a temporary surface barrier on the paper was developed to prevent the infused resin from breaching the paper's surface. This minimized the resin on the composite's surface and allowed its surface conductivity to remain high. There was a relationship between EMI shielding/lightning protection and the electric conductivity of composite panel surfaces. Therefore, the conductivity properties of CNFP played a determined role in the EMI shielding and the lightning protection of composite panels. By adding nickel nanostrand into the carbon nanofiber papers, the higher SE value and lightning strike tolerance were obtained which provide another good choice for EMI shielding application and lightning protection of the aircraft.

CHAPTER SEVEN: ELECTRO ACTUATION OF CARBON NANOFIBER-BASED SHAPE MEMORY POLYMER NANOCOMPOSITES

7.1. Introduction

Shape memory polymers (SMPs) are a kind of smart material which is capable to be deformed and fixed into a temporary shape and recover the original permanent shape on exposure of external stimuli such as heat, electricity, light etc. Recently, shape memory polymers (SMPs) have gained lots of attraction due to their outstanding properties. Compare to traditional shape memory alloy materials, SMPs process many advantages such as easy to fabricate, high elastic deformation capability and tailored recovery temperature in comparison with traditional shape memory alloy materials [53-55]. SMPs have wide applications, such as textile and clothing manufacturing, biomedical engineering, aerospace engineering, and so on [55-58]. Same as the other types of shape memory materials, with application domain of SMPs growing explored, direct temperature heating is almost the only actuation method of shape recovery. However, lots of researches have been carried out on the actuation for SMPs and SMP composites. Different kinds of actuation methods are explored including infrared light heating [57], laser light heating [58], electrical resistive heating [59], magnetic field [60,61] or solvent [62-64].

Significant achievements have been made for SMP composite so far and shape recovery actuation could be achieved by electrically resistive heating. However,

almost all previous works are just simply blended conductive filler into pure polymer. This approach will arise many problems once the polymer is used as matrix for fiber reinforced polymer composites and manufacture by resin transfer molding (RTM) processing. On this motivation, a unique technique of making conductive CNFs into paper form has been explored for functional materials [65, 66]. High-quality self-assembled CNF papers are produced by filtrating on hydrophilic or hydrophobic membrane. It's well known that CNF nanocomposites can significantly improve the mechanical performance of polymer, ceramic and teal matrix with a small amount of CNFs. Meanwhile, based on the excellent electrical properties of pure CNF paper, it is expected that the composites incorporated with CNF paper will possess an outstanding electrical properties.

The salient features of SMPs have made them promising in a growing number of applications. For examples, some SMPs can be used to develop biodegradable sutures, actuators, catheters, and stents for medical applications if made of the correct material [67,68]; the SMPs are excellent materials for deployable and morphing structures of aircraft and spacecraft[69], ranging from array bearing hinges to thin-film structures [70] due to the material's light weight and malleability. To make SMPs effective in those applications, precisely controlling the deflection of them are necessary. The objective of the control system in this paper is to precisely and repeatedly drive the deflection angle of the sample SMP to a desired value using the

position information of the interested dots on the surface of the SMP and measured from the vision system.

In this study, we explored self-assembly CNFs paper incorporated with the epoxy-based SMP (Veriflex®E2) to fabricate the electro induced SMP composites. The synergistic effect of carbon nanofiber (CNF) and carbon nanofiber paper (CNFP) on shape memory polymer (SMP) nanocomposites actuation has been investigated. The deformation of SMPs sample has been detected and analyzed by a vision based 3D coordinate prediction system. The dynamic mechanical analysis (DMA) also been carried out in order to predict its thermal-mechanical properties. Over a hundred times control tests have been conducted to investigate the accuracy and repeatability of SMP nanocomposites.

Substantially more attention has been given in the past to shape memory alloys and shape memory ceramics than to shape memory polymers because unreinforced shape memory polymers have much lower stiffness and recovery force potential than shape memory alloys and shape memory ceramics. However, when incorporated into a fiber-reinforced composite, both the stiffness and the recovery force of a shape memory polymer can be dramatically improved [53]. In order to increase the mechanical properties of the SMP, the unidirectional carbon fabric are incorporated with the resin. Successful actuation of continuous fiber reinforced SMP nanocomposites leads their application as the structure material. Thermal-mechanical properties of SMP nanocomposites have been investigate by the dynamic mechanical

analysis (DMA). The mechanical property degradation of SMP nanocomposites after different cycle actuation has been investigated.

7.2. Electro Actuation of SMP coated with carbon nanofiber paper

7.2.1. Materials

Carbon nanofibers (Pyrograf®-III, PR-HHT-25) were provided in powder from Applied Sciences Inc., Cedarville, Ohio, USA. The nanofibers have a diameter of 50-100 nm and length of 30-100 μ m. CNFs have excellent electrical conductivity (0.75S/cm) and thermal conductivity (2×10^7 W·K⁻¹·m⁻¹). Deionized water was used as the solvent. Meanwhile, the non-ionic surfactant (Triton X-100) was used to aid the dispersion of CNFs. The epoxy-based SMP resin Veriflex®E2 was supplied from Cornerstone Research Group, Inc., Dayton, Ohio, USA. The Veriflex E2 which comes as two-parts is a fully formable thermoset shape memory polymer (SMP) resin system. The mixing ratio of part A and part B is 100:27.08. The Veriflex E2 resin is engineered with a glass transition temperature (T_g) of 104 °C, and the cured resin has unique “shape memory” properties and can be bent, stretched and twisted, without the any loss of the shape memory effect.

7.2.2. Fabrication of CNFs Paper and the CNFP-based SMP Composites

The carbon nanofibers were divided into several parts evenly, and then were transferred into 1000ml beakers and 400 ml deionized water was added in each beaker. In order to disperse the CNFs even into the water, 4ml of surfactant Triton-X100 was

added into the solution. The solution was subsequently sonicated using a high intensive probe sonicator for with 30 min. After that, the solution was cooled down to room temperature and Ten drops of surfactant were added into the solution. Then the solution was sonicated twice again with 30 min interval and was cooled down to room temperature. Finally the as-prepared suspensions were sonicated two minutes and immediately transferred into filtration system. The carbon nanofiber paper was made by filtering the suspension through 0.4 μm hydrophilic polycarbonate membrane under a high-pressure (100psi) filtration system. Once the paper was made, the filter with the carbon nanopaper was carefully removed and placed onto a piece of paper where the filter was detached. The papers were about 12.5 cm in diameter. The remaining paper was put into oven at temperature of 120°C for two hours. In this research, four groups of samples are made, and the weights of CNFPs include 1.2g and 2.4g, whose thickness equal to 0.5mm and 1mm, respectively.

After the CNFP was ready, resin transfer molding (RTM) process was used to fabricate the SMP nanocomposite. In order to increase the bulk thermal and electrical conductivity, CNFs were added into SMP resin. Two parts of Veriflex E2 resin were firstly mixed together using a high shear mixer. The CNFs were blended into the SMP resin with 1% weight fractions. The resulting mixture was degasified in a vacuum oven to completely remove air bubbles. To further investigate the effect of the thickness of the CNPs, different thicknesses of CNFPs (0.5mm, 1mm) were placed on the inside bottom of the mold. The SMP resin modified with CNFs was then injected

into the mold. The curing cycle for the resin is: Ramping to 120 °C and hold 4 hrs, then Ramping to 150 °C and hold another 4 hrs. Then, the SMP, with CNFP on its surface, is fabricated.

7.2.3. Results and Discussion

Morphological characterization of CNF paper and its SMP composites

In order to study their morphologies and network structures, the CNFPs and its composites were characterized with scanning electron microscope (SEM) (ZIESS Ultra-55, at 5 kV). The samples were coated with about 10 nm of Au on its surface in order to enhance SEM imaging. The SEM images of CNFPs and CNFPs infused with SMP resin are shown in Figure 29. The CNFs are homogenous dispersed almost without any aggregation. As we know CNFs is one of the best conductive materials, each individual CNF is the conductive path of electrons. The continuous network structure is observed, which further enhances the conductivity of CNFPs. Figure 29 (b) clearly shows the cross section of CNFPs after resin infusion and the net structure still remain which lead the nonconductive polymer to be as a conductor through the conductive network. Therefore, electro inducing the SMP can be obtained.

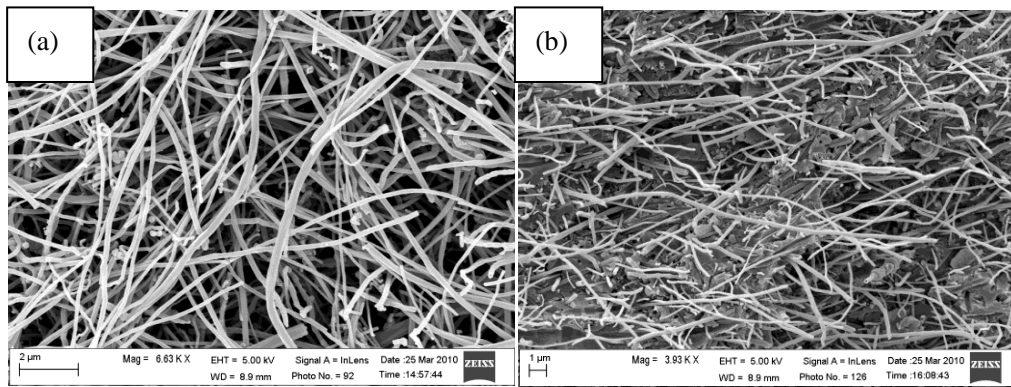


Figure 29 SEM images of (a) CNFPs and (b) CNFPs infused with SMP resin.

Electrical Resistivity of CNFPs incorporated SPM Composites

The electrical resistivity of the neat SMP and their hybrid filler filled composites were measured by a standard four-probe method (SIGNATONE QUADPRO system) using a precision multi-meter incorporated with a four-point cylindrical probe. The apparatus has four probes in a straight line with an equal inter-probe spacing of 1.56 mm. The radius of the probe needle is 100 μm . A constant current passes through two outer probes and an output voltage is measured across the inner probes with the voltmeter.

The resistivity of different groups of SPM samples is shown in Figure 30. The resistivity of group1 (SMP coated with 0.5 CNFP) is 0.54 $\text{ohm}^{\wedge}\text{cm}$, which is about 2×10^{16} times less than pure SMP (about $10^{16} \text{ohm}^{\wedge}\text{cm}$). As mentioned before, due to intrinsic excellent conductivity of CNFs, more efficient conductive path for electrons are provided. The network structure of CNFP further improves the conductive structure and enhances the conductivity of SMP composite. Compare Group 1 with Group 2 (SMP coated with 1mm thick CNFP), the resistivity decrease as the thickness

of CNFP increases due to more conductive paths were involved. After blended with CNFs into the resin system, the resistivity of SMP composites is even less, and the value is 0.340 ohm^{cm} for group 3 and 0.307 for group 4. This indicates the CNFs blended into the SMP resin system create additional conductive paths inside of SMP composite.

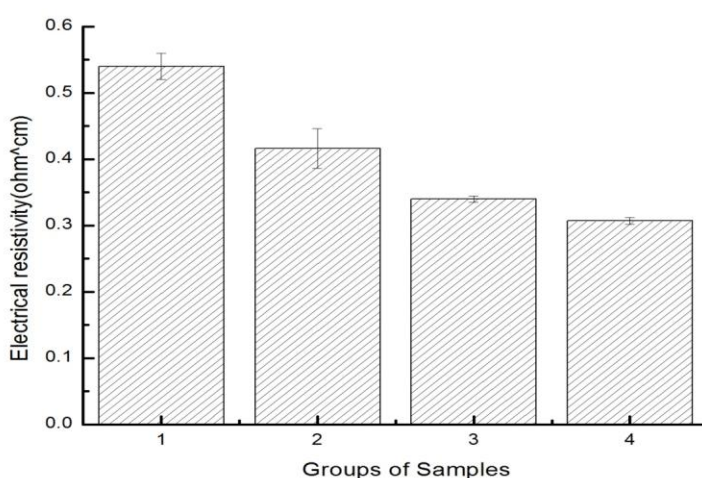


Figure 30 the electrical resistivity of different groups of sample. Column 1 is SMP incorporated with 0.5mm CNFP on its surface, column 2 is SMP coated with 1.0mm CNFP, column 3 is SMP blend with 1wt% CNFs and meanwhile, coated with 0.5mm CNFP, and column 4 is SMP blend with 1wt% CNFs and coated with 1mm CNFP.

Dynamic Mechanical Analysis (DMA)

In order to investigate the dynamic mechanical property of SMP composites, DMA was carried out using TA Instruments DMA Q800. Dynamic mechanical properties refer to the response of a material as it is subjected to an oscillating load. These properties may be expressed in terms of a storage modulus, a loss modulus, and a tangent delta (damping). The testing temperature ranges from 60 °C to 170.00 °C

and the heating rate is 10.00 °C/min. The frequency is 1.0Hz. The testing results are presented in figure31. The storage modulus, loss modulus and tangent delta of four groups of SMP sample are plotted vs temperature. Storage modulus describes elastic property of SMP composites which is related to the Young's modulus. The loss modulus stands for the viscous property which associated with energy dissipation in the form of heat upon deformation. The peak value of tangent delta indicates the glass transition temperature (T_g) of the SMP composites. The peak values of four groups of samples are quite similar which tells good thermal stability of SMP composites after mixed with CNFs.

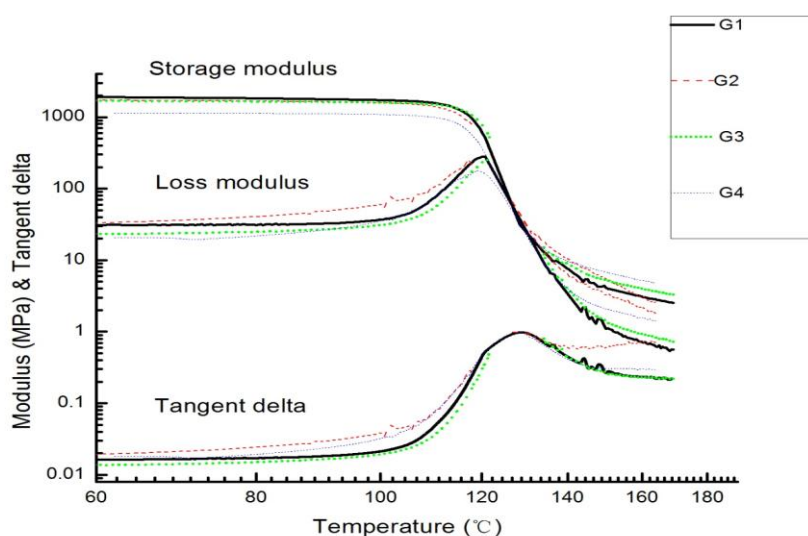


Figure 31 Storage modulus, loss modulus and tangent delta curves for G1-G4 samples.

Column 1 is SMP incorporated with 0.5mm CNFP on its surface, column 2 is SMP coated with 1.0mm CNFP, column 3 is SMP blend with 1wt% CNFs and meanwhile, coated with 0.5mm CNFP, and column 4 is SMP blend with 1wt% CNFs and coated with 1mm CNFP

Characterization results of shape recovery effect of SMPs by vision based coordinate measurement system

In order to obtain the deformation information of arbitrary points on the polymer material with current and voltage applied, a low-cost vision based 3D coordinate measurement system is designed. Figure 32 shows the experiment setup, in which a material sample marked with different colors in different locations is placed in front of two webcams of known orientations. The projection to the camera system allows a 3D reconstruction of those points in real time.

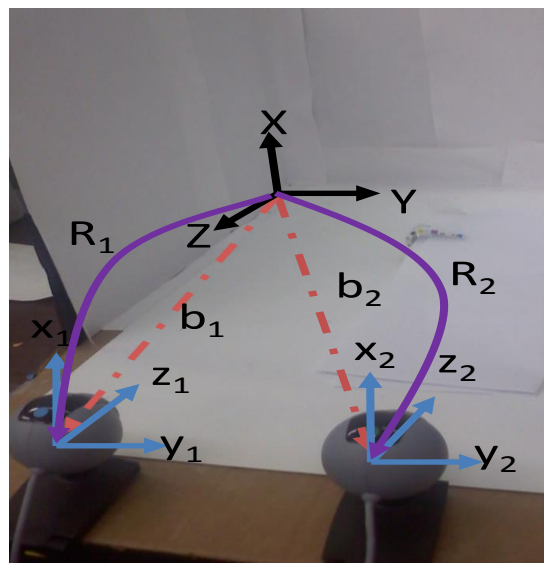


Figure 32 Camera Setup

Sample

While samples varied in composition, the general size of samples was maintained constant. A typical sample was three to four inches long and placed in the same location for each test. This size and location was chosen in an effort to keep the

projected image close to the center of the cameras to ensure accurate 3D position reconstruction. Voltage was applied through alligator clips held in place by sticky tack and a white sheet of paper was placed over the clips and tack to prevent confusion between the yellow tack and yellow dots on the sample.

Point Tracking

A number of colored dots were painted or placed, depending on the size of the sample, along the side of the sample with more being placed along areas of a high curvature as shown in Figure 34. Prior to applying a voltage, the entire images from both cameras were compared to the specific RGB and range values thresholds for each camera and each dot. If all dots are found in user accepted locations, the program stored the points and used a reduced search area centered on the latest known location of each dot for the current search (Figure 35). In the event that a dot is not found in its reduced search area, the program searches the entire frame for the dot which typically adds roughly 112ms to runtime for the current system. To reduce background noise, the test bed was covered in white paper before the placement of the sample.

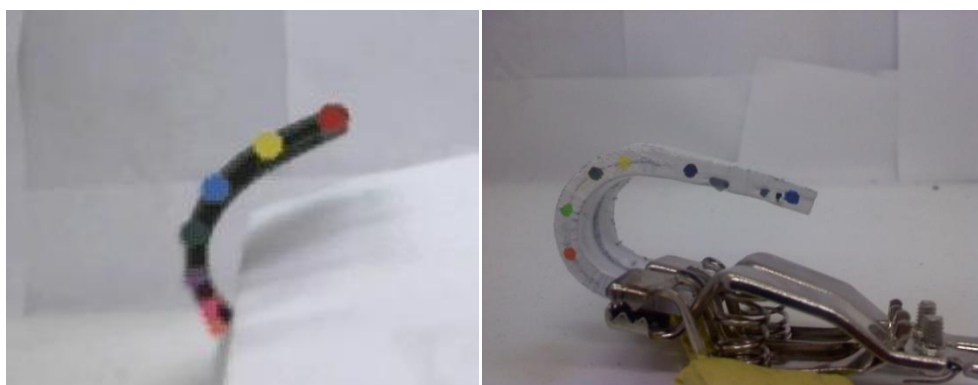


Figure 33 Sample with placed colored dots (left) and painted dots (right)

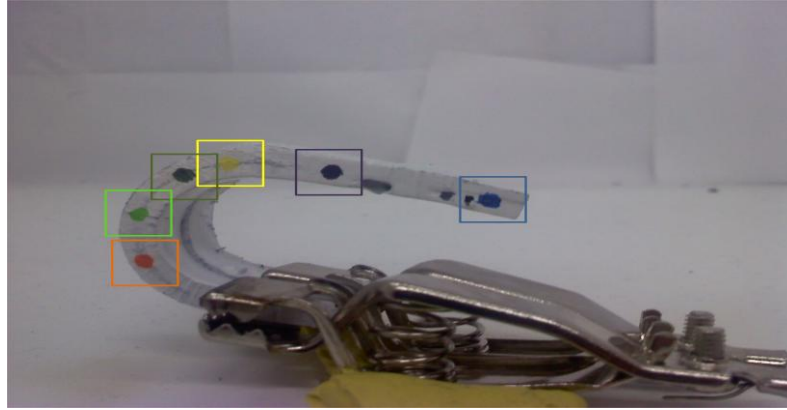


Figure 34 reduced search area and associated dots

Angle Characterization

Using the topmost two dots on the material sample, the current state can be found by calculating the angle from the horizontal, ω , where the starting angle is typically close to 180° and the current desired ending angle is 0°

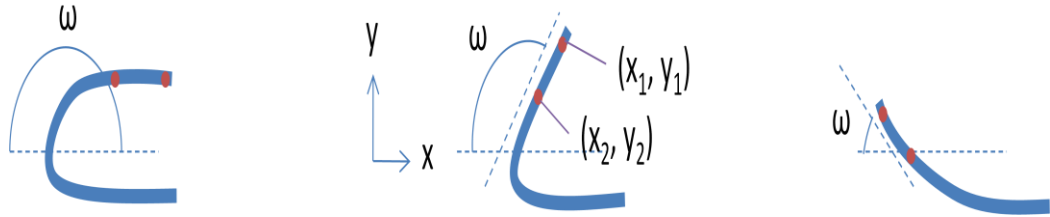


Figure 35 Idealized sample deformation over time

where

$$\omega = \tan^{-1} \left(\frac{y_1 - y_2}{-(x_1 - x_2)} \right) \quad (7)$$

Shape memory effect of SMPs

Figure 37 demonstrate the macroscopic shape memory effect of the SMP composite. The permanent shape is a flat strip, and the temporary shape is an “n” shape. It can be seen that, at the same actuation voltage, the recovery time four samples is 5123s, 582s, 110s and 94s, respectively. That means the response of the actuation is improved by coating thicker CPNs due to more CNFs involve to the surface conductive network. Meanwhile, bending 1wt% into SMP will further facilitates the recovery of SMP which is result of the increase of bulk thermal and electrical conductivity. Due to this synergistic effect, we can see that G4 is dramatically less then 95seconds, which is less than 1/10.

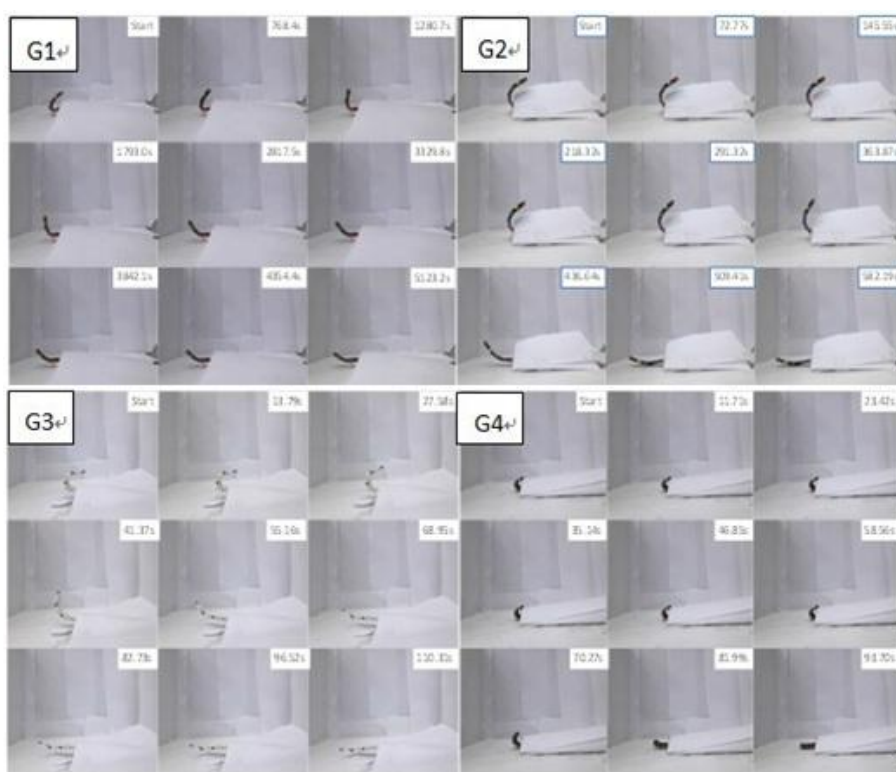


Figure 36 Series of photographs showing the macroscopic shape-memory effect of SMP composite for G1-G4. The permanent shape is a flat strip of composite material, and the temporary shape is deformed as right-angled shape.

7.2.4. Control tests of SMP nanocomposites

Control System

As can be seen in Figure 38, pixel coordinates u and v from each camera are obtained using the vision system discussed in the previous section. This camera data is used in reconstruction to obtain the states x_i, y_i , and z_i calculate Θ . This deflection angle is compared to the desired angle, Θ_d , creating the error signal $e = \Theta_d - \Theta$. As will be explained in a later section, a command voltage V_c is calculated from the PID controller and sent through the voltage regulator in conjunction with the power supply and applied to the sample as V_{input} . This voltage heats the material through resistive heating causing a change in position as T_m approaches and surpasses T_g .

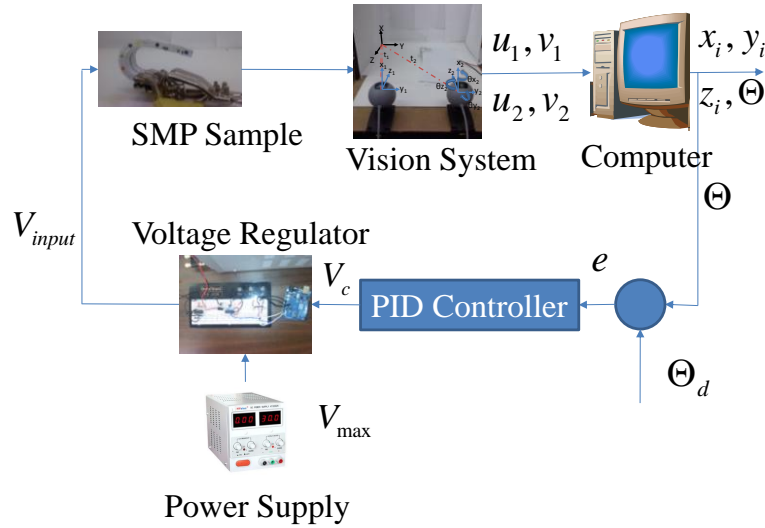


Figure 37 Block diagram of control system

Voltage Regulator

The control input to the SMP is generated through the voltage regulator. As shown in Figure 39, an SN754410 Quad Half H-Bridge, an Arduino Uno, and a DC Power Supply HY3002 are included. According to the voltage command calculated by the controller, a pulse width modulation signal at a frequency of 500Hz is sent to the H-Bridge which alternates the voltage input between $[0, V_{\max}]$ with a resolution of $V_{\max} / 255$. V_{\max} is the maximum voltage determined by the power supply, and in our experiment, $V_{\max} = 25V$.

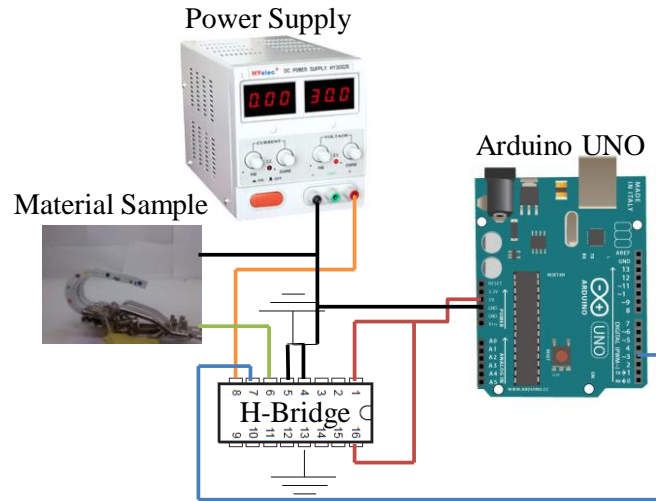


Figure 38 Circuit diagram of voltage Regulator

Results of PID control of SMP nanocomposites

The figure 40 shows the final results of a PID controller after iterative tuning of its parameters ($k_p = 20, k_i = 15, k_d = 4$). Each sample was first heated with a voltage of 25v until malleable, deformed under loading to ~ 180 degrees from the memorized state, and allowed to cool back to room temperature before testing. These

had a reasonably fast response of ~90 seconds and could be repeatedly commanded to the desired angle within 5%.

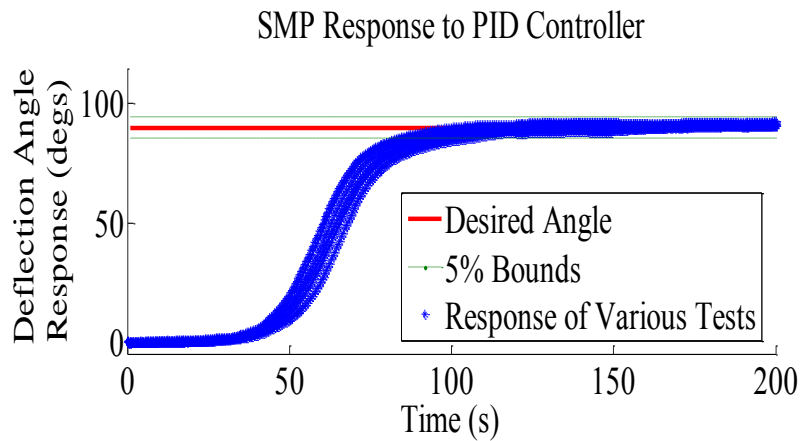


Figure 39 PI control response for varying values of k_p and k_i

In a typical response, the proportional gain (Figure 41) drove the response of the sample in each test for around 50 seconds. Saturation control and the resetting function in the iterative gain kept this initial input acting as the standard step input seen in most SMP testing.

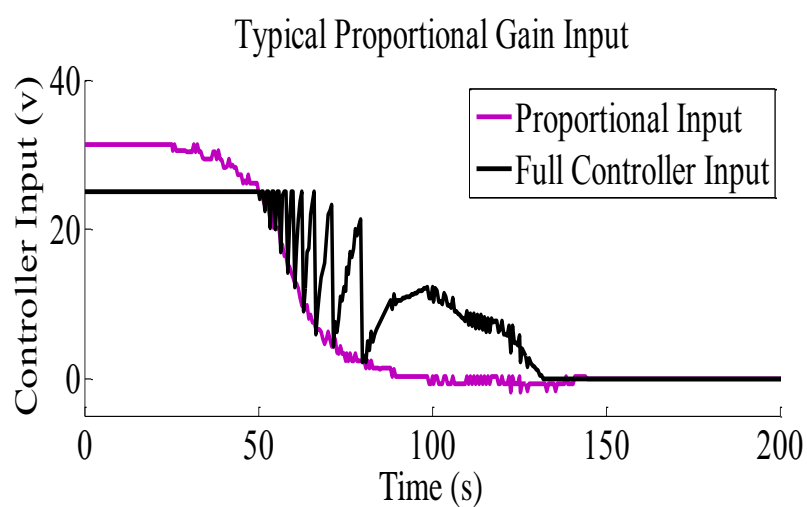


Figure 40 Typical Proportional Gain Input

With time, however the error signal becomes small enough to almost negate the proportional gain and the integral gain (Figure 42) becomes the dominant driver of the voltage.

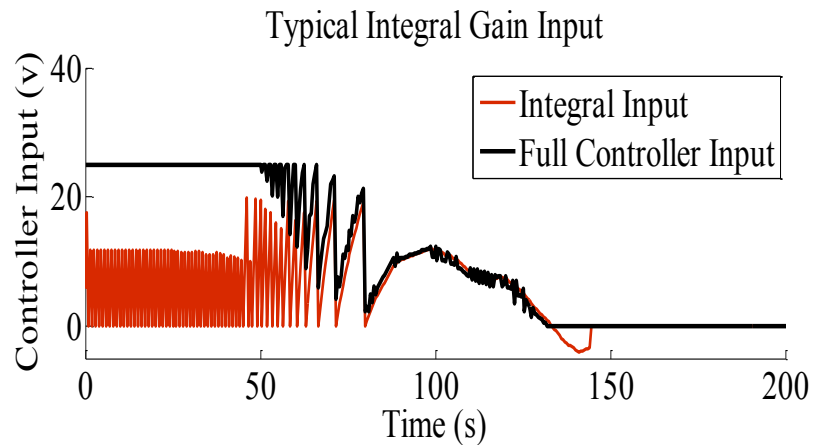


Figure 41 Typical Integral Gain Input

It was found that in the pursuit of a fast response, a small derivative gain was desirable thus making its contribution to the voltage input minimal. Larger values increased the response time by up to 40 seconds, while only decreasing the overshoot 2 degrees (best case).

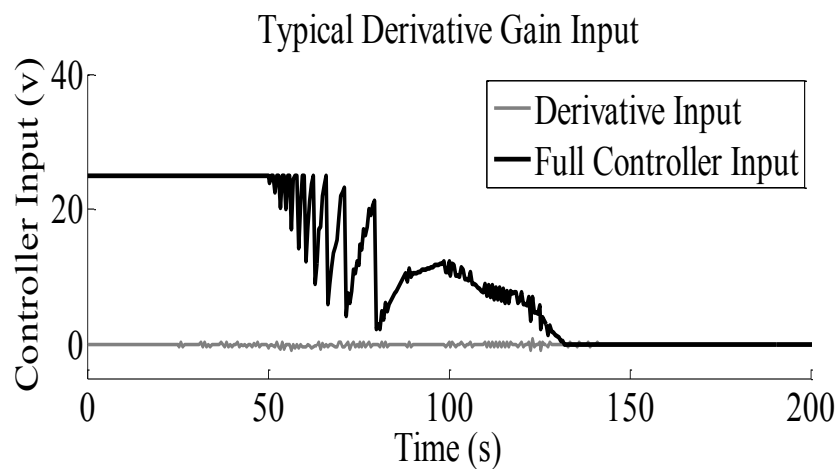


Figure 42 Typical Proportional Gain Input

7.3. Electro Actuation of continuous carbon fiber reinforced SMP nanocomposites

7.3.1. Raw materials

Highly conductive PR 25 Carbon nanofiber is provided by ASI as mentioned before. Unidirectional carbon fabric (GA090) is provided by Hexcel utilizing the 12k AS4 fiber. The PAN based fiber AS4 with continuous, high strength, and high strain, is the used primarily in aerospace applications. The polyurethane-based SMP (MP5510), provided form SMP Technologies Inc. (Japan), is potting type thermoset resin. The chemical ingredient includes about 70% Dimethylformamide and 30% Polyurethane. A variety of application has been developed based on this type of SMP resin, such as Spoon, scissors, tooth brush and kitchen knife for Handicapped Wig net Dole Hair Water-proofing film tape bandage, Printing for leather, Transforming photo to canvas, Surgical cast, Lining of Inner Pipe, Artificial Nail, Toys, Development structures for outer space, Readily decomposable, Fasteners.

7.3.2. Experimental Results and Discussion

Dynamic Mechanical Analysis (DMA)

In order to investigate the dynamic mechanical property of fiber reinforced SMP composites, DMA was carried out using TA Instruments DMA Q800. Dynamic mechanical properties refer to the response of a material as it is subjected to an oscillating load. Tensile mode has been employed for this test. In the tensile mode, one end of the sample is fixed and movable part of the system providing the oscillatory force is attached to the other end. Pretension is applied to prevent the

sample from bending or buckling during the oscillation. This mode is most suitable for films, fibers and thin bars. The advantage is that the clamping of the sample has practically no influence on the deformation of the sample.

Four groups of sample have been tested, including pure SMP, SMP coated with CNFP, SMP incorporated with carbon fabric, and SMP incorporated with carbon fabric and CNFP. These DMA properties may be expressed in terms of a storage modulus, a loss modulus, and a tangent delta (damping). The testing temperature ranges from 0 °C to 190.00 °C and the heating rate is 10.00 °C/min. The frequency is 1.0Hz. The testing results are presented in figure 44-46. The storage modulus and tangent delta of four groups of SMP sample are plotted vs temperature. Storage modulus describes elastic property of SMP composites which is related to the Young's modulus. The peak value of tangent delta indicates the glass transition temperature (T_g) of the SMP composites. The peak values of pure SMP, SMP coated with CNFP, SMP incorporated with carbon fabric, and SMP incorporated with carbon fabric and CNFP are 73°C, 74°C, 78°C, 84°C, which indicates the thermal stability of SMP composites has been significantly improved by incorporating with CNFP and carbon fabric. The mechanism could be better heat absorption and dissipation provided by CNF and carbon fabrics.

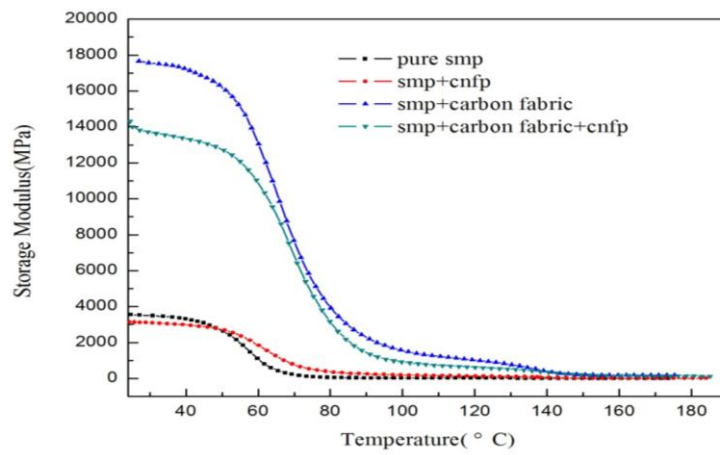


Figure 43 Storage Modulus of SMP samples

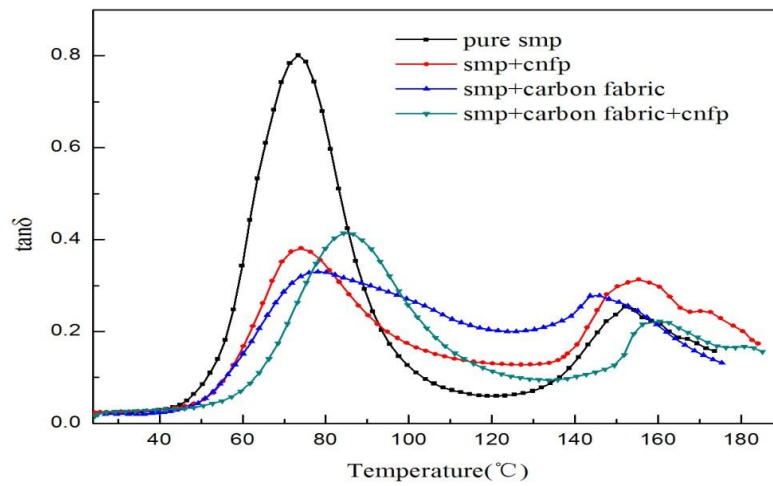


Figure 44 $\tan\delta$ of SMP samples

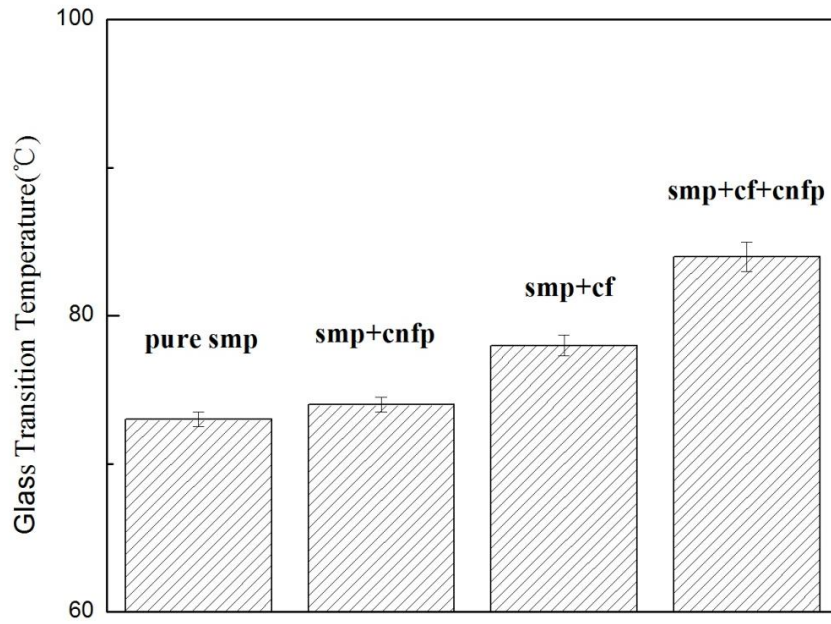


Figure 45 Glass transition temperature of SMP sample

7.4. Mechanical Property Degradation of Fiber Reinforced SMP Nanocomposites

Due to the organic nature of polymer, durability is a critical issue for all kind of polymer based composites, since the degradation of the polymer composites is inevitable. The repeatability of shape memory effect of CNFP coated SMP has already discussed in above. In this section, the bending property degradation of fiber reinforced SMP nanocomposites will be investigated. The nanocomposites panels were fabricated by autoclave processing with the same curing cycle as mentioned before. The three point bending test was carried out according the ASTM standard D790. As recommended, specimen dimension is 127mm ×12.7mm× 3.2mm (as figure shows). The test facility is MTS Insight 5kN Electromechanical Load Frame Model # Insight 5 SL (as figure shows).

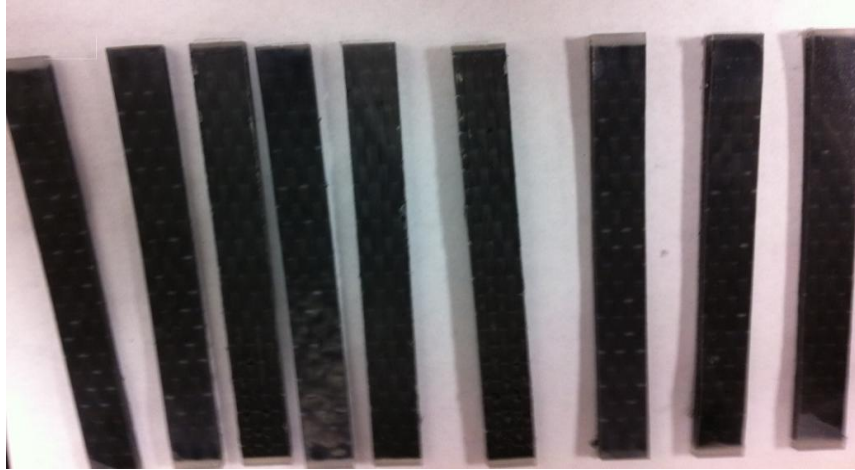


Figure 46 Three point bending samples



Figure 47 MTS machine for three point bending test

From the three point bending test, the load at a given point on the load-deflection curve and deflection of the center of the beam can be obtained. So the flexural stress and strain can be calculated by the equation below.

Flexural Stress (δ_f):

$$\delta_f = \frac{3PL}{2bd^2} \quad (8)$$

where: δ is the stress in the outer fibers at midpoint, MPa (psi), P is the load at a given

point on the load-deflection curve, N (lbf), L is the support span, mm (in.), b is the width of beam tested, mm (in.), and d is the depth of beam tested, mm (in.).

Flexural Strain, (ϵ_f):

$$\epsilon_f = \frac{6Dd}{L^2} \quad (9)$$

where: ϵ = strain in the outer surface, mm/mm (in./in.), D = maximum deflection of the center of the beam, mm (in.), L = support span, mm (in.), and d = depth, mm (in.).

After the flexural stress and stain were obtained, the flexural modulus can be calculated by the equation below.

Flexural modulus (E_B)

$$E_B = \frac{L^3 m}{4bd^3} \quad (10)$$

where: E_B is the modulus of elasticity in bending, MPa (psi), L is the support span, mm (in.), b is the width of beam tested, mm (in.), d is the depth of beam tested, mm (in.), and m is the slope of the tangent to the initial straight-line portion of the load-deflection curve, N/mm (lbf/in.) of deflection.

Five groups of sample were prepared, which have been actuated by 0 time, 5 times, 10 times, 20 times, and 50 times, respectively. The three point bending test results are shown below. The stress-strain curves are consistent. All groups of the sample shown an initial linearly behavior, and then a loading redistribution after primary crack, and then a brittle fracture occurred. Next figure shows the ultimate strength of the sample. There is a 15% decrease of the ultimate strength after 5 times actuation, which is due to the thermal degradation of SMP suffered from the

actuation process. Then ultimate strength almost stays the same for the sample of 5 times, 10 times, 20 times. Even after 50 times actuation, there is 25% decrease of the ultimate strength. So, this material obviously shows good durability. The next figure of bending modulus is even more convincing. The bending modulus of five group sample barely changed, and there is only less 2% decrease of the bending modulus even after 50 times actuation.

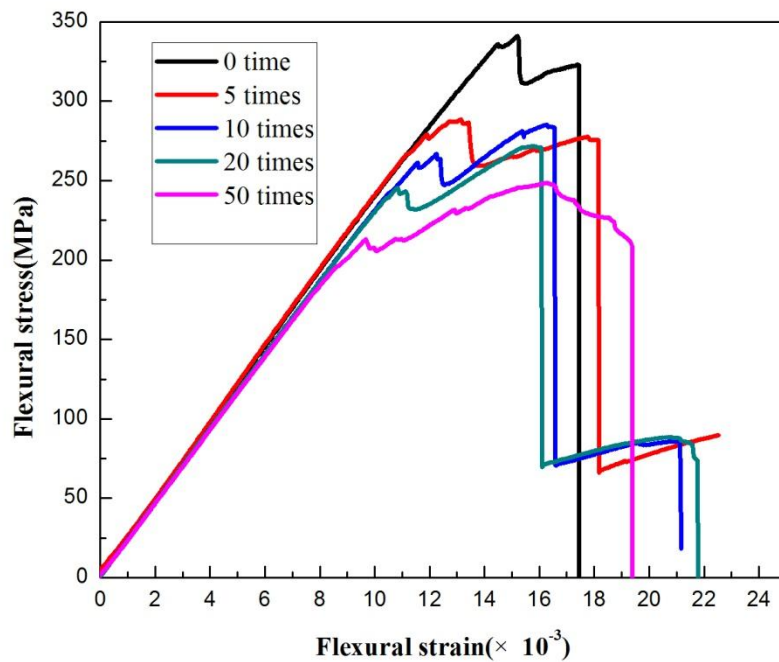


Figure 48 Flexural stress-strain curves of SMP samples

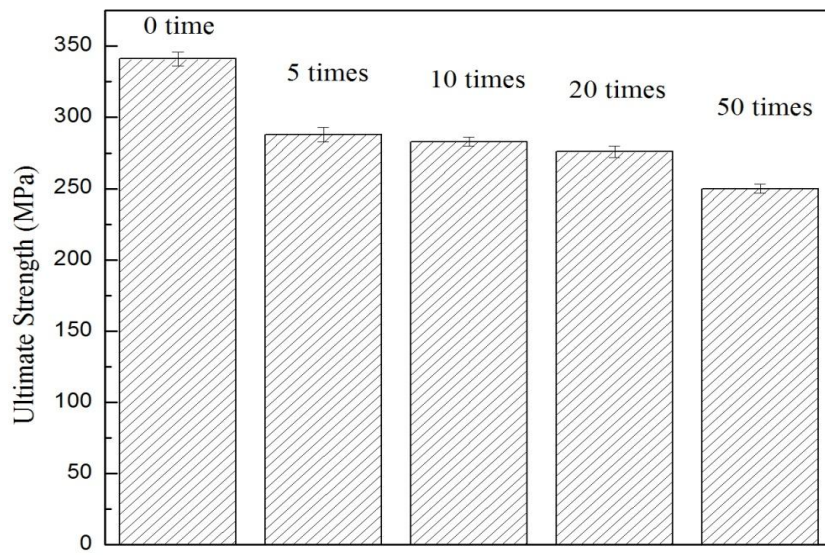


Figure 49 Ultimate strength of SMP samples

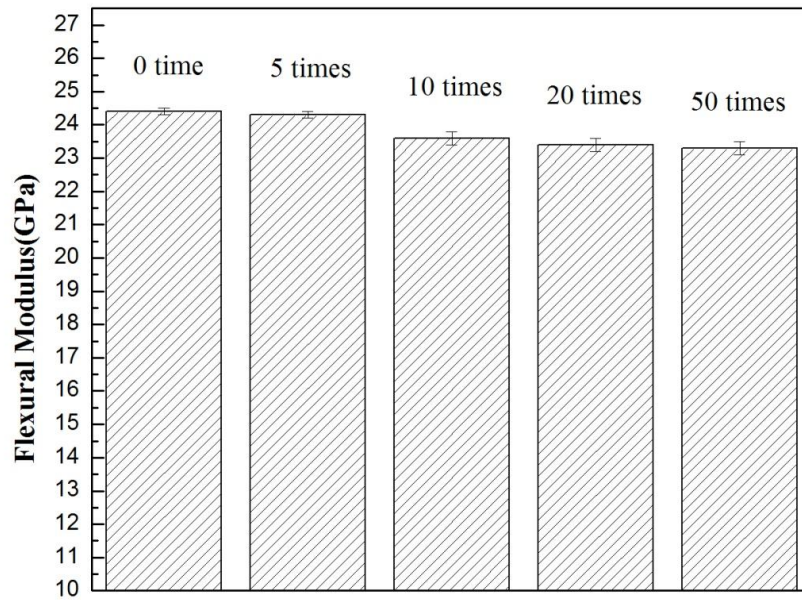


Figure 50 Flexural Modulus of SMP samples

7.5. Characterization results of shape recovery effect of carbon fiber reinforced SMP composites by vision based coordinate measurement system

The fabrication method of the sample is the same as the sample for three point bending test. The characterization method of shape memory effect of carbon fiber reinforced SMP composites is the same as mentioned previously. Three groups of sample were prepared. All the sample were coated with 0.5mm thick CNFP. The fiber volume fractions of the sample are 0%, 35.1%, 55.2%, respectively. Below are the test results. From the result, the both recovery speed and recovery rate are improved by incorporating carbon fabric with SMP resin, which are due to better heat transfer created by adding continuous carbon fiber into the nanocomposites.

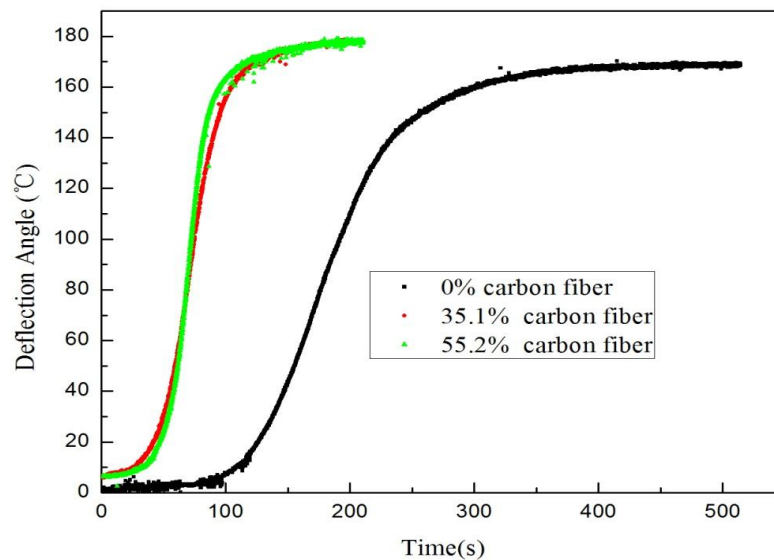


Figure 51 Deflection Angle of sample with 0%, 35.1%, 55.2% fiber volume fraction

7.6. Summary

In this research, electro induction of the CNF paper integrated with SMP is achieved by electrical resistive heating. This unique composite is combined with excellent electroactive responsive and behavior shape memory effect. Series of experiments were conduct to study the synergistic effect of carbon nanofiber and carbon nanopaper on the shape recovery of the SMP composites. The actuation of the SMP composites was achieved by the electrical resistive heating of carbon nanopaper. The conductivity of SMP is greatly reduced by incorporating CNP into SMP and further reduced by blending CNFs into SMP, and then the shape memory response is significantly accelerated. Therefore, it is expected that the recovery progress of SMP can be designed through tailoring the dispersion of individual CNF and controlling the thickness of CNF paper. Meanwhile, a vision-based control system was developed, which offered a noninvasive approach to measure and precisely control the shape of the SMP nanocomposites. The actuation test results show that the responses of the SMP nanocomposites under this controller were fast and accurate, and the performance was repeatable.

CHAPTER EIGHT: COVELENT FUNCTIONALIZATION OF CARBON FIBERS WITH POLYHEDRAL OLIGOMERIC SILSEQUIOXANE AND THEIR APPLICATION IN SUPERHRDROPHOBICITY AND FLAME RETARDANCY

8.1. Introduction

Carbon nanofibers (CNFs), with excellent mechanical, electrical, and thermal properties, have gained numerous attentions, and the application of carbon nanofibers includes nanosensors, full cell, Li battery and fiber reinforced composites [71-77]. CNFs also have been used as a fire retardant additive in polymer matrix [78-82]. Kashiwagi et al. reported the first study on the flammability of polymer/CNTs composites [78, 79]. Significant reduction in heat release rate (HRR) was observed after CNFs were incorporated into poly (methyl methacrylate) and polypropylene at a very low loading. It was reported that a jammed network structure covering the entire sample surface was formed to act as a heat shield to slow down the thermal degradation of the polymer.

Polyhedral oligomeric silsequioxane (POSS) is a candidate material for the design of polymer composites [83-87]. Adding POSS to polymers results in significant improvements in the properties of the polymers such as thermal stability, oxidative resistance, mechanical properties and flammability resistance and hydrophobicity. The diameter of the POSS cage is ca.0.45nm. However, it can reach the dimension of 1-3 nm when an organic decoration is included. The POSS molecules are decorated on the outer surface with organic hydrophobic residues and

covalently bonded to Si atoms, which could facilitate the dispersion in polymer. This enables a large variability of POSS derivatives. POSS is completely nonpolar. But the polarity can be induced with the appropriate organic derivatives [84, 85]. The excellent properties of POSS macromonomer inspire to prepare functionalized POSS cages, which can be used as the modification agents of CNFs to prepare the composite combining the two types of nano-reinforcement agents.

In our previous study [87], POSS and carbon nanofiber (CNF) were fabricated as flame retardant sheet and coated onto the surface of polymer composites. The preformed sheet worked as a protective layer which prevented the transmission of an external heat to the underlying polyester resin and limited the diffusion of the volatilization gases to the surface to feed the flame. However, the previous study revealed that the CNF/POSS sheet was not effective enough to improve the fire retardant performance. The possible reasons include the POSS aggregate during the paper making process and the low thermal stability of POSS particles.

In this study, carbon nanofibers (CNFs) were grafted with POSS (CNF-g-POSS) and subsequently used to prepare a nanopaper. It is anticipated that the grafting of POSS onto CNF will enhance the dispersion of POSS particles, thermal stability and the flame retardancy of polymer composites. The morphology, thermal properties, surface characteristics and flammability of the hybrid nanopaper are discussed in this study.

8.2. Experimental

Materials

Pyrograf-IIITM carbon nanofibers (PR-PS-25) were supplied from Applied Sciences Inc., Cedarville, Ohio. The nanofibers have diameter of 100-150 nm and length of 30-100 μm . Aminopropylisooctyl-POSS (AM0270) was supplied from Hybrid Plastics, Inc. All chemicals (such as H_2SO_4 , CHCl_3 etc.) were supplied from Fisher Scientific, Inc. The unsaturated polyester resin (product code: 712-6117, Eastman Chemical Company) was used as matrix material with the methyl ethyl ketone peroxide as hardener at a weight ratio of 100:1.

Functionalization of CNFs and the preparation of nanopaper

Figure 53 illustrates the preparation of POSS covalently functionalized CNFs. The obtained CNFs were oxidized with a mixture of nitric acid and sulfuric acid (1/3 by volume) in an ultrasonic bath at 40 $^{\circ}\text{C}$ for 2h and then were refluxed for 2h. After cooling down to room temperature, the mixture was diluted with a large amount of deionized water, followed by a vacuum filtering through a polycarbonate film. The acid-modified CNFs were washed with deionized water until the pH value of water was about 7. The modified CNFs were dried at 60 $^{\circ}\text{C}$ in a vacuum oven for 2h and then grinded into powder with a mortar. A mixture of acid-modified CNFs (4g), thionyl chloride (1000ml) and N, N-dimethylformamide was dispersed in an ultrasonic bath about 3h and refluxed at 70 $^{\circ}\text{C}$ for 24 h. The residual SOCl_2 was removed by the reduced pressure distillation to yield acyl chloride functionalized

CNFs (CNFs-COCl). CNFs-COCl (4g), POSS-NH₂ (20g), and 5 ml Et₃N were added into a glass flask and dispersed by CHCl₃. The mixture was suspended in an ultrasonic bath at 40 °C for 2 h, and stirred by magnetic stirrer for 72 h in an oil bath under high purified N₂ atmosphere. The product obtained was vacuum-filtered and washed five times with excess CHCl₃ to remove the residual of POSS molecules then dried to yield neat CNF-g-POSS.

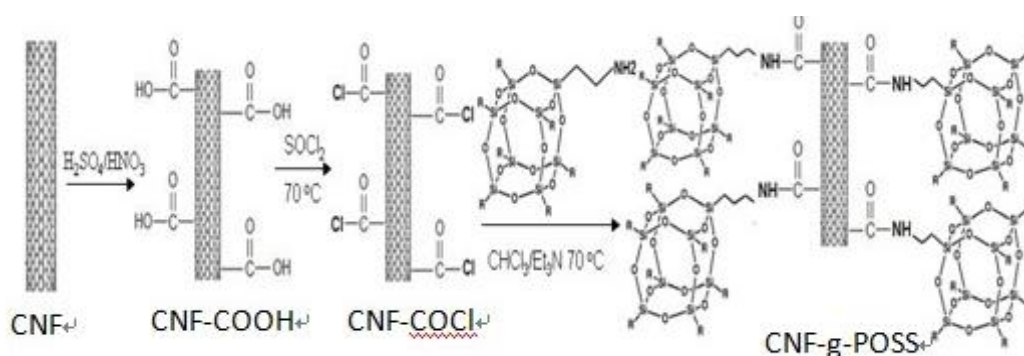


Figure 52 Illustration for the synthesis of CNF-g-POSS.

The pristine CNF or CNF-g-POSS was dispersed in distilled water with an aid of surfactant Triton-X100. The mixture was subsequently sonicated using a high intensity probe sonicator (600-watt Sonicator 3000 from Misonix Inc.) for about 90 min to make a stable suspension. The nanopaper were prepared by the infiltration of the suspension through a 0.4 μm polycarbonate membrane under a high-pressure compressed air system, and then the papers were washed with distilled water to remove the surfactant. The prepared papers were dried in an oven at 120 °C for 2 h. The schematic of the papermaking process is shown in Figure 54.

The CNF or CNF-g-POSS film was prepared as following: A CNF or

CNF-g-POSS suspension was obtained by mixing CNF or CNF-g-POSS in chloroform and sonicated for 90 min with an ultrasonic bath. The superhydrophobic films were prepared by drop casting the suspension onto a substrate and then the solvent was allowed to evaporate in the fume hood.

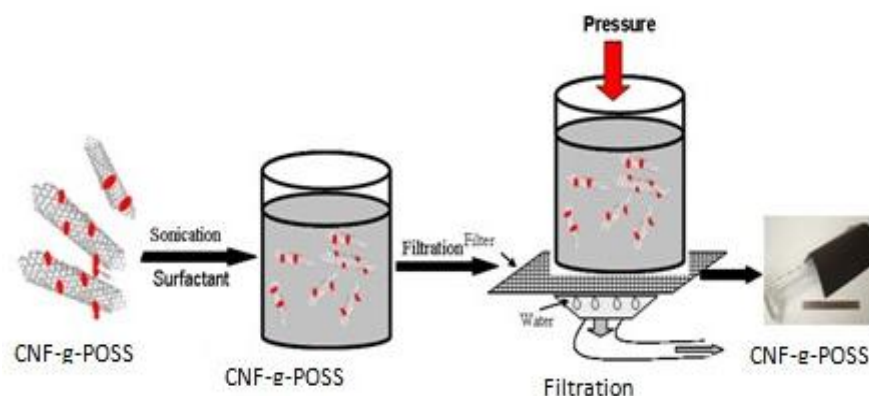


Figure 53. Illustration for the preparation of nanopaper.

8.3. Measurements

Characterization of CNF-g-POSS

The Fourier Transform Infrared Spectra (FTIR) spectra were recorded by a Nicolet 6700 spectrometer using KBr pellets. Raman spectroscopy was conducted with a Renishaw Raman RM-1000 spectrometer with a 532 nm laser source. The scanning electron microscopy (SEM) images were obtained with SEM (Zeiss Ultra-55) at 10 kV. Prior to imaging the nanopaper and its composites were aputter-coated with a conductive gold layer.

Contact angle measurements

The static contact angle was acquired by a “DropImage” contact angle

measurement system at room temperature. The deionized water (10 μ L) was introduced using a micro-syringe and images were captured to measure the angle of the liquid-solid interface. Five measurements were taken and averaged.

Thermal stability analysis

Thermo-gravimetric analysis (TGA) was conducted using a Thermal analyzer (TGA-Q5000, TA Co., USA). The characterization of the sample was conducted in nitrogen flow from 25 to 700 $^{\circ}$ C at a rate of 10 $^{\circ}$ C/min. The weight of the sample was about 10mg.

Flammability evaluation

Heat release rate (HRR) is one of the most important parameters to evaluate the flammability of polymer materials. It is obtained by conducting cone calorimeter test. A sketch of the instrument is shown in the Figure 55. Besides the HRR, other useful information can also be obtained from the test, such as the total heat released, peak heat release rate (PHRR), time to ignition, mass loss rate, and production of smoke, CO and CO₂. According to the standard ASTM E 1345-10 (ISO 5660-1), the fire retardant performance of the composites with and without nanopaper coatings was evaluated by a FTT cone calorimeter (manufactured by Fire Testing Technology Ltd) with an incident heat flux of 50kw/m². For all the samples, the unexposed surfaces and side edges were wrapped in an aluminum foil. There was ceramic wool within the sample holder of the cone calorimeter. Therefore the unexposed surfaces of the samples were insulated. The samples were evaluated in a horizontal position with

the surfaces coated with nanopapers, when applicable, directly exposing to the heat flux during cone calorimeter tests. The dimension of the sample is 100mm ×100mm×6m, with CNFs weight fraction of approximately 1%. The experiments were repeated 2 times for all of the samples. The results showed less than 10% variation. The flammability data reported in this study was the average of the 2 replicated tests.

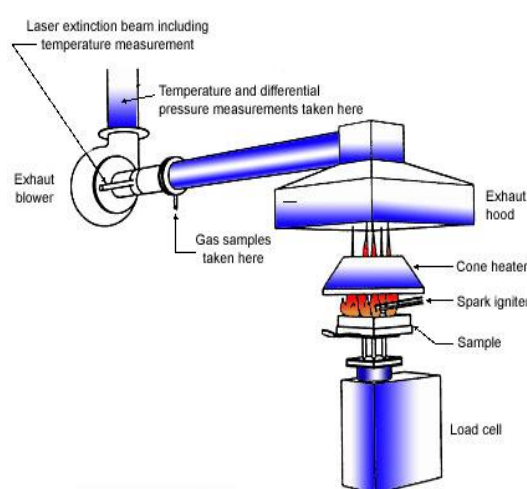


Figure 54 The schematic representation of the ASTM E1345-10 cone calorimeter test method

The sample was heated up to 900 °C at a constant rate of 1°C/s. The peak heat release rate (PHRR) in Watts per gram of sample (W/g) was calculated from the oxygen depleting measurements. The total heat release (THR) in kJ/g was obtained by integrating the HRR curve.

8.4. Results and discussion

The preparation of POSS covalently functionalized CNF was illustrated in Figure 53. The FTIR spectra of pristine CNF, POSS and CNF-g-POSS are shown in

Figure 56. After the covalent functionalization, a broad band at around 1700 cm^{-1} corresponding to the stretching vibration of the C=O group of the amide functionality was observed in the CNF-g-POSS. Another new peak appeared at around 1110 cm^{-1} , which was attributed to the symmetric stretching vibration of Si-O bond [81]. These results indicate that POSS particles were associated to the surface of CNF.

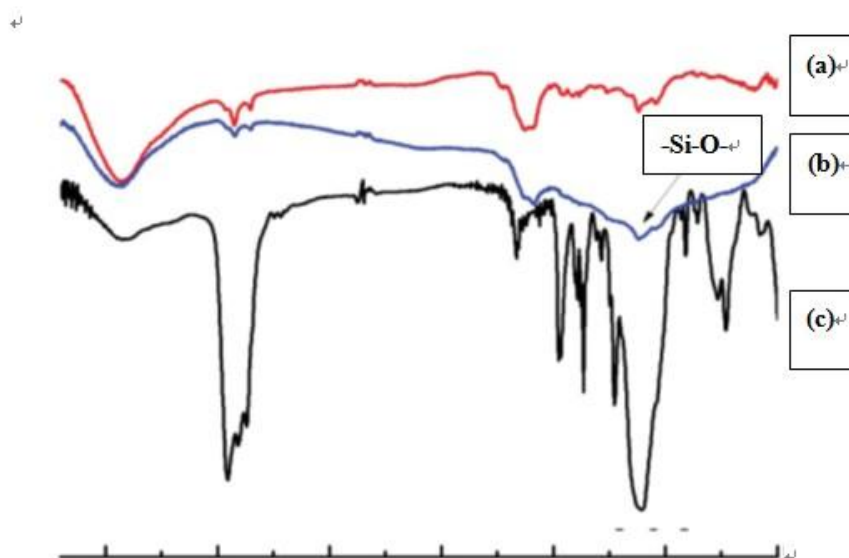


Figure 55 FTIR spectra of: (a) pristine CNTs; (b) CNT-g-POSS; (c) POSS.

Figure 57 illustrates the Raman spectra of the pristine CNF and CNF-g-POSS. The D-band at around 1350 cm^{-1} is assigned to the disordered graphite structure or sp^3 hybridized carbon of CNF [89]. The G-band at around 1580 cm^{-1} is attributed to in-plane stretching mode of graphite, which reflects the structural intensity of the sp^2 -hybridized carbon atoms. The peak intensity ratio (I_D/I_G) increases from 0.58 to 0.80, as shown in Figure 57, indicating many defects or functionalization in the nanofibers. In addition, a smooth shoulder band located at around 1610 cm^{-1} is observed for the CNF-g-POSS. The D' band is also associated with the defects or

disorder in the nanofibers, which is an evidence of the disruption of the aromatic system of p electrons by the attached molecules [90, 91]. Both the increase in I_D/I_G and the enhancement of the D' band of CNF-g-POSS is the evidence of covalent functionalization of POSS onto CNFs.

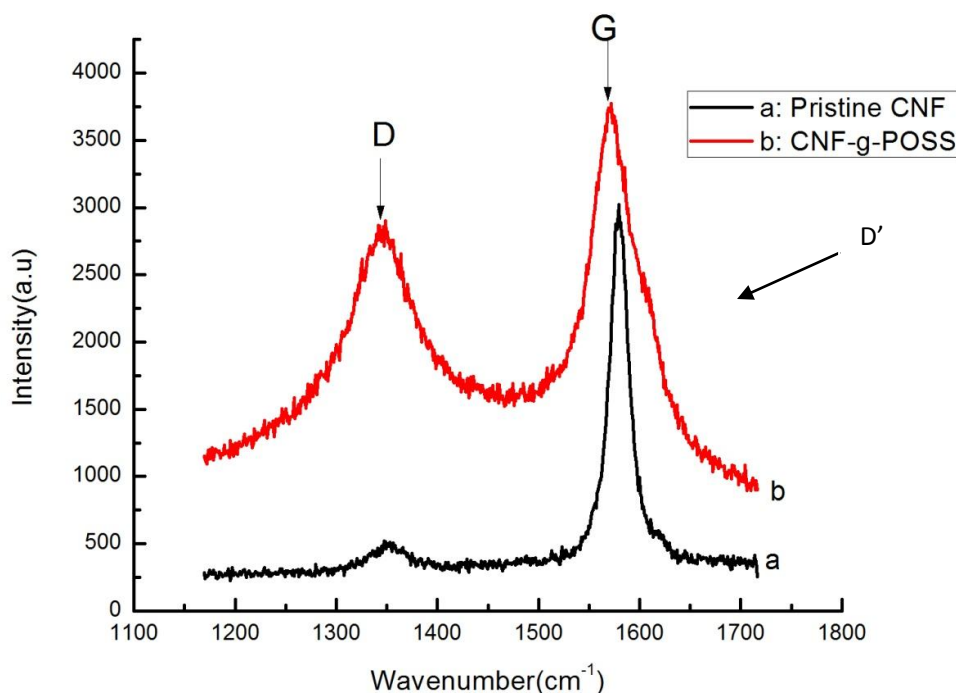


Figure 56 Raman spectra of: (a) pristine CNF; (b) CNF-g-POSS.

The nanopapers were fabricated with CNF-g-POSS and CNF respectively. The morphologies of CNF and CNF-g-POSS nanopaper are shown in figure 58, respectively. In figure 58(a), CNFs are uniformly dispersed and highly entangled with each other, which forms a random interconnected network. A more compact and entangled network is observed in CNF-g-POSS nanopaper, as shown in Figure 58(b).

The nanofibers seem to be much shorter, which is due to the oxidation with strong acids.

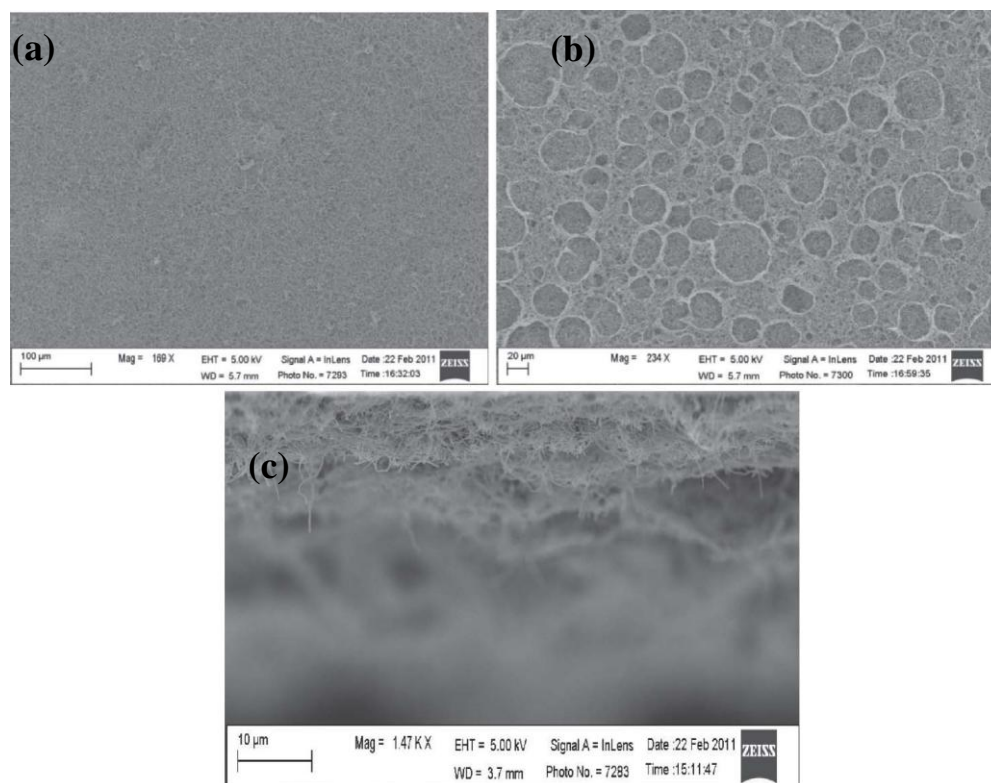


Figure 57 SEM images of: (a) surface of CNF paper, (b) POSS-g-CNF paper, (c) the ‘wall’ in (b) at high magnification.

Figure 58 shows the measurements of water contact angle. The water contact angle of pristine a CNF film is found to be $140.4 \pm 0.4^\circ$, which suggests that the surface of CNFs film is hydrophobic. The contact angle measured with water is significantly increased to $160.5 \pm 0.1^\circ$ in the case of CNF-g-POSS film. The remarkable increase in hydrophobicity is attributed to the POSS molecules attached covalently to the nanofibers surface, which lowers the surface energy of the nanofibers [92]. Another possible reason for the superhydrophobicity is surface roughness [92]. A difference in the surface morphologies of the films was observed in figure 58. The CNF film shows

a relatively smooth surface decorated with wrinkles. However, the CNF-g-POSS film exhibits a honeycomb-like structure with a diameter of the cell ranging from 10 to 100 μm . A high magnification SEM image reveals that the “wall” of honeycomb is composed of entangled CNF-g-POSS, as shown in figure 57(c). This honeycomb structure makes a contribution to the super hydrophobicity, by decreasing the contact area between the water droplet and the surface [93, 94]. The formation of honeycomb structure, although it has not been fully understood, may result from the change in the surface tension of the solution and self-assembly of CNF-g-POSS [95, 96]. The solution always tends to decrease its Gibbs free energy, which is proportional to the surface tension. When the suspension is casted onto a substrate, the solvent begins to evaporate. In the case of CNF/ CHCl_3 solution, CNF may precipitate because of the low solubility. Due to the good compatibility between CNF-g-POSS and solvent, the amount of CNF-g-POSS will assembly on the surface of the solution and form a thin surface film, which will decrease the surface energy of the system. With the volatilization of the solvent, the capillary forces are exerted upon the nanofibers, and as a result some nanofibers are reoriented parallel to the direction of the liquid retraction. After the solvent evaporates completely, the honeycomb structure remains. The stability of the superhydrophobic surface is a critical issue that needs to be addressed from a practical point of view. A main drawback of superhydrophobic surfaces made from CNFs, as reported in Lau and his co-workers’ work [97], is that the superhydrophobicity can only last for several minutes. The superhydrophobicity

then decreases even disappears, owing to the water droplet penetration into the void of the film. However, the superhydrophobicity of the sample in this study is very stable. After the sample was exposed to a high-humidity environment for three weeks, the water contact angle was $150\pm0.3^\circ$, which indicates the surface is still superhydrophobic.

The thermal stability of the nanopaper is related to the fire performance of composites. TGA is one of the most widely used techniques for a rapid evaluation of the thermal stability of various polymer composites [81]. The thermal properties of pristine CNF, POSS and CNF-g-POSS were studied by TGA under N_2 atmosphere, as shown in Figure 60 and Table 10. The decomposition of POSS particles occurs at about $225^\circ C$ with 1 wt% residue at the end of decomposition. The pristine CNF decomposes at around $650^\circ C$ and 95 wt% residue remains at $700^\circ C$. However, the CNF-g-POSS is less thermally stable; the decomposition temperature drops to $380^\circ C$. The relative amount of grafted POSS onto CNF can be estimated by the TGA analysis. The difference in weight at $700^\circ C$ between CNF-g-POSS and pristine CNF showed that the content of covalently grafted POSS is approximately 20 wt%.

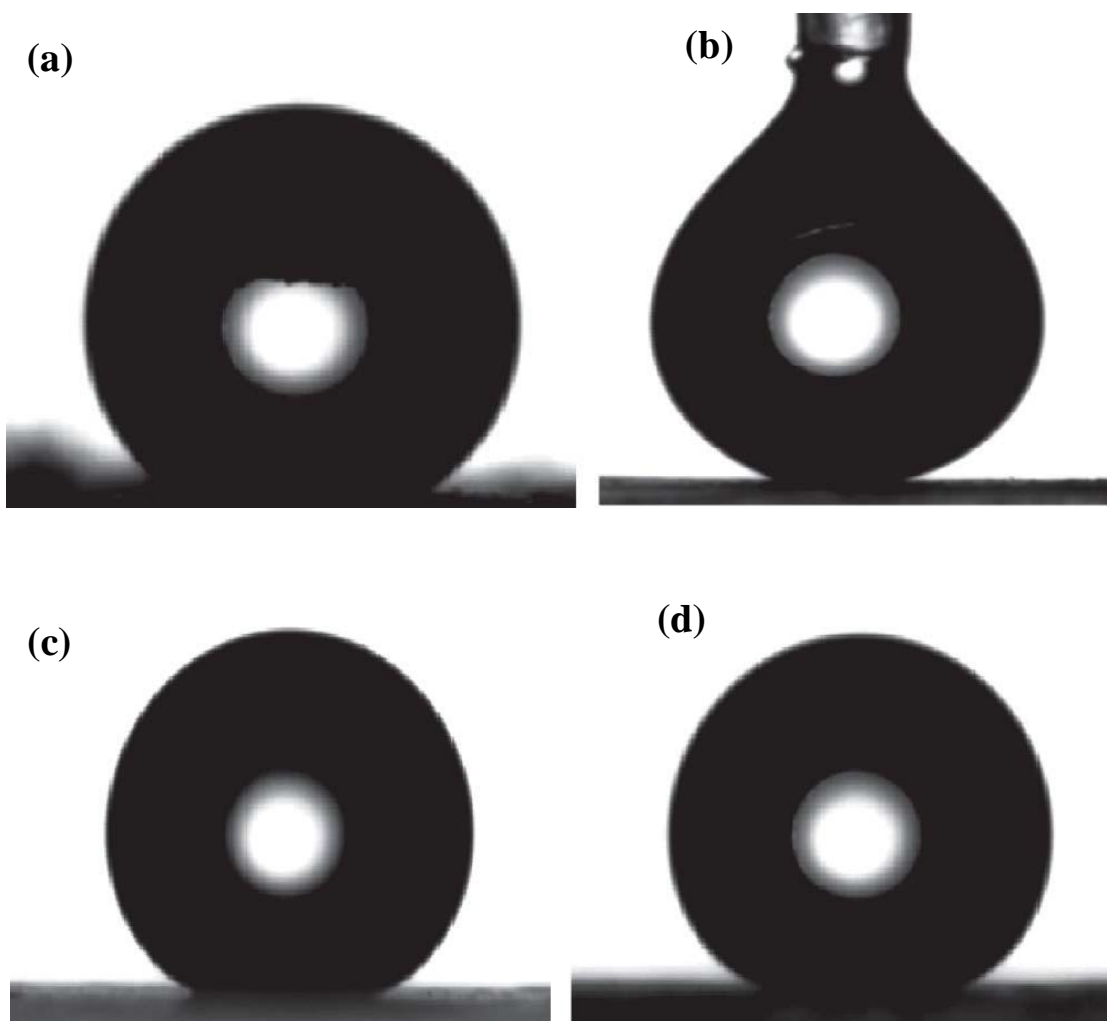


Figure 58 Photo images of a 15 μL water droplet on surfaces: (a) CNF film; (b) A droplet sticks on CNF-g-POSS film; (c) stays on CNF-g-POSS film; (d) the same measured CNF-g-POSS film after exposure to a high-humidity environment for three weeks.

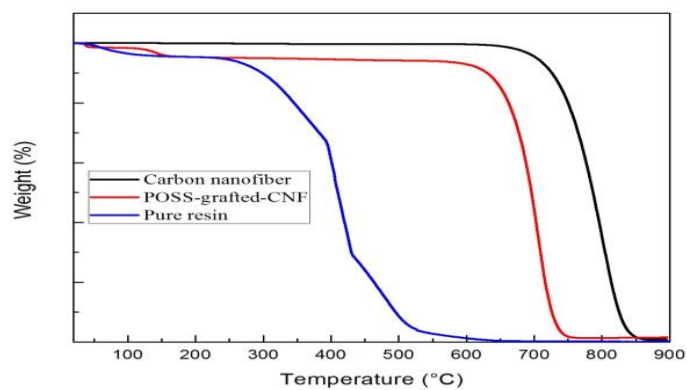


Figure 59 TGA results of pure POSS, CNF, and POSS-grafted-CNF

Table 10 Thermal properties of particles, nanopaper with resin from TGA.

TGA Test Samples	T-5 wt% (°C) *	Char (wt%) @ 700 °C
Pristine CNF	700	94.9
CNF-g-POSS	301	45.1
Aminopropylisooctyl-POSS	227	1

Table 11 PHRR and Char of samples

Test Samples	PHRR(kW/m ²)	Char (wt%) @ 700 °C	Time to ignition (s)
Neat resin	621	0.03	23
CNF+resin	384	38	15
POSS-g-CNF	346	40.3	26.1

Figure 64, 65 illustrates the plots of Mass Loss, and HRR versus temperature of neat resin and CNF, and POSS-grafted-CNF infused with resin. The PHRR, time to ignition and Char are summarized in Table 11. The neat resin exhibits the highest PHRR of 621 W/g. For the sample of pristine CNF with resin, the PHRR is significantly suppressed by 38%, from 621 W/g to 384 W/g. Further reduction of PHRR from 384 kW/m² to 346 kW/m² is observed for CNFs-g-POSS paper with resin, which is reduced by approximately 45%. The decrease of PHRR and Mass loss indicates that the incorporation of the POSS-g-CNF into polymer composites can restrict the fire development.



Figure 60 Pure resin panel after cone test



Figure 61 Resin with 1% CNF panel after cone test



Figure 62 Resin with POSS-grafted-CNF panel after cone test

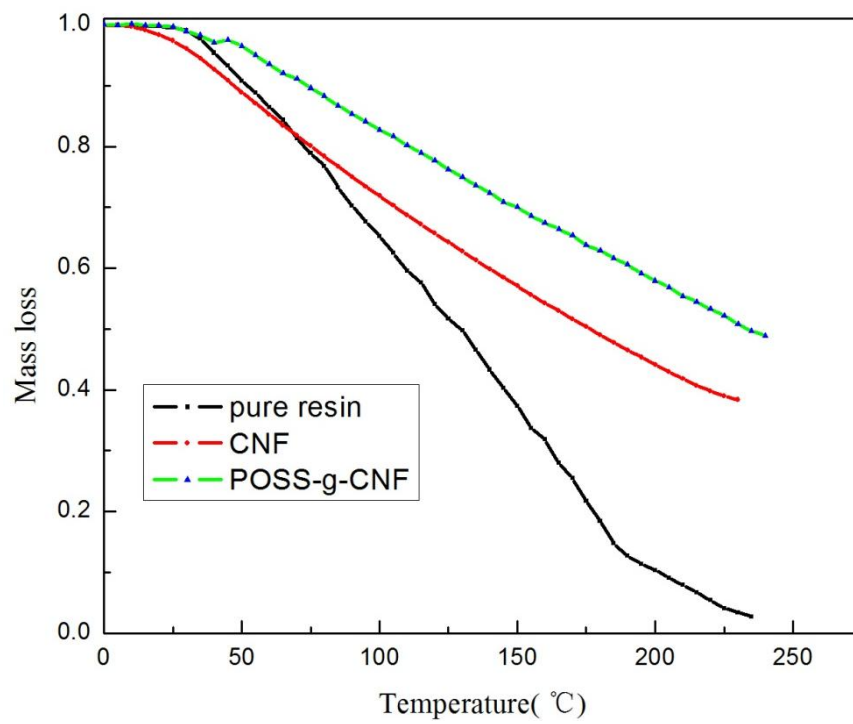


Figure 63 the mass loss of the cone test

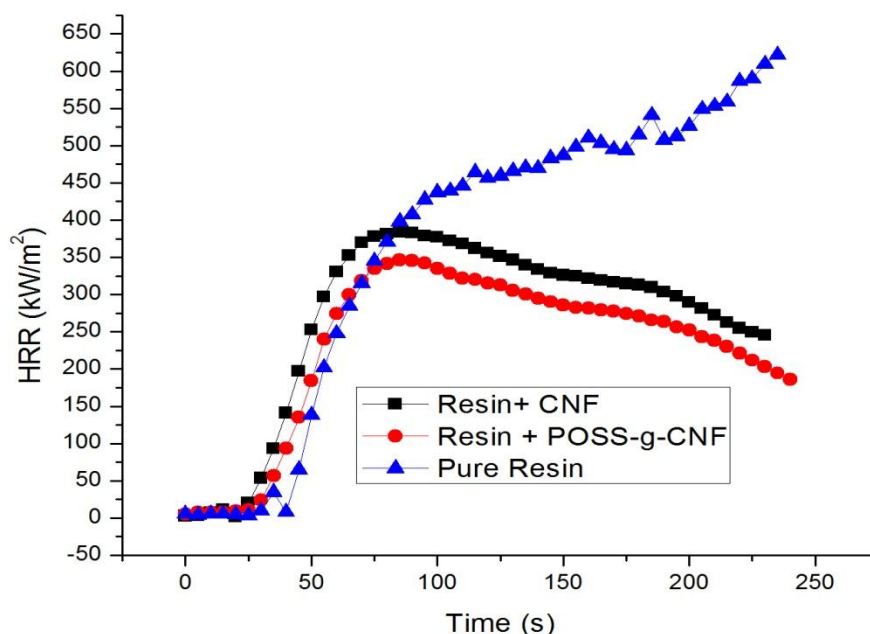


Figure 64 HHR of the cone tsest

Moreover, the efficiency of CNF-g-POSS in fire retardancy is higher than pristine CNF due to the char formation. The images of the char morphologies are shown in Figure 61, 62, 63. In the residue of CNF and CNF-g-POSS with resin, the nanofibers are entangled together with the char materials. The entire structure could effectively act as barrier to limit the diffusion of flammable gases to the surface and slow down the combustion and degradation of the resin.

8.5. Summary

CNF-g-POSS were synthesized by reacting POSS-NH₂ with the functionalized CNF, which was prepared by the modification of pristine CNF with H₂SO₄/HNO₃ followed by SOCl₂. The CNF-g-POSS samples were characterized by FTIR, Raman

spectroscopy and TEM-EDAX. The results indicated that POSS was chemically grafted to CNF, and the grafting amount of the POSS determined by TGA, was approximately 25 wt%. The CNF-g-POSS film exhibits a stable superhydrophobicity even exposed to a high-humidity environment over a long period. The nanocomposites were fabricated with CNF-g-POSS and CNF. The flame retardant performance of the nanocomposites was evaluated by cone test. A significant reduction in PHRR was observed for CNF-g-POSS nanopaper with resin. The CNF-g-POSS composite exhibits high efficiency in fire retardancy compared to CNF composite. This is due to the char formation during combustion, which could effectively limit the heat and mass transfer and the diffusion of the flammable gases and therefore slow down the combustion and degradation of the resin.

CHAPTER NINE: CONCLUSION AND FUTURE WORK

In this study, multifunctional carbon nanofiber papers have been developed and optimized as a platform material. Carbon nanofiber paper can be integrated into polymer composites through resin transfer molding (RTM) processing and Autoclave processing. Vibrational test results have shown significant increase in damping ratios of the nanocomposite laminates which is critical for the structural stability and dynamic response, position control, and durability of dynamic system. The friction between carbon nanofibers and polymer resin are expected to be responsible for energy dissipation in the nanocomposite laminates. Hybrid nanopapers are developed to improve the tribology properties of polymer composites. Test result shows both reduce for COF and ware rate and the surface ware properties are greatly enhanced.

The conductivity and shielding effectiveness (SE) of carbon nanopapers/nanofilms and the lightning strike tolerance on these composite panels are measured in this study, respectively. The test results showed a good correlation between the EMI shielding/lightning strike tolerance and the surface electrical conductivity. Carbon nanofiber paper can be used for lightning strike protection by incorporating Nickel nanostrands because the highly conductive surface could provide safe conductive paths.

A series of experiments were conduct to study the synergistic effect of carbon nanofiber and carbon nanopaper on the shape recovery of the SMP composites. The actuation of the SMP composites was achieved by the electrical resistive heating of

carbon nanopaper. The conductivity of SMP is greatly reduced by incorporating CNP into SMP and further reduced by blending CNFs into SMP, and then the shape memory response is significantly accelerated. Meanwhile, a vision-based control system was developed, which offered a noninvasive approach to measure and precisely control the shape of the SMP nanocomposites. The actuation test results show that the responses of the SMP nanocomposites under this controller were fast and accurate, and the performance was repeatable. Carbon fiber reinforced SMP nanocomposites were fabricated. These carbon fiber reinforced SMP nanocomposites have shown good durability and easy to actuate by resistivity heat, which lead their application as a structure material.

CNF-g-POSS were synthesized by reacting POSS-NH² with the functionalized CNF, which was prepared by the modification of pristine CNF with H₂SO₄/HNO₃ followed by SOCl₂. The CNF-g-POSS samples were characterized by FTIR, Raman spectroscopy. The results indicated that POSS was chemically grafted to CNF, and the grafting amount of the POSS determined by TGA, was approximately 15 wt%. The CNF-g-POSS film exhibits a stable superhydrophobicity even exposed to a high-humidity environment over a long period. The nanopapers were fabricated with CNF-g-POSS and CNF. The flame retardant performance of the composites was evaluated by cone calorimeter test. A significant reduction in PHRR was observed for CNF-g-POSS mixed with resin. The CNF-g-POSS paper exhibits high efficiency in fire retardancy compared to CNF and pure resin. This is due to the char formation

during combustion, which could effectively limit the heat and mass transfer and the diffusion of the flammable gases and therefore slow down the combustion and degradation of the resin.

The research results have shown significant improvement of electrical and mechanical properties of CNF-based nanocomposite. For the future work, efforts could be carried out in several aspects. For the nanopaper, more work can be done in the alignment. The conductivity could be significantly improved by controlling orientation of the CNF. Also, new particle could be hybrid into the paper, such as graphene. However, it should be noticed that because of the layer structure of graphene, the porosity of the nanopaper will be greatly reduced, which makes the resin infusion much more challenging. For SMP research, fundamental experiments could be done, such as monitoring the temperature change of the sample during actuation. The recovery force should be investigated.

REFERENCE

- [1] J. Hale. Boeing 787 from the Ground Up. Aero. 2006; 4: 17-24.
- [2] Lucintel, Growth opportunities in the Global Composite Materials Industry, SPE, ACCE, 2011
- [3] <<http://www.sonifier.com>>, sonifier products, Branson ultrasonics corp.
- [4] J. Liu, A. G. Rinzler, H. J. Dai, et al. “Fullerene pipes”. Science, 1998; 280(5367): 1253
- [5] H. Ago, K. Petritsch, M. S. P. Shaffer, et al. “Composites of carbon nanotubes and conjugated polymers for photovoltaic devices”. Adv. Mater., 1999; 11(15): 1281
- [6] Y. H. Li, Y. M. Zhao, M. Roe, et al. “In-plane large single walled carbon nanotube films: In situ synthesis and field emission properties”. Small, 2006; 2(89):1026
- [7] R. T. Lv, S. Tsuge, X. C. Gui et al. “In situ synthesis and magnetic anisotropy of ferromagnetic buckypaper”. Carbon, 2009; 47(4): 1141
- [8] J. A. Sung, Y. W. Zhu, S. H. Lee, Stoller M. D., T. Emilsson, S.J. Park, A. Velamakanni, J.H. An, and R. S. Ruoff, Thin Film Fabrication and Simultaneous Anodic Reduction of Deposited Graphene Oxide Platelets by Electrophoretic Deposition, J. Phys. Chem. Lett., 2010; 1, 1259–1263
- [9] M. Zhang, S. Fang, A. Zakhidov, S. B. Lee, A. E. Aliev, C. D. Williams, K. R. Atkinson, R. H. Baughman, Strong, Transparent, Multifunctional, Carbon Nanotube Sheets, Science, 2005; 309, 1215.
- [10] V. P. Veedu, A. Cao, X.S. Li, K.G. MA, C. Soldano, S. Kar, P. M. Ajayan AND

M. N. Ghasemi-Hejhad, Multifunctional composites using reinforced laminate with carbon-nanotube forests, *nature materials*, 2006; 5, 457-462.

[11] W. Liao and K. Wang. On the Analysis of Viscoelastic Materials for Active Constrained Layer Damping Treatments. *Journal of Sound and Vibration*, 1997; 207, 319.

[12] C. Brackbill, L. Ruhl, G. Lesieutre and E. Smith. Characterization and Modeling of the Low Strain Amplitude and Frequency Dependent Behavior of Elastomeric Damper Materials. *Journal of the American Helicopter Society*; 2000; 45, 34.

[13] 3M Bonding Systems Division. Material Data Sheets, 1999; 1000, 55144.

[14] J. M. Biggerstaff and J. B. Kosmatka, *Journal of Composite Materials*, 1998; 32, 21.

[15] S. Iijima. Helical microtubules of graphite carbon. *Nature* , 1991; 8, 354.

[16] J. R. Maly and C. D. Johnson, *SPIE Proceedings on smart structures and Materials*, 1996; 365.

[17] J. P. Lu, *Physical Review Letter*, 1997; 79, 1297.

[18] E. Hernandez, C. Goze, P. Bernier and A. Rubio, *Physical Review Letter*, 1998; 80, 4502.

[19] M. M. J. Treacy, T. W. Ebbesen and J. M. Gibson, *Nature*, 1996; 381, 678.

[20] P. Poncharal, Z. L. Wang, D. Ugarte and W. A. de Heer, *Science*, 1999; 283, 1513.

[21] M. Yu, O. Lourie, M. J. Dyer, K. Moloni, T. E. Kelley and R. S. Ruoff, *Science*,

2000; 287, 637.

[22] N. Koratkar, B. Q. Wei and P. M. Ajayan, *Advanced Materials*, 2002; 14, 997.

[23] J. Suhr, N. Koratkar, N. P. Keblinski and P. M. Ajayan, *Nature Material*, 2005; 4, 134.

[24] J. Suhr, W. Zhang, P. M. Ajayan and N. Korathar, *Nano Letters*, 2006; 6, 219.

[25] A. Buldum, J.P. Lu. Atomic scale sliding and rolling of carbon nanotubes. *Phys Rev Lett*, 1999; 83, 5050.

[26] H. Holscher, U.D. Schwarz, O. Zworner, R. Wiesendanger. Consequences of the stick-slip movement for the scanning force microscopy imaging of graphite. *Phys Rev B*, 1998 ; 57, 2477.

[27] R. Himanshu and J. Nader, *Composites Science and Technology*, 2005; 65, 2079.

[28] I. C. Finegan, G. G. Tibbetts and R. F. Gibson, *Composites Science and Technology*, 2003; 63, 1629.

[29] V. Rooij, W.A. Timmer. Roughness sensitivity considerations for thick rotor blade airfoils. *Trans ASME*; 2003; 125, 468–78.

[30] D. D. L. Chung, *Electromagnetic Interference Shielding Effectiveness of Carbon Materials*, *Carbon*, 2001; 39, 279-285.

[31] K.K.S. Kumar, S. Geetha, and D.C. Trivedi, *Freestanding Conducting Polyaniline Film for the Control of Electromagnetic Radiations*, *Current Applied Physics*, 2005; 5, 603-608.

- [32] S. Wen and D.D.L. Chung, Electromagnetic Interference Shielding Reaching 70 dB in Steel Fiber Cement, *Cement and Concrete Research*, 2004; 34, 329-332.
- [33] S. Yang, K. Lozano, A. Lomeli, H. D. Foltz, and R. Jones, Electromagnetic Interference Shielding Effectiveness of Carbon Nanofiber/LCP Composites, *Composites Part A*, 2005; 36, 691-697.
- [34] U. Lundgren, J. Ekman, and J. Delsing, Shielding Effectiveness Data on Commercial Thermoplastic Materials, *IEEE Transactions on Electromagnetic Compatibility*, 2006; 48, 766-773.
- [35] B. Wang, R. Liang, O. Marietta-Tondin, S. Wang, C. Zhang, L. Kramer, and P. Funchess, EMI Shielding Effectiveness of Carbon Nanotube Buckypaper Nanocomposite/Foam Sandwich Structures, *Multifunctional Nanocomposites*, 2006.
- [36] D. Yuping, L. Shunhua, and G. Hongtao, Investigation of Electrical Conductivity and Electromagnetic Shielding Effectiveness of Polyaniline Composite, *Science and Technology of Advanced Materials*, 2005; 6, 513-518.
- [37] M. S. Kim, H. K. Kim, S. W. Byun, S. H. Jeong, Y. K. Hong, J. S. Joo, K. T. Song, J. K. Kim, C. J. Lee, and J. K. Lee, PET Fabric/Polypyrrole Composite With High Electrical Conductivity for EMI Shielding, *Synthetic Metals*, 2002; 126, 233-239.
- [38] N. A. Aal, F. El-Tantawy, A. Al-Hajry, and M. Bououdina, New Antistatic Charge and Electromagnetic Shielding Effectiveness from Conductive Epoxy Resin/Plasticized Carbon Black Composites, *Polymer Composites*, 2008, 125-132.

- [39] P. B. Jana, A. K. Mallick, and S. K. De, Effects of Sample Thickness and Fiber Aspect Ratio on EMI Shielding Effectiveness of Carbon Fiber Filled Polychloroprene Composites in the X-Band Frequency Range, *IEEE Transactions on Electromagnetic Compatibility*, 1992; 34, 478-481.
- [40] Y. Yang, M. C. Gupta, K. L. Dudley, and R. W. Lawrence, Novel Carbon Nanotube-Polystyrene Foam Composites for Electromagnetic Interference Shielding, *Nano Letters*, 2005; 5, 2131-2134.
- [41] J. R. Gaier, Intercalated Graphite Fiber Composites as EMI Shields in Aerospace Structures, *IEEE Transactions on Electromagnetic Compatibility*, 1992; 34, 351-356.
- [42] T. Wang, G. Chen, C. Wu, and D. Wu, Study on the Graphite Nanosheets/Resin Shielding Coatings, *Progress in Organic Coatings*, 2007; 59, 101-105.
- [43] B. O. Lee, W. J. Woo, and M.-S. Kim, EMI Shielding Effectiveness of Carbon Nanofiber Filled Poly(vinyl alcohol) Coating Materials, *Macromolecular Materials and Engineering*, 2001; 286, 114-118.
- [44] B. O. Lee, W. J. Woo, H. S. Park, H. S. Hahm, J. P. Wu, and M. S. Kim, Influence of Aspect Ratio and Skin Effect on EMI Shielding of Coating Materials Fabricated With Carbon Nanofiber/PVDF, *Journal of Materials Science*, 2002, 37, 1839-1843.
- [45] Y. Yang, M. C. Gupta, and K. L. Dudley, Toward Cost-Efficient EMI Shielding Materials Using Carbon Nanostructure-Based Nanocomposites, *Nanotechnology*, 2007; 18.

- [46] Y. Yang, M. C. Gupta, K. L. Dudley, and R. W. Lawrence, Conductive Carbon Nanofiber-Polymer Foam Structures, *Advanced Materials*, 2005; 17, 1999-2003.
- [47] D. D. L. Chung, Comparison of Submicron-Diameter Carbon Filaments and Conventional Carbon Fibers as Fillers in Composite Materials, *Carbon*, 2001; 39 1119-1125.
- [48] X. Luo and D. D. L. Chung, Electromagnetic Interference Shielding Using Continuous Carbon-Fiber Carbon-Matrix and Polymer-Matrix Composites, *Composites Part B*, 1999; 227-231.
- [49] E.M. Bazelyan, and Y. Raizer, *Lightning Physics and Lightning Protection*, Nicki Dennis, London, 2000.
- [50] F.H. Gojny, M.H.G. Wichmann, B. Fiedler, W. Bauhofer and K. Schulte Influence of nano-modification on the mechanical and electrical properties of conventional fibre-reinforced composites, *Composites Part A*, 2005; 36, 1525.
- [51] J. Gou, Z.Y. Liang and B. Wang, Investigation of Molecular Interaction between (10, 10) Single-Walled Nanotube and Epon 862 Resin/DETDA Curing Agent Molecules, *Int. J. Nanosci*, 2004; 365, 228-234.
- [52] J. Gou, S. O'Braint, H. Gu and G. Song, Damping Augmentation of Nanocomposites Using Carbon Nanofiber Paper, *J. Nanomateri*, 2006; 2006, 1.
- [53] A. Lendlein, H. Jiang, O. Junger, R. Langer, Light-induced shape-memory polymers, *Nature*, 2005; 434, 879-882.
- [54] A. Lendlein, S. Kelch, Shape-memory polymers, *Angew. Chem. Int. Ed.*, 2002;

41, 2034-2057.

[55] J.S. Leng, H.B. Lu, Y.J. Liu, W.M. Huang, S. Y. Du, Shape-memory polymers: A class of novel smart material, *MRS Bulletin*, 2009; 34, 848-855.

[56] I. Bellin, S. Kelch, R. Langer, A. Lendlein, Polymeric Triple Shape Materials, *Proc. Natl Acad. Sci. USA*, 2006; 103, 18043-18047.

[57] R. Vaia, Nanocomposites-Remote-controlled actuators, *Nature Mater.*, 2005; 4, 429-430.

[58] D.J. Maitland, M.F. Metzger, D. Schumann, A. Lee, T.S. Wilson, Laser Activated Shape Memory Polymer Microactuator for Treating Ischemic Stroke, *Lasers Surg Med.*, 2002; 3, 01-11.

[59] N.G. Sahoo, Y.C. Jung, N.S. Goo, J.W. Cho, Conducting shape memory polyurethane-polypyrrole composites for an electroactive actuator, *Macromolr Mater Eng.*, 2005; 290, 1049-1055.

[60] A.M. Schmidt, Electromagnetic activation of shape memory polymer networks containing magnetic nanoparticles, *Macromol. Rapid Commun.*, 2006; 271168-1172.

[61] M.Y. Razzaq, M. Anhalt, L. Frormann, B. Weidenfeller, Mechanical spectroscopy of magnetite filled polyurethane shape memory polymers, *Mater. Sci. Eng. A-Struct. Mater. Prop. Microstruct. Process.*, 2007; 471, 57-62.

[62] J.S. Leng, H.B. Lv, Y.J. Liu, S.Y. Du, Comment on "Water-driven programmable polyurethane shape memory polymer: Demonstration and mechanism" [*Appl. Phys. Lett.* 86, 114105, (2005)], *Appl. Phys. Lett.*, 2008; 92, 206105.

- [63] H.B. Lv, J.S. Leng, Y.J. Liu, S.Y. Du, Shape-memory polymer in response to solution, *Adv. Eng. Mater.*, 2008; 10, 592-595.
- [64] H.B. Lu, Y.J. Liu, J.S. Leng, S.Y. Du, Qualitative separation of the effect of solubility parameter on the recovery behavior of shape-memory polymer, *Smart Mater. Struct.*, 2009; 18, 085003.
- [65] J. Gou, S.O. Braint, H. Gu, G. Song, Damping augmentation of composites using carbon nanofiber paper, *J Nanomater.*, 2006; 2006, 1-7.
- [66] J. Gou, Single-walled nanotube bucky paper and composites, *Polym Inter.*, 2006; 55, 1283-1288.
- [67] A. Lendlein, et al., Biodegradable, Elastic Shape-Memory Polymers for Potential Biomedical Applications, *Science*, 2002; 296, 1673-1676.
- [68] Langer, et al. Designing materials for biology and medicine, *Nature*, 2004; 428, 487-492.
- [69] A.L. Browne, N.L. Johnson, Method for controlling airflow, United States Patent 7178859, 2007.
- [70] Xin, et al., Fiber reinforced shape-memory polymer composite and its application in a deployable hinge, *Smart Mater. Struct.*, 2009; 18
- [71] S. Iijima, Helical microtubules of graphitic carbon, *Nature*, 1991, 354, 56.
- [72] Y.C. Choi, W. Choi, Synthesis of Y-junction single-wall carbon nanotubes, *Carbon*, 2005; 43, 2737-2741.
- [73] D. Eder, Carbon Nanotube/Inorganic Hybrids, *Chem. Rev.* 2010; 110, 1348.

- [74] J. Wang, R.P. Deo, P. Poulin, M. Mangey, Electrochemical sensing platform based on the carbon nanotubes/redox mediators-biopolymer system, *J. Am. Chem. Soc.* 2003, 125, 14706.
- [75] J. Zou, L. Liu, H. Chen, S.I Khondaker, R.D. Mccullough, Q. Huo, L. Zhai, Dispersion of pristine carbon nanotubes using conjugated block copolymers, *Adv. Mater.*, 2008; 20, 2055.
- [76] L. Ci, J. Suhr, V. Pushparaj, X. Zhang, P.M. Ajayan, Continuous Carbon Nanotube Reinforced Composites, *Nano Lett.*, 2008; 8, 2762.
- [77] T. Chatterjee, A. Jackson, R. Krishnamoorti, J. Hierarchical, Hierarchical structure of carbon nanotube networks, *Am. Chem. Soc.*, 2008; 130, 6934.
- [78] T. Kashiwagi, F. Du, J.F. Douglas, K.I. Winey, Harris Jr RH, Shields J.R. Nanoparticle Networks Reduce the Flammability of Polymer Nanocomposites, *Nat. Mater.*, 2005; 4, 9928.
- [79] T. Kashiwagi, E. Grulke, J. Hilding, R. Harris, W. Awad, J. Douglas, Thermal Degradation and Flammability Properties of Polypropylene-Carbon Nanotube Composites, *Macromol. Rapid Commun.*, 2002; 23, 761.
- [80] S. Peeterbroeck, F. Laoutid, B. Swoboda, J.M. Lopez-Cuesta, N. Moreau, J.B. Nagy, M. Alexandre, P. Dubois, How Carbon Nanotube Crushing can Improve Flame Retardant Behaviour in Polymer Nanocomposites, *Macromol. Rapid Commun.*, 2007; 28, 260.
- [81] H. Lu, C.A. Wilkie, Synergistic effect of carbon nanotubes and

decabromodiphenyl oxide/Sb₂O₃ in improving the flame retardancy of polystyrene, 2010; Polym. Degrad. Stab. 95, 564.

[82] Wu Q, Zhu W, Zhang C, Liang Z, Wang B, Study of fire retardant behavior of carbon nanotube membranes and carbon nanofiber paper in carbon fiber reinforced epoxy composites, Carbon, 2010; 48, 1799.

[83] Y. Tang, M. Lewin, Migration and surface modification in polypropylene (PP)/polyhedral oligomeric silsesquioxane (POSS) nanocomposites, Polym. Adv. Technol., 2009; 20, 1.

[84] A. Lee, J. D. Lichtenhan, Thermal and viscoelastic property of epoxy–clay and hybrid inorganic–organic epoxy nanocomposites, J. Appl. Polym. Sci., 1999; 73, 1993.

[85] A.J. Waddon, L. Zheng, R.J. Farris, E.B. Coughlin, Nanostructured polyethylene-POSS copolymers: control of crystallization and aggregation, Nano Lett., 2002; 2, 1149.

[86] D.M. Fox, P.H. Maupin, R.H. Harris, J.W. Gilman, D.V. Eldred, D. Katsoulis, P.C. Trulove, H.C. De Long, Use of a polyhedral oligomeric silsesquioxane (POSS)-imidazolium cation as an organic modifier for montmorillonite, Langmuir, 2007; 23, 7707.

[87] R. Misra, B.X. Fu, S.E. Morgan, Surface energetics, dispersion, and nanotribomechanical behavior of POSS/PP hybrid nanocomposites, 2007; J. Polym. Sci.: Part B: Polym. Physics, 45, 2441.

- [88] Tang Y, Zhuge J, Gou J, Chen R, Ibeh C, Hu Y, Morphology, thermal stability, and flammability of polymer matrix composites coated with hybrid nanopapers, *Polym. Adv. Technol.*, 2011; 10, 1043.
- [89] H. Wu, R. Tong, X. Qiu, H. Yang, Y. Lin. R. Cai. S. Qian, Functionalization of multiwalled carbon nanotubes with polystyrene under atom transfer radical polymerization conditions, *Carbon*, 2007; 45, 152
- [90] A.M. Rao, A. Jorio, M.A. Pimenta, M.S.S. Dantas, R. Saito, G. Dresselhaus, Polarized Raman study of single-wall semiconducting carbon nanotubes, *Phys. Rev. Lett.*, 2000; 84, 1820.
- [91] S.M. Cooper, H.F. Chuang, M. Cinke, B.A. Cruden, M. Meyyappan, Gas permeability of a buckypaper membrane, *Nano Lett.*, 2003; 3, 189.
- [92] X. Zhang, F. Shi, J. Niu, Y. Jiang, Z. Wang, Superhydrophobic surfaces: from structural control to functional application, *J. Mater. Chem.*, 2008; 18, 621.
- [93] X. Zhang, F. Shi, J. Niu, Y. Jiang, Z. Wang, Superhydrophobic surfaces: from structural control to functional application, *J. Mater. Chem*, 2008; 18, 621.
- [94] S. Li, H. Li, X. Wang, Y. Song, Y. Liu, L. Jiang, D. Zhu, *J. Phys.Chem. B*, 2002; 106, 9274.
- [95] Y. Tian, Q. Jiao, H. Ding, Y. Shi, B. Liu, *Polymer*, 2006; 47, 3866.
- [96] J. Chen, W. A. Weimer, *J. Am.Chem.Soc.* 2002; 124, 758.
- [97] K. K. S. Lau, J. Bico, K.B.K. Teo, M. Chhowalla, G.A.J. Amaratunga, W.I. Milne, H. G. Mckinley, K.K. Gleason, *Nano Lett.*, 2003; 3, 1701.